CRREL REPORT 96-9

CRREL

Physical System Dynamics and White Phosphorus Fate and Transport, 1994, Eagle River Flats, Fort Richardson, Alaska

Daniel E. Lawson, Lewis E. Hunter, Susan R. Bigl,
Beth M. Nadeau, Patricia B. Weyrick and John H. Bodette

August 1996

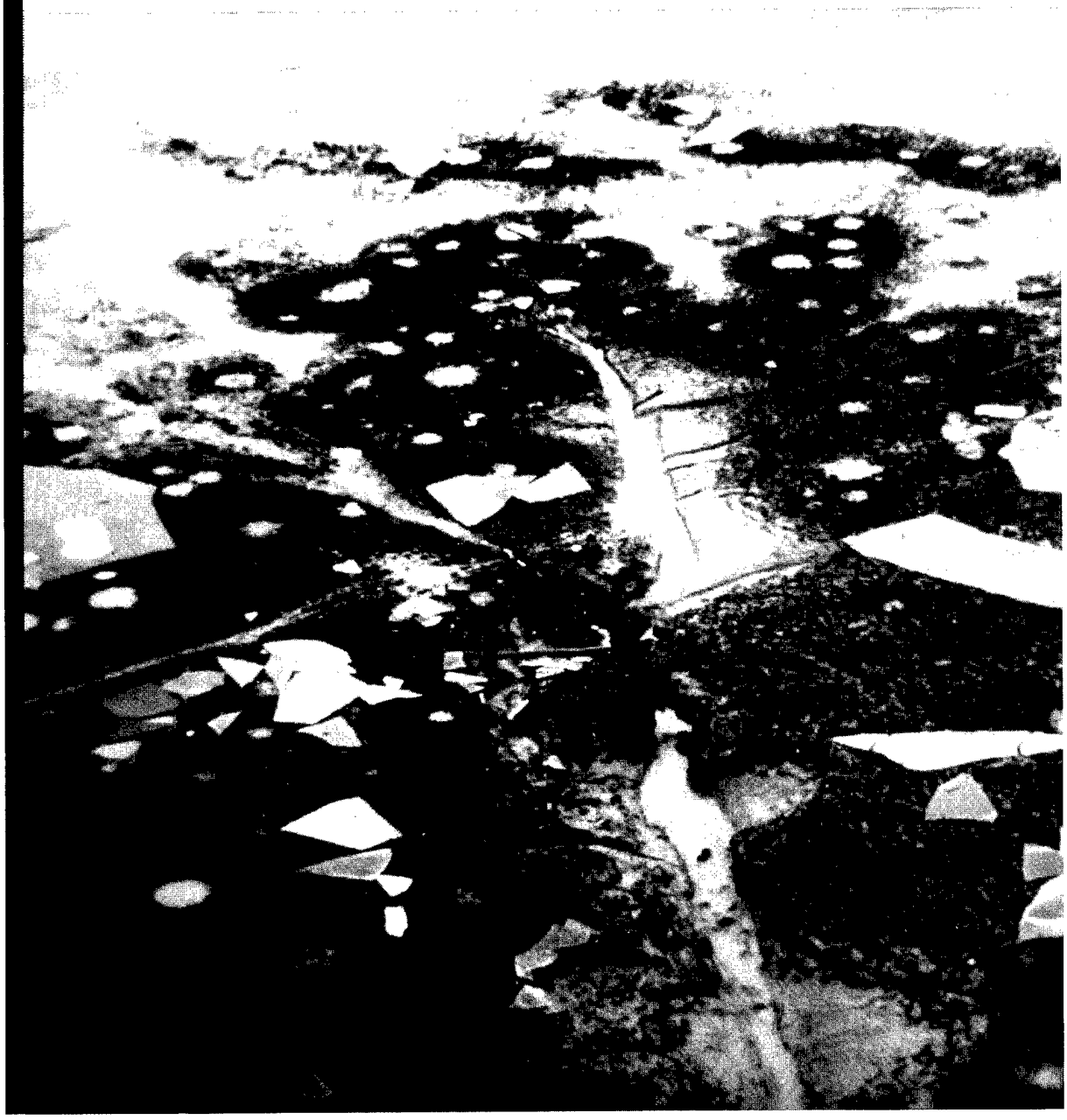

Abstract: Eagle River Flats (ERF) is a subarctic estuarine salt marsh where human and natural forces are causing significant changes in the environment. Multiple internal and external forces govern the physical and chemical processes by actively altering surface conditions, sometimes in unpredictable ways. ERF is also used as an artillery range by the U.S. Army, where past use has resulted in white phosphorous (WP) contamination of the sediments within ponds and mudflats. Bottom-feeding waterfowl ingest this WP, which causes rapid death. This report documents analyses of the physical environment, describing the nature of the physical systems and factors controlling them. It includes data on sedimentation, erosion and hydrology. These investigations provide knowledge necessary to designing and evaluating remedial technologies. They also help determine the system's capacity to naturally attenuate the WP contamination.

Cover: Aerial view of In-Between Gully (center) with stranded ice floes adjacent to it. WP-contaminated sediments can be transported by ice pulled from ponds during tidal flooding.

How to get copies of CRREL technical publications:

Department of Defense personnel and contractors may order reports through the Defense Technical Information Center:

DTIC-BR SUITE 0944
8725 JOHN J KINGMAN RD
FT BELVOIR VA 22060-6218
Telephone 1 800 225 3842
E-mail help@dtic.mil
msorders@dtic.mil
WWW http://www.dtic.dla.mil/

All others may order reports through the National Technical Information Service:

NTIS
5285 PORT ROYAL RD
SPRINGFIELD VA 22161
Telephone 1 703 487 4650
1 703 487 4639 (TDD for the hearing-impaired)
E-mail orders@ntis.fedworld.gov
WWW http://www.fedworld.gov/ntis/ntishome.html

A complete list of all CRREL technical publications is available from:

USACRREL (CECRL-TL)
72 LYME RD
HANOVER NH 03755-1290
Telephone 1 603 646 4338
E-mail techpubs@crrel.usace.army.mil

For information on all aspects of the Cold Regions Research and Engineering Laboratory, visit our World Wide Web site:
http://www.crrel.usace.army.mil

DISCLAIMER NOTICE

THIS DOCUMENT IS BEST QUALITY AVAILABLE. THE COPY FURNISHED TO DTIC CONTAINED A SIGNIFICANT NUMBER OF PAGES WHICH DO NOT REPRODUCE LEGIBLY.

CRREL Report 96-9

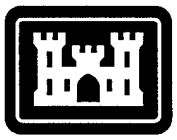

US Army Corps of Engineers
Cold Regions Research & Engineering Laboratory

Physical System Dynamics and White Phosphorus Fate and Transport, 1994, Eagle River Flats, Fort Richardson, Alaska

Daniel E. Lawson, Lewis E. Hunter, Susan R. Bigl,
Beth M. Nadeau, Patricia B. Weyrick and John H. Bodette

August 1996

Prepared for
U.S. ARMY ALASKA, FORT RICHARDSON, ALASKA
and
U.S. ARMY ENGINEER DISTRICT, ALASKA

PREFACE

This report was prepared by Dr. Daniel E. Lawson, Research Physical Scientist, Geological Sciences Division, Susan R. Bigl, Research Physical Scientist, Civil and Geotechnical Engineering Research Division, Lewis E. Hunter, Research Physical Scientist, Geological Sciences Division, Beth M. Nadeau, Physical Scientist, Geological Sciences Division, Patricia B. Weyrick, Physical Science Technician, Snow and Ice Division, and John H. Bodette, Civil Engineering Technician, Civil and Geotechnical Engineering Research Division, Research and Engineering Directorate, U.S. Army Cold Regions Research and Engineering Laboratory.

Funding and support for this research was provided through the U.S. Army Engineer District, Alaska, by the U.S. Army Alaska, Fort Richardson, Alaska. The authors thank William Gossweiler, Douglas Johnson, William Smith and Laurie Angell for helpful discussions, logistical support and assistance in the field, as well as for their continuing support, and Dr. Charles Racine, Marianne Walsh and Charles Collins for numerous discussions on the Eagle River Flats project and their assistance in the field and laboratory. Also thanked are Dennis Lambert, Troy Arnold and Ron Bailey for their assistance in the field, and Cora Farnsworth for her contribution in preparing the report. Earlier versions of this report have been reviewed by Larry Gatto and Jeffrey Strasser.

CONTENTS

ILLUSTRATIONS

Figure Page

Figure Page

TABLES

Table

EXECUTIVE SUMMARY

Eagle River Flats (ERF) is an estuarine salt marsh where natural and human forces are causing changes in the physical environment. The natural system is governed by a high tidal range, glacial river influences with a high sediment influx, a subarctic coastal climate and an active tectonic setting that make ERF susceptible to rapid and unpredictable changes. Ground explosions from the U.S. Army's use of ERF as an artillery range also cause physical changes to the terrain, hydrology and surface drainage. Smoke-producing rounds detonated above or on the ground have introduced White Phosphorus (WP), which is now distributed in the near-surface sediments of the ponds and marshes (Racine et al. 1992a).

Previous studies have shown that the unusually high duck mortality at ERF is linked to ingestion of WP particles by bottom-feeding waterfowl (Racine et al. 1992a,b). This study aims at understanding the physical environment of ERF to evaluate the fate and transport of WP, which is critical to developing remedial technologies for clean-up.

In this complex and dynamic environment, it is extremely difficult to predict the effects remedial measures will have on the physical system, and vice versa. Thus, knowledge of the overall system response, site-specific conditions, and process interactions is required before appropriate decisions on remedies can be made. In addition, natural attenuation of WP contamination can result from the site's physical and chemical processes, but the potential for this attenuation, and the length of time for attenuation to take place, requires an understanding of the physical processes. So, salinity, temperature, dissolved oxygen (DO), pH and turbidity were monitored to assess tidal and river dynamics during the flood and ebb cycle. Hydrological controls, including drainage pattern, channel gradients, channel cross sections and flow velocity, were also analyzed to calculate ebb discharge, sediment and WP particle transport rates, and to model sediment and water flux.

Tidal height fluctuations were measured in 1994 in concert with water level changes in eight gullies and the Eagle River where it discharges into ERF. Tidal currents measured in three gullies indicate that velocities are higher during ebb than during flood; thus, sediment transport and channel erosion are potentially greatest during ebb. Eagle River provides an avenue for tidal waters to inundate the innermost reaches of the Flats. Preliminary analyses show that sedimentation in the northern two-thirds of ERF is tidally dominated, whereas the southern one-third is river dominated. Sedimentation ranged from several millimeters per year on levees, 10–15 mm per year on mudflats, and up to 20–40 mm per year in ponds. Sediment is derived predominantly from the Knik Arm.

Suspended sediment concentrations were measured in the Eagle River, tidal gullies draining the ponds and mudflats, and the Knik Arm to define the sediment sources and to determine the timing of sediment transport. During a tidal cycle, TSS increases steadily with the flooding tide and decreases at a slower rate during the ebb. Seasonally, TSS values in gully and Knik Arm waters increase from spring to fall. Continuously recorded optical backscatter values of turbidity show a similar seasonal relationship, but with a high degree of variability.

Surveyed longitudinal profiles of tidal gully thalwegs revealed that the gullies are receding into the mudflats and ponds. There are several sharp increases in gradient (knickpoints) in each gully, marking channel adjustment to the progressive extension of the tidal gully into the mudflats and ponds. Two gully headwalls, one on the western side of Bread Truck and the other near the pond complex between Bread Truck and C ponds, are advancing at a rate sufficient to increase the drainage of those ponds in the next 15–30 years, if the current average rates persist.

Chemical analyses of sediment trap and plankton net samples indicate that WP does move and redeposit in ERF proper, and is transported as well through tidal

gullies to the Eagle River and Knik Arm. Bathymetric profiling of Knik Arm located several potential sites where WP-contaminated sediments may be deposited.

The physical system of ERF is dynamic and changing over seasons, years and decades. The relative importance of erosional and depositional processes vary from area to area in response to tidal and river hydrology. Natural sedimentation rates are high and may aid in the infilling of dredged areas and provide a natural method of WP burial, thereby reducing the risk of WP ingestion by waterfowl. The drainage system is actively changing through expansion of tidal gullies into adjacent mudflats and ponds, with certain pond areas likely to be drained in the next 10–20 years. Erosion will continue to release WP from mudflat and pond sediments over time, while existing ice and water transport mechanisms will move WP particles into tidal gullies, the Eagle River and Knik Arm. Whether these particles survive mechanical transport and persist in Knik Arm is unknown, but chemical analyses of deposits in the river and the Arm, coupled with laboratory flume tests of WP particle resistance to abrasion, could determine if transport may physically destroy them.

Our investigations of the physical system have significantly improved knowledge of the processes actively changing ERF and determining the flux of sediment and water in the system. Additional work is required to address the basic issue of whether these initial data and process relationships are representative of the variability in the ERF physical system. Further evaluation of the potential for natural attenuation of WP is also required. Site-specific investigations of contaminated areas requiring remediation are still necessary to develop criteria and a methodology to evaluate the potential effectiveness of remedial technologies at each location.

Physical System Dynamics and White Phosphorus Fate and Transport, 1994, Eagle River Flats, Fort Richardson, Alaska

DANIEL E. LAWSON, LEWIS E. HUNTER, SUSAN R. BIGL,
BETH M. NADEAU, PATRICIA B. WEYRICK AND JOHN H. BODETTE

INTRODUCTION

Eagle River Flats (ERF) is an 865-ha tidal flat and salt marsh at the mouth of Eagle River on Knik Arm, northeast of Anchorage, Alaska (Fig. 1). The tidal flat has been used as an artillery range since the early 1940s. Previous work by CRREL has shown that an unusually high mortality of migratory waterfowl, particularly ducks, is attributable to the ingestion of elemental white phosphorus (WP) particles (Racine et al. 1992a,b). White phosphorus particles were introduced by smoke rounds detonated during military training (Racine et al. 1992a, 1993). Particles of WP are now present in near-surface sediments at numerous locations in ERF, most notably in pond and marsh bottom sediments where dabbling ducks ingest them during feeding.

This report describes the results of 1994 investigations of the physical component of the Eagle River Flats ecosystem. These studies included analyses of the tidal and river hydrology that are critical for evaluating remedial technologies for WP contamination. Proposed remedies, which include removal of WP by dredging, in-situ degradation by temporary or permanent drainage and drying of ponds, and reduced risk by use of covers (possibly geotextiles), sedimentation and burial, will affect the ERF physical ecosystem in largely unknown ways. Studies of specific sites to be remediated are critical and their influence on the whole physical system must be considered.

ENVIRONMENTAL CONDITIONS

Eagle River Flats is one of several estuarine tidal flats and salt marshes in the upper Cook Inlet region of south-central Alaska (Fig. 1). Located at the mouth of the Eagle River, ERF is

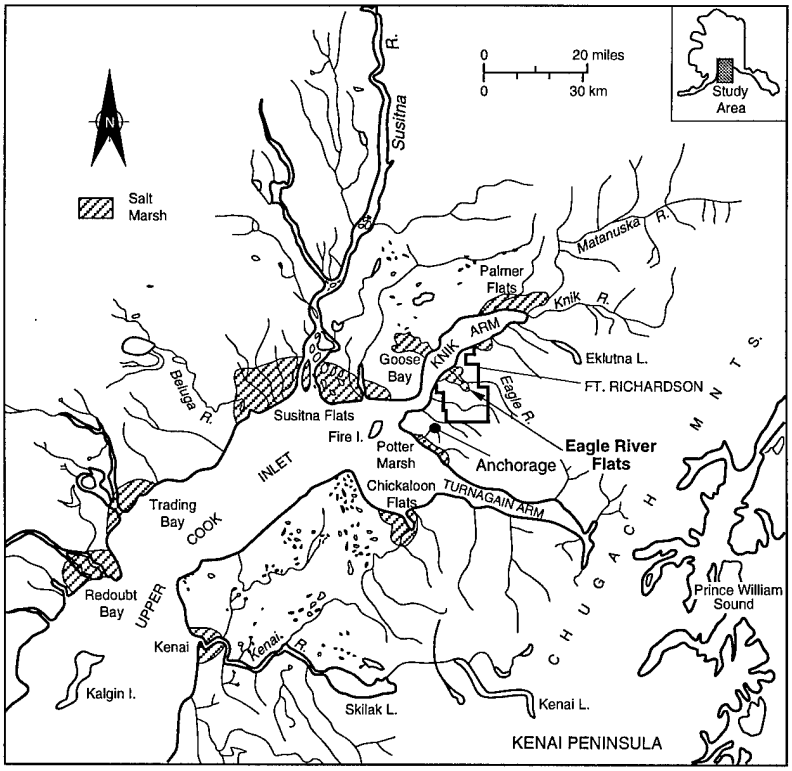

Figure 1. Upper Cook Inlet region, showing ERF and several other estuarine salt marshes (shaded areas).

about 2.8 km wide at the coast and narrows inland. This subarctic region has a transitional maritime to continental climate, with moderate annual temperatures (daily mean 1.9°C; minimum mean –2.2°C) and precipitation (330–508 mm; Evans et al. 1972). ERF is inundated by the semidiurnal macrotidal fluctuations (9 to 11 m) in Knik Arm and the resulting overflow from the Eagle River as it meets the rising tide.

The Eagle River drains a 497-km^2 basin in the Chugach Mountains, 13% of which is covered by glaciers, yet it takes only a few percent glacier cover to significantly modify the runoff and sediment yield of the drainage basin (e.g., Lawson 1993). Glaciers modify peak discharges, the timing and volume of hourly, daily and seasonal discharges, the lag between precipitation and the increase in runoff it causes, and long-term trends in annual discharge of the basin (e.g., Gurnell and Clark 1987, Lawson 1993).

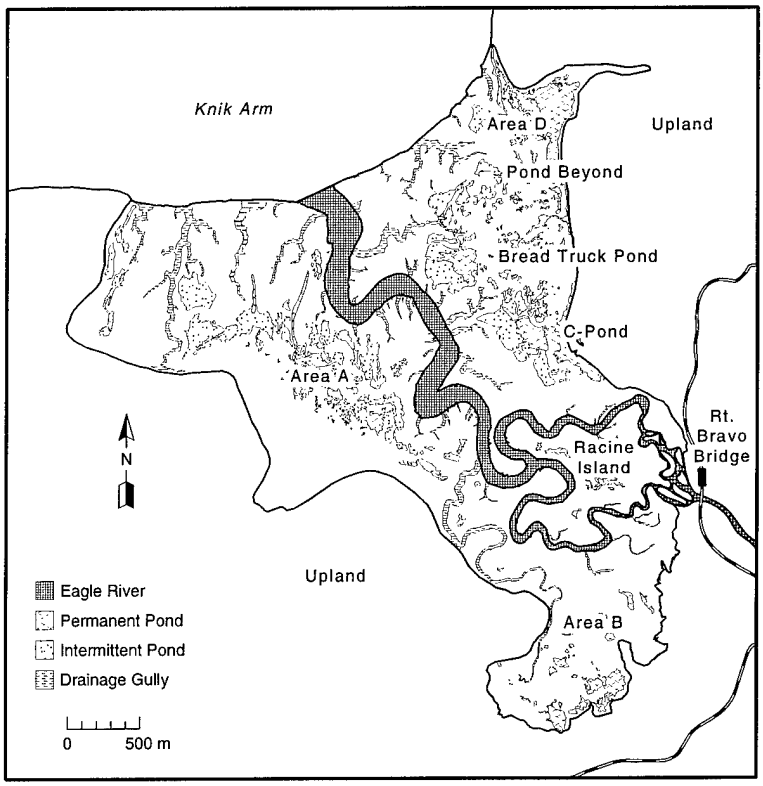

Figure 2. General distribution of ponds and the primary drainage system.

Because of this glacial influence, the primary melt season of July and August sees the maximum and peak discharges. River discharge and sediment fluxes vary daily, seasonally and annually, primarily because of glacial meltwater fluxes (Lawson 1993). Massive quantities of silt- and clay-size particles are transported in suspension by the large rivers draining glacierized basins in the Alaska Range, Chugach Mountains and Kenai Peninsula (e.g., Susitna, Knik and Matanuska river basins, Fig. 1) and are discharged into Knik Arm. These materials can remain suspended in the Arm for extended periods and flow into intertidal wetlands during tidal inundation.

Average discharge of Eagle River from 1966 to 1981 was about 14.7 m^3/s, with a peak discharge of 177 m^3/s having occurred on 18 September 1967 (USGS 1981). During a 10-year observation period (1966–1975), average monthly river discharge was observed to be lowest in February (1.4 m^3/s), with a minimum of 0.68 m^3/s having occurred between 29 January and 5 February 1974. The highest monthly discharges came during July and August, with mean discharges of 46.9 and 43.5 m^3/s respectively. However, owing to the variability in glacier melting and rainfall, average discharge for these months ranged widely from 24.7 to 62.9 m^3/s, with peak discharges exceeding 100 m^3/s when rainfall-induced floods took place during high melt periods (USGS 1981).

The Eagle River cuts approximately through the middle of ERF. The ponds and marshes primarily drain into it through vegetated channels and drainageways, and through unvegetated tidal gullies that form a dendritic network (Fig. 2). Where gullies and drainageways do not follow a dendritic course, their location appears to be controlled by relict drainage networks abandoned during the evolution of ERF (see Fig. 4a). The northern and coastal 20% of ERF is drained through gullies that discharge directly into Knik Arm. Surface water enters ERF from uplands on the east, west and southern boundaries; uplands are composed of glacial deposits and are covered by spruce and birch forests.

As with other estuarine salt marshes in Cook Inlet (e.g., Hanson 1951, Vince and Snow 1984, Rosenberg 1986), vegetation grows in zones that are commonly determined by elevation and related to the landforms of ERF (Fig. 3). We believe this relationship to be a function of flooding frequency, salt tolerance, drainage capacity and sedi-

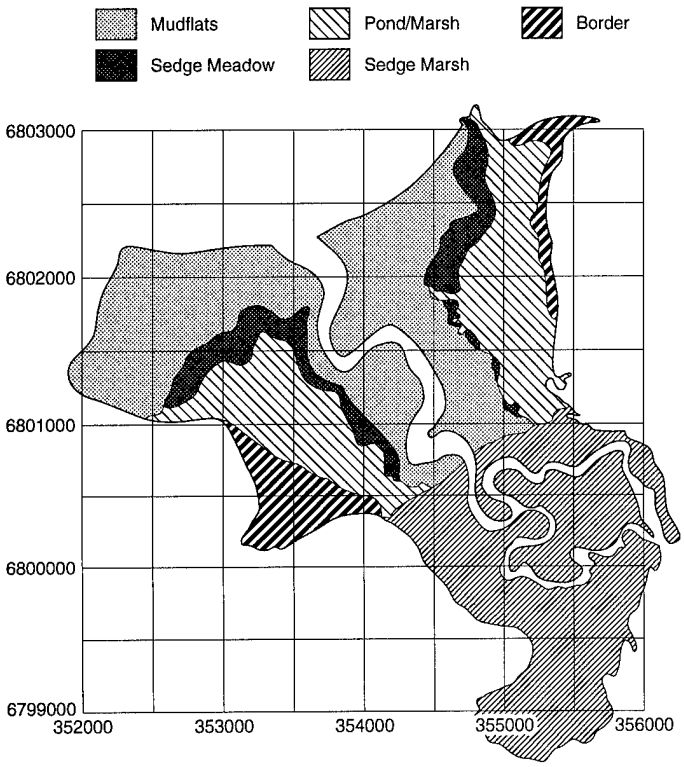

Figure 3. Distribution of primary landform–vegetation units (from Racine et al. 1993).

mentation rates. Levees, mudflats, marshes and shallow ponds (to 50 cm depth) approximately parallel the Eagle River and coastline (Racine et al. 1992a). Freshwater ponds or shrub bogs lie along the uplands on the northeast and southwest.

BACKGROUND AND PREVIOUS STUDIES

The fundamental sedimentary and hydrological processes of subarctic and arctic tidal flats and salt marshes are not well understood (e.g., Boon 1975, Frostick and McCave 1979, Carling 1981, Collins et al. 1987, Dionne 1988, Stoddart et al. 1989, Reed 1990, Andrew and Cooper 1993). The roles of glacial rivers and glacial-marine sediment discharges in tidal flat and salt marsh sedimentology have received only limited attention (Ovenshine et al. 1976a,b; McCann et al. 1981; Bartsch-Winkler and Ovenshine 1984). Neither the sediment flux nor sediment budget of tidal flats and salt marshes are sufficiently defined to link their hydrology and sedimentology (e.g., Frostick and McCave 1979, Kohsiek et al. 1981).

Short-term sediment accumulation is related to elevation, and thus to the frequency and depth of inundation and annual sediment supply, but eustatic rise in sea level may be more important to long-term rates (e.g., Krone 1987; Allen 1990a,b; French 1991, 1993; McLaren et al. 1993; French and Spencer 1993). The texture and composition of sediment deposited in tidal flats and salt marshes vary in space because of tidal channels and gullies as well as tidal currents (e.g., Carling 1982, Allen 1992).

The sediment balance, the accretion or erosion of sediment, in tidal flats and salt marshes has been estimated using short-term vertical sedimentation rates (e.g., Harrison and Bloom 1977, Richard 1978, Letzch and Frey 1980, Stoddart et al. 1989). Longer-term estimates have been made by dating subsurface horizons (e.g., Hubbard and Stebbings 1968, Allen and Rae 1988) and creating radionuclide profiles (e.g., Keene 1971, Bloom 1984, Kearney and Ward 1986). Both estimates, however, may be misleading owing to compaction after deposition in the former case and time-dependent accretion rates in the latter (French 1993).

The initial analyses of ERF sedimentation and erosion (Lawson and Brockett 1993, Lawson et al. 1995) indicate that the forces of erosion and deposition are actively changing the morphology of the drainage system, ponds and mudflats. Past migration of the Eagle River has apparently reworked a significant amount of sediment, as indicated by meander scars and channel cut-offs (Fig. 4b). Limited sampling during early studies has shown that WP-bearing sediments from gullies probably move into the Eagle River during tidal ebb, potentially increasing the accessibility of WP particles to migratory waterfowl, invertebrates, fish or other organisms. We also evaluated factors controlling these physical processes in the tidal flats, but the data are still insufficient to assess the short- and long-term response.

Processes of erosion, transport and deposition vary seasonally (Tables 1 to 6). Their importance may likewise vary across ERF in response to a number of internal factors (Table 7). The relationship of these factors to physical processes are under investigation; our understanding of the process relationships are presented in subsequent sections of this report.

External controls (Table 7) are more difficult to define because they are affected by a number of

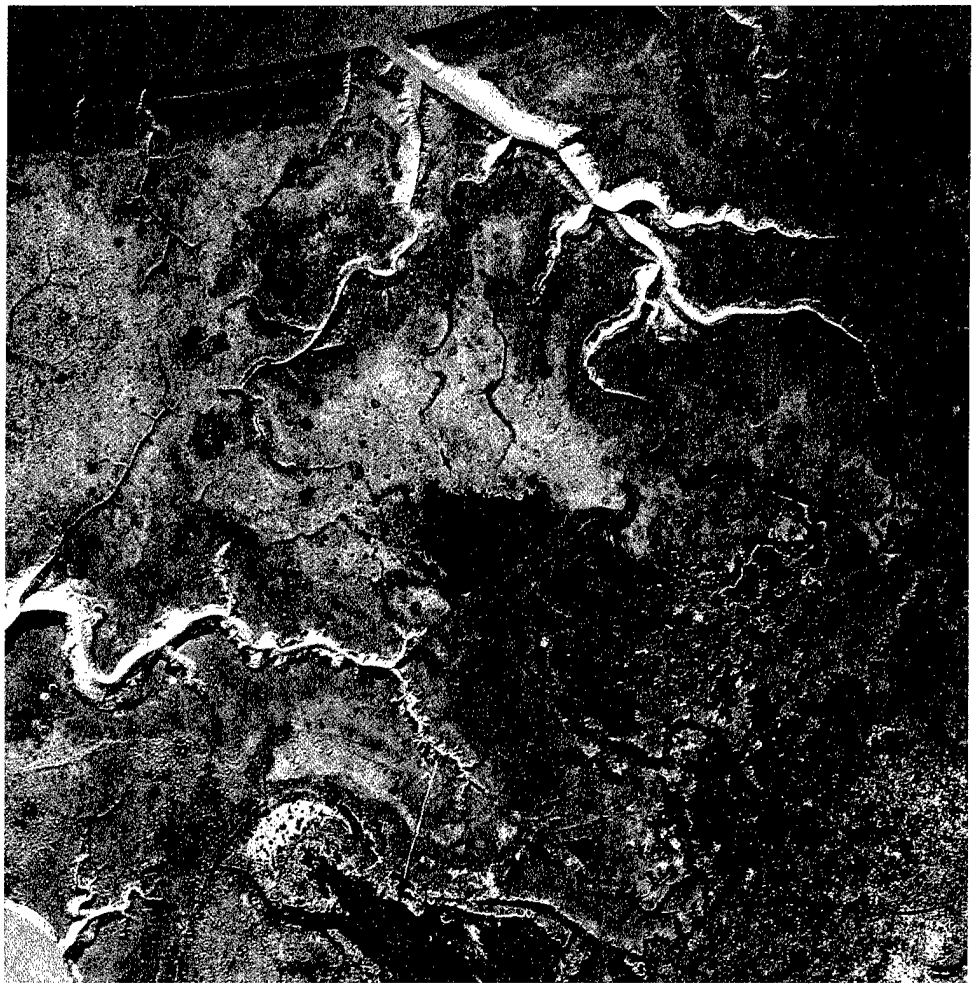

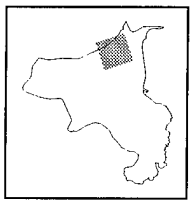

a. Typical active gully erosion following courses of relief drainageways.

Figure 4. 1994 aerial photographs of ERF (originally color infrared).

other factors, most of which lie beyond the scope of our analysis. In particular, tectonic, and especially earthquake, activity is virtually impossible to predict; however, its impact on the physical system of ERF may be enormous.

Eagle River Flats was last severely struck by the 1964 Alaskan Earthquake (magnitude 9.2 on the Richter Scale [Cohen et al. 1995]), with both sedimentary and tectonic subsidence affecting the site's elevation (Small and Wharton 1969) and thus its physical processes. A tectonic drop of about 0.6–0.7 m was recorded in the Anchorage region (Brown et al. 1977). Subsidence caused by sediment liquefication and solidification probably reduced the pond elevations by an amount similar to that found near the Portage area of Turnagain Arm (Ovenshine et al. 1976a). Since the earthquake, the region has been rising at about 1.5 cm/year, although the rate has been decreasing over time (Brown et al. 1977).

How the physical system responded to these changes in elevation is unknown; however, an increase in pond water depths may have resulted in an increase in sedimentation rates, in keeping with what happened in Turnagain Arm (Ovenshine et al. 1976a). In addition, after the elevation drop, the tidal flat hydrology would be out of equilibrium, bringing a response from the physical system. Disequilibrium would have been maintained by the uplift following the earthquake.

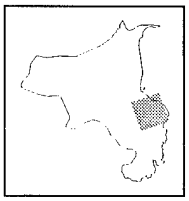

b. Meander scars along the side of the Eagle River.

Figure 4 (cont'd).

Table 1. Summer erosional processes.

Morphological unit	*Processes*	
Marshes	Currents (rare)	Wind waves (rare)
Ponds	Wind waves	Tidal currents
	Wind currents	Debris impacts (e.g., logs)
	Ducks and other bottom-feeding organisms	Bioturbation
Gullies	Currents	Ground water
	–tidal	–piping
	–runoff	–sapping
	Overland flow	Gravitational slope processes
	–sheet	–slump
	–rill	–block collapse
	Wind waves	–sediment gravity flow
Mudflats	Currents	Debris impacts (e.g., logs)
	–wind	Rain drop impact
	–tidal	Bioturbation
	Overland flow	
	–sheet	
	–rill	
Levees	Currents	Debris impacts
	–tidal	Wind waves
	–river	
Coast	Current scour	Debris impacts
	Wind waves	Overland flow

Table 2. Winter erosional processes.

Morphological unit	*Processes*
Marshes	Ice plucking
Ponds	Freeze-on and ice plucking
	Ice shove
	Ice scour
Gullies	Plunge pool undercutting
	Freeze–thaw cycling
	Ice segregation and thaw
	Ice directed current scour
Mudflats	Ice plucking
	Ice shove (floating–expansion)
	Ice scour
	Ice cover confined scour
	Freeze–thaw cycling
Levees	Ice scour
	Freeze–thaw cycling
	Ice shove
	Ice-directed current scour
Coast	Ice plucking
	Ice shove (floating–expansion)
	Ice scour
	Ice block confined scour
	Freeze–thaw cycling
	Current scour
	Wind waves

Table 3. Summer transport processes.

Currents (river)
Suspended load
Bedload
Saltation
Wind currents (pond–mudflats)
Suspended load
Bedload
Gravitational slope processes
Currents (tidal–gully)
Flood
Ebb
Ground water
Piping

Table 4. Winter transport processes.

Ice floes
Freeze-on
Freeze-in
Ice shove
Frazil ice
Anchor ice
Freeze-on
Freeze-in

Table 5. Summer depositional processes.

Morphological unit	*Processes*
Ponds	Suspension sedimentation
	–settling-out
	–vegetation trapping
Gullies	Suspension sedimentation
	–settling-out
	Bedload deposition
	Sediment gravity flows
	Slumping
Mudflats	Suspension sedimentation
	–settling-out
	–vegetation trapping
Marshes	Suspension sedimentation
	–vegetation trapping
Levees	Suspension sedimentation
	–settling-out
	–vegetation trapping

Table 6. Winter depositional processes.

Morphological unit	*Processes*
Ponds	Ice entrapment and in-situ melting
Mudflats	Ice freeze-on and in-situ melting
	Snow filtering and in-situ melting
	Ice growth entrapment and in-situ melting
	Ice cover confined suspension settling-out
Levees	Ice freeze-on and in-situ melting (sediment–organics)
	Snow filtering and in-situ melting
	Ice growth entrapment and in-situ melting
	Ice cover confined suspension settling-out
Gullies	Ice growth entrapment and in-situ melting
	Ice cover confined settling-out

Table 7. Controls on physical processes.

Internal
River
Tides
Glacial sediment–water sources
Substrate material properties
Vegetation
Sediment influx–efflux
Weather–climate
Human activity
Ground water conditions
External
Earthquakes
Tectonic activity
Eustatic sea level rise
Isostatic rebound
Subarctic climate
Glaciers
Surface and ground water systems

Other important external forces include the regional surface and ground water systems, subarctic climate, eustatic rise in sea level, and glaciers as sediment and water sources (Table 1). Each of these factors must be considered when interpreting the physical dynamics of the Flats.

Tidal and river water dynamics control the amount of material available for deposition in ERF and affect the locations and rates of erosion. The amount of sediment transported in flood waters is a primary factor determining the erosion and transport of sediments during ebb. This capacity changes seasonally, as sediment discharge is reduced in winter, while water temperature decreases and salinity increases, causing a net increase in water density. Higher density water can erode and transport more sediment during the winter, although the total volume transported is reduced.

Aerial photographs show that tidal gullies have significantly extended into the mudflats by headward erosion (Fig. 5). Short- or long-term treatments for WP contamination may be compromised if such large-scale physical changes occur shortly after their implementation. The aerial photos also show large-scale changes resulting from riverine processes, which include abandonment of a primary river channel in the southern part of the Flats in the last 40 years, channel migration of various amounts from near the Route Bravo bridge north to the river mouth at Knik Arm, and the apparent burial of marsh and gully terrain in the Racine Island area.

It is not known whether the seasonal and annual variability of sediment discharge in the glacial rivers is evident in the tidal waters of Knik Arm. The Eagle River, as do other glacial rivers, transports an insignificant amount of suspended

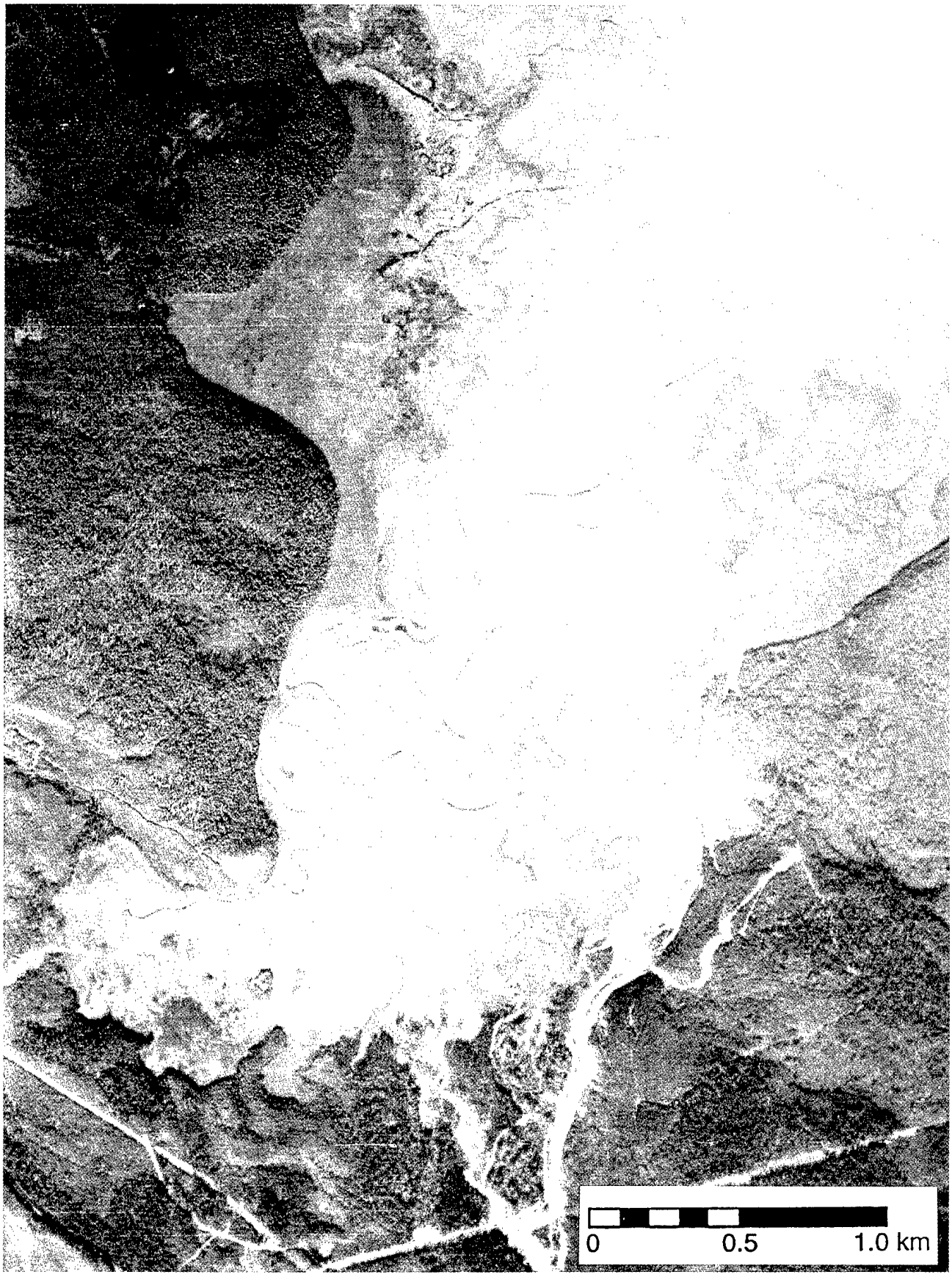

a. 1950.

Figure 5. Aerial photographs of ERF.

b. 1967.

Figure 5 (cont'd). Aerial photographs of ERF.

c. 1993.
Figure 5 (cont'd).

sediment during the fall through early spring, when glacial discharge is limited primarily to ground water sources (e.g., Lawson 1993). Samples from along the coast in Knik Arm in January, March and November of 1994 indicated that sediment remains in suspension through the winter, but in lesser quantities than during the summer. The continued presence of suspended sediment during winter is important, because it is the only source available for deposition in ERF during that time.

Expanding the above discussion, we note that aerial photographs from 1950, 1967 and 1993 reveal changes in the channel pattern entering ERF. Two main channels entered the Flats in 1950, but by 1967 the southern channel was abandoned and the northern channel diverged northwest of the Route Bravo bridge. The two primary channels entering the Flats today are partially braided and have a divergent pattern characteristic of an alluvial fan (Fig. 5c). Both characteristics indicate a significant decrease in channel gradient near the bridge, leading to a reduction in carrying capacity and the deposition of sediments in transport, as well as a fundamental change in the channel configuration (e.g., Leopold et al. 1964). In addition, the 1993 image shows a well-defined change in surface texture where these channels merge into a single meandering channel (Fig. 5c). This textural change probably bespeaks a change in physical characteristics such as elevation, gradient or the grain size and mineralogy of the substrate materials.

In addition, landforms in this part of ERF are mainly levees, vegetated marshes and abandoned channels and point bars, except in the center of the Racine Island area (Fig. 5c). Here, an abandoned gully within the center of an intertidal pond exists, while surrounding it, the deposits are relatively featureless and probably consist of overbank deposits from Eagle River flooding. In contrast, the northern two thirds of ERF have landforms more typical of tidal flats near river mouths elsewhere in this region (e.g., Ovenshine et al. 1976b).

Both the tributary channel and the meandering main channel deepen downstream, becoming incised by over 5 m. Near-vertical scarps and evidence of recent slumping characterize river banks that are actively eroding. Aerial photographic analyses reveal that, historically, banks have receded several tens of meters at some locations.

The relatively tight meander loops in the lower section of the river have significantly changed over the last 40 years. Meander scars and abandoned point bars are common along the length of the active channel and are especially evident in photographs of the southern reaches of the Flats (Fig. 5c). Channel changes are a natural progression resulting from the erosion and recession of the outer banks of meander bends, deposition of sediments as point bars in the inner parts of each bend, and a general downstream migration of the channel (e.g., Allen 1982). At some locations, a breaching of tight meander loops causes their abandonment.

Channel changes remobilize bank sediments, which may be transported either downstream or upstream, depending on the timing of collapse. In the idealized river model, they would move to the next point bar and be redeposited; however, redeposition will be controlled by the interaction among tidal and river processes, particle grain size, and water properties affecting density (e.g., temperature and salinity) and flocculation. Sediments may therefore be redeposited in the ponds and mudflats during flooding tides, or they may be transported towards the Knik Arm during the ebb cycle.

Gullies in the mudflats have also lengthened and deepened during the last 40 years, in some cases extending over 200 to 300 m. A significant extension of gullies toward the ponds and marshes is particularly evident in Figures 5b (1967) and 5c (1993). Headwalls recede during flood or ebb flow, as water is funneled into and out of the ponds and mudflats through the drainage system. The cause of gully expansion is not proven. But the tectonic activity during and following the 1964 Alaskan earthquake or large-scale river channel changes caused by flooding can cause the gully expansion. We must further quantitatively analyze historical aerial photographs and deposits in the alluvial landforms to find its cause.

Tributary channels with dendritic patterns, called vegetated drainageways, drain water from the mudflats and ponds into the gullies (Fig. 6). A second set of channels intercepted by the active tributary system unconformably crosses other landforms, including ponds (such as C and Bread Truck) where they lie below the pond water surface. Their pattern is irregular and unrelated to the active gully drainage system. We interpreted these secondary channels as relict drainages that reveal significant changes to the ERF drainage system in the past. The cause of such change is unknown, but may also be related to larger scale forces such as river avulsion, flood-induced channel migration, or earthquake-induced subsidence.

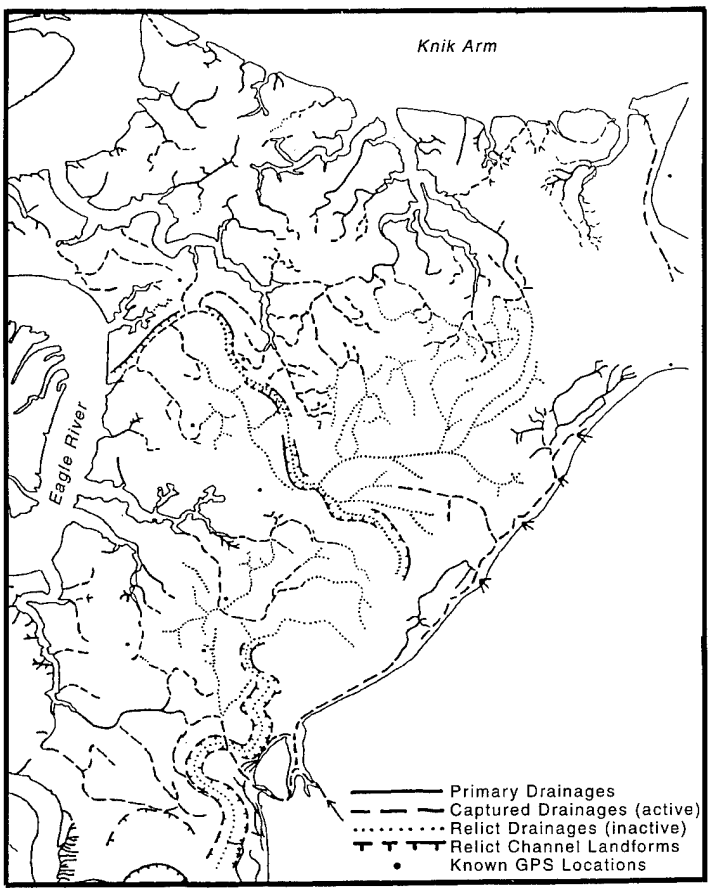

Figure 6. Drainage pattern analysis of 1993 aerial photograph of C and D areas.

STUDY OBJECTIVES

The objectives of this multi-year investigation are to:

1. Conduct quantitative analyses of ERF's physical system dynamics, particularly hydrological, sedimentological and hydraulic processes controlling erosion, transport, deposition and burial of WP-bearing sediments. We will develop a conceptual framework for the ERF physical ecosystem and the fate and transport of WP particles, including the potential for off-site migration.

2. Evaluate the short- and long-term response and sensitivity of the physical processes and terrain to modifications caused by proposed remedial technologies, particularly temporary or permanent pond drainage, dredging, capping, geotextiles or others as proposed.

3. Assess the effects of the physical system on the effectiveness and stability of proposed remedial measures for WP contamination and develop strategies for restoring areas of dredging, artificial drainage, or other proposed measures.

This report summarizes the current results of this study, synthesizing previous work of 1992 and 1993 with the 1994 investigations, and addresses elements of Objective 1.

STUDY SITES AND METHODS

Transects

We established our transects to include representative morphological units, with 11 transects set out in May 1992 (Lawson and Brockett 1993), 1 in June 1993, and 11 in 1994 (Fig. 7). We surveyed the transects using an electronic theodolite to determine ground surface elevations relative to local benchmarks and the UTM grid. Grab samples of surface sediment (to 5-cm depth) were taken at each survey point along the transects for analyzing the grain size distribution using standard sieving and hydrometer techniques. These data are necessary for us to delineate surfacial textural trends and to evaluate the relative importance of the tidal and riverine sediment sources to sedimentation and landform development.

Sedimentation and erosion

Sedimentation rates in ponds and marshes are difficult to measure accurately because only a slight disturbance of the water column will resuspend the fine-grained bottom sediments. If these sediments are caught in sediment traps, sedimentation will be over-sampled and the resulting rates high. We, therefore, used several methods to measure primary sedimentation rates and related surface erosion and secondary rates of resedimentation resulting from resuspension of pond bottom materials. Rates of sedimentation and surface erosion at mudflat, levee and tidal gully sites were measured using other techniques.

We used "sedimentation stakes" to measure erosion and deposition at transect points where the surface was wet or standing water was present (Fig. 8). These stakes consist of a rod and a square, rigid plate (about 7 cm^2) that slides freely on the rod as used by Ovenshine et al. (1976a,b) in Turnagain Arm, Alaska. Erosion depth is defined by the increase in distance between the top of the rod and the top of the plate, as measured periodi-

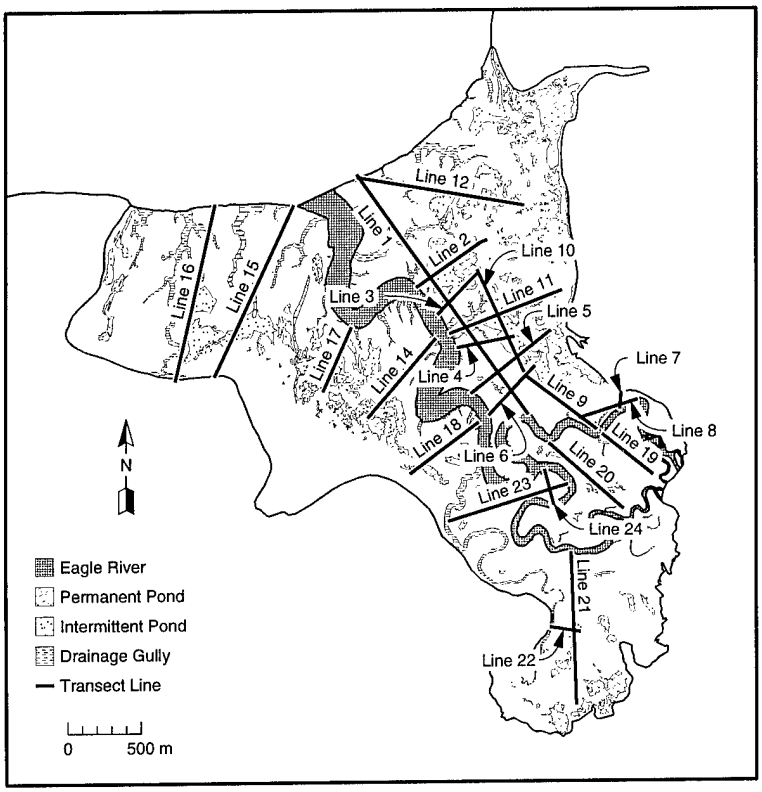

Figure 7. Transect locations.

cally to the nearest 0.5 mm. The amount of accretion is the thickness of sediment deposited on the plate surface. The difference between these two readings defines the net sedimentation (or erosion) rate. Monthly rates were measured in July, August and September 1992 following each monthly period of tidal flooding, while seasonal rates were measured in May and September of both 1993 and 1994.

The amount of accretion at transect survey points was also monitored by spraying an area (~30 × 30 cm) on the ground surface with pavement marking paint and locating the corners of this area with wire survey flags (see also Vince and Snow 1984). Net accumulated sediment is measured by cutting and removing a ~2- × 2-in. (~0.03- × 0.03-m) block of sediment with a putty knife (Fig. 9). The thickness of sediment above the paint layer is then measured to the nearest 0.5 mm. Paint was applied at certain sites in June 1992, August 1992, August 1993 and May–June 1994. In contrast to sedimentation stakes that are broken or removed during winter, the wire flags and the persistence of buried paint horizons allow us to acquire a continuous record of net sedimentation rates. Use of the method allows us to account for sediment compaction through time.

Sedimentation rates in ponds were also measured at 10 sites following tidal inundations in

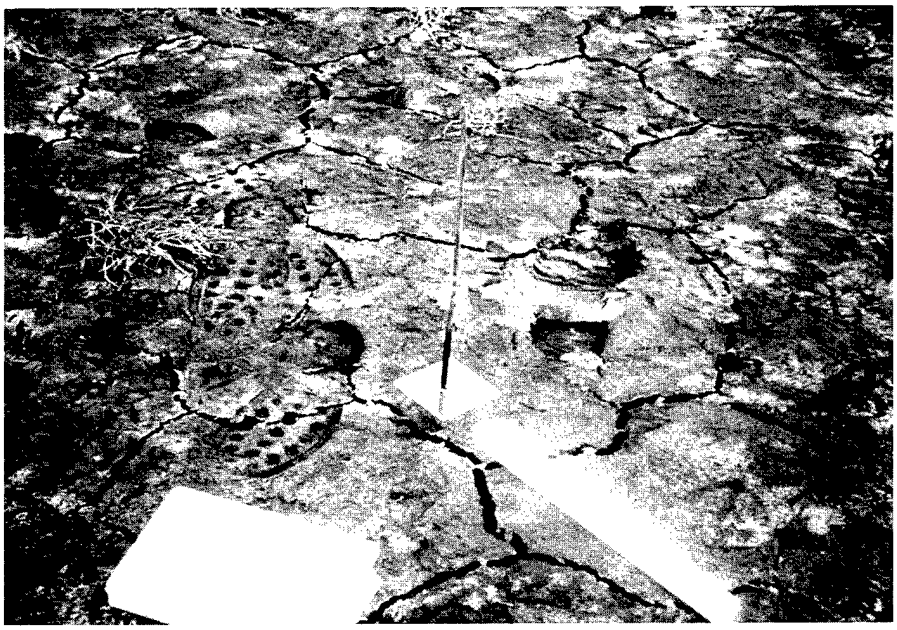

a. Sedimentation stake with plate that slides freely on the rod.

Figure 8. Sedimentation measurement techniques.

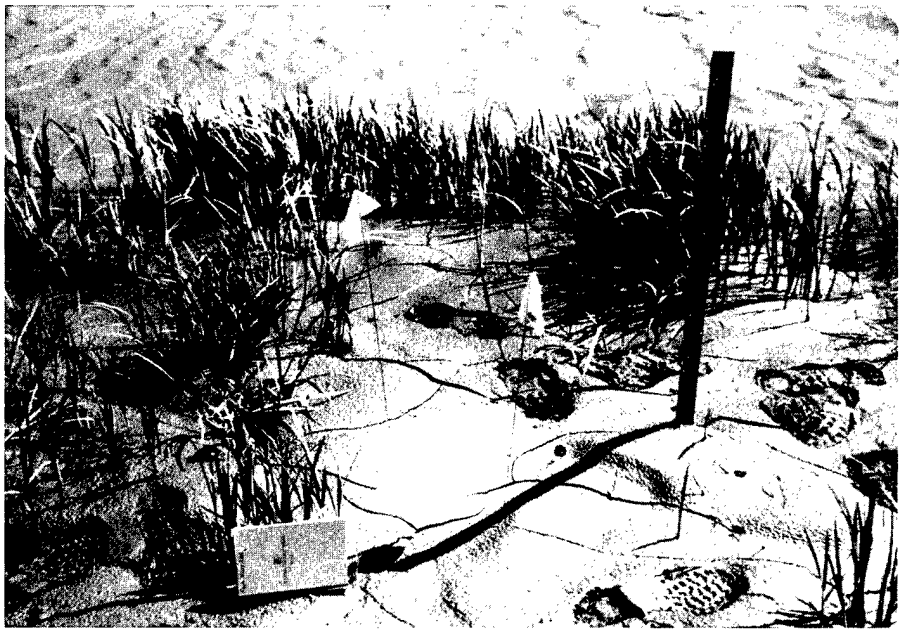

b. Wire flags mark an area of painted ground.

Figure 8 (cont'd).

Figure 9. Paint layer depth within block of sediment is measured to define sedimentation rates.

June, August and September 1992, May and September 1993 and May and September 1994 (Fig. 10). Samplers were installed in eight additional sites in 1994. Gross pond deposition was measured in a sediment trap consisting of a 4-in.-diam. (10.2-cm-diam.) schedule-40 PVC pipe end cap glued to a short length of 2-in.-diam. (5-cm-diam.) schedule-40 PVC pipe. The pipe was inserted into the pond until the bottom of the cup was in contact with the bed (Fig. 11b and 12). Sediment trapped in the cup includes new sediment brought into the ponds by tidal inundation and river currents, and materials resuspended by wind waves, dabbling ducks or other mechanisms.

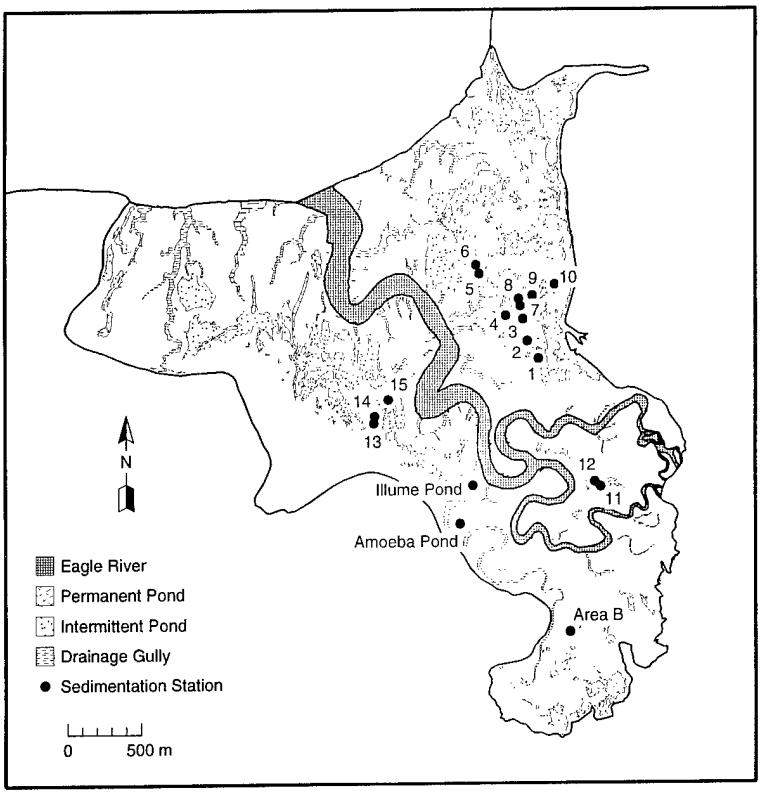

Figure 10. Pond sedimentation stations.

We measured the quantity of accumulated sediment to the nearest 0.5 mm by inserting a graduated scale into the sediments at three places. After measurement, the sediment in the cup is cleared or saved in plastic bags for WP analysis.

Net sedimentation rate in ponds is measured using a thin, rigid plastic plate of about 30 cm square that is pushed gently into the pond bottom until the plate surface is flush with the pond bottom surface. The corners of the plate are secured by aluminum tent pegs (Fig. 11 and 12). Sediment in suspension settles onto this plate, but this sediment can also be reworked and resuspended by wind or other mechanisms, thereby delineating a net rate. Plates become covered by sediment and aquatic vegetation in 1 to 2 weeks.

Initially, in 1992, a stake with a millimeter-graduated scale on its face was inserted into the pond bottom, and the height of the pond bottom and the water column were measured to provide a second tally of the net sedimentation rate (Fig. 11a). However, surface waves and glare commonly made this a difficult measurement to obtain. In addition, aquatic vegetation on the bed commonly covered the base of the scale. For these reasons, only water levels are measured on these scales.

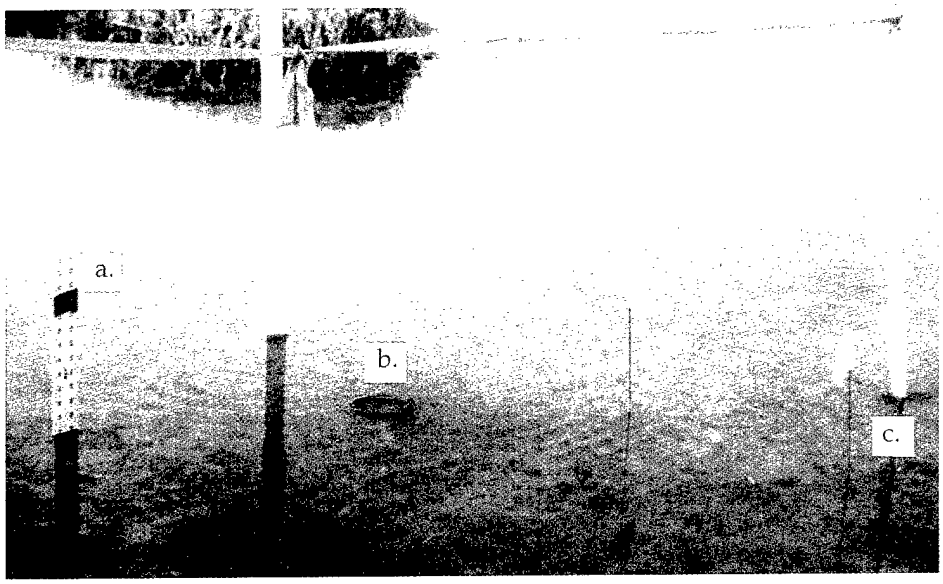

Figure 11. Sedimentation station in a pond site. A meter stake (a), cup sampler (b) and plate sampler (c) are shown in position. The plate sampler is located between the two survey flags.

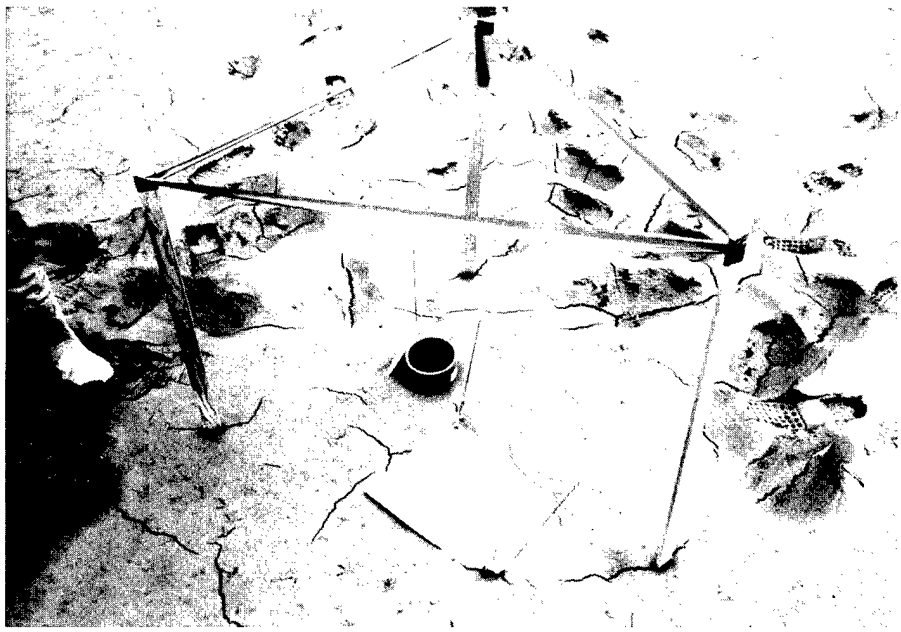

Figure 12. Example of sedimentation station at intermittent pond location showing layout of cup and plate sampler.

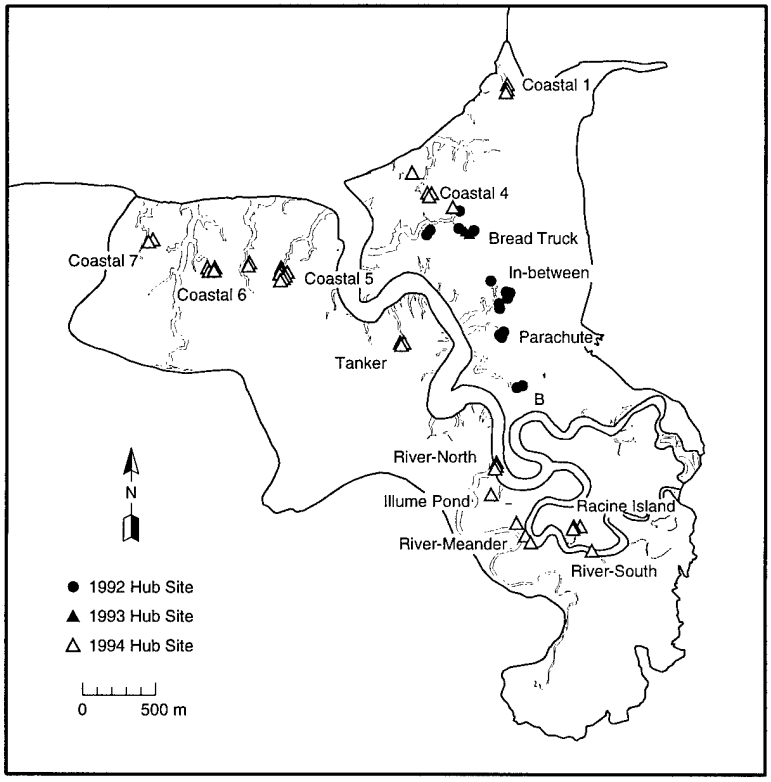

Figure 13. Gully headwall and lateral wall erosion sites.

Gully erosion and recession

Gullies draining the ponds and mudflats are actively extending inland by headwall and lateral wall erosion. We established 57 sites to evaluate retreat rates (Fig. 13)—11 sites were established in June 1992, 3 in June 1993, 3 in September 1993, 1 in May 1994 and 39 in July 1994. At each site, stakes were driven into the ground along a straight line at known distances from one another and from the crest of a gully scarp (Fig. 14). A "hub" stake was set at a known distance from this stake line. The distance between the hub and the crest

a. B-Gully

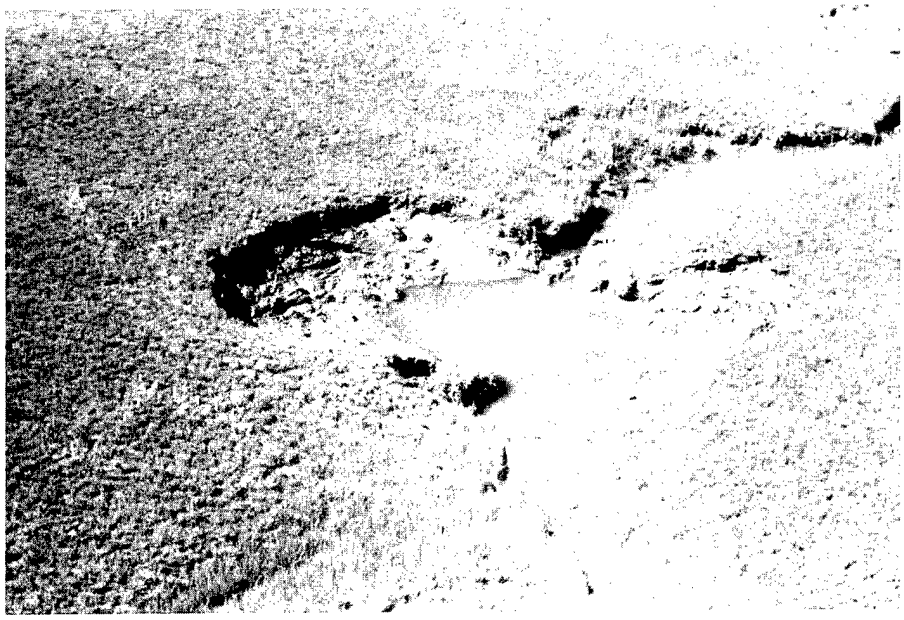

b. Aerial view of Coastal 6 Gully.

Figure 14. Examples of gully erosion sites. Line stakes are established along a line approximately parallel to the gully scarp. Hub stakes are located away from the line stakes and were used as the origin of measurements to scarp.

of the gully scarp was measured across the top of each line stake with a tape measure. We measured the position of the gully scarp by lowering a plumb bob by string from the tape measure, so that a horizontal distance could be read where the string and measuring tape met. We then placed flagged wire stakes at each point of measurement along the headwall. By repeating these measurements, we could monitor changes in scarp geometry with time while providing seasonal and annual data on gully recession and erosion rates.

Recession was measured in September 1992, June and September 1993, and May, September and November 1994. The September measurements delineate summer rates, while those of May or June delineate winter rates. The November 1994

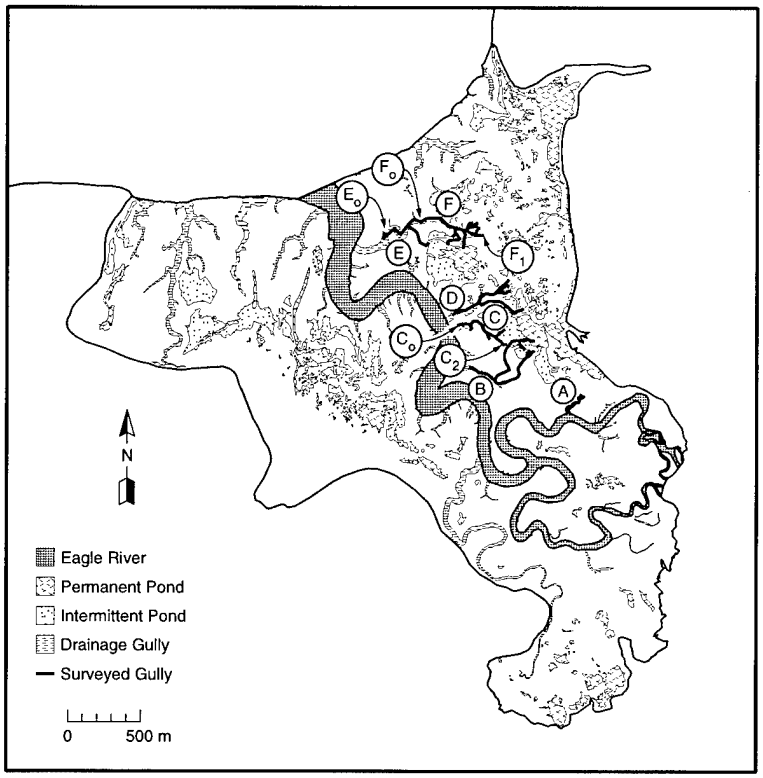

Figure 15. Location of surveyed longitudinal cross sections of gullies.

data will define the amount of erosion occurring between September and the initial period of freezeup. Repeat measurements at points without any retreat (as indicated by the continuing presence of wire flags) show that they are reproducible to ± 2–5 cm. The accuracy, however, is limited by how well the crest of the gully scarp can be defined; the gully scarp is highly irregular and, therefore, accuracy is probably limited to ±10 cm in the worst case.

Longitudinal cross-sections of nine gullies were surveyed in 1993, beginning at or near the Eagle River and continuing into the ponds (Fig. 15). Gradients were calculated from these data for characteristic reaches of each gully. Gradients were incorporated into empirical estimates of gully discharge at surveyed cross sections for maximum or bankfull ebb (Lawson et al. 1995). These data signify the relative stability of the drainage system, and therefore may provide information to allow us to assess both short- and long-term trends in gully erosion and pond stability.

Water quality parameters

Various types of data have been collected at several sites to help us assess the surface hydrology and water quality of ERF. A majority of sampling sites were in small plunge pools at the heads of tidal gullies throughout the Flats (Fig. 16). The Mortar and Spring gully sites are located along drainages that receive tidal waters directly from Knik Arm. The sites at Bread Truck, Parachute, B, Tanker and Otter gullies are located in drainages that flow to the Eagle River. The Otter Creek site represents drainage from the southwestern uplands as well as Area B mudflats. The two final sites represent the primary source waters: the Eagle River upstream of where it enters ERF, and the Knik Arm just north of the coast (Fig. 16).

At the nine gully locations (hydrostation sites) (Fig. 16), a basic suite of water characterization data was collected at 4-minute intervals. These data include temperature (measured by thermistor or a Hydrolab H_2O multiparameter sensor, or both); salinity, pH, redox and dissolved oxygen (Hydrolab); turbidity (OBS3 optical backscatter sensor); and water surface elevation (Druck pressure transducer) (Table 8). From August to September 1993, data were collected at three sites: Parachute Gully, Bread Truck Gully and Eagle River. These three sites were reestablished in May 1994, and other sites were added later as equipment became available throughout the 1994 season (Fig. 17). In addition, 500-mL water samples were collected for analyzing Total Suspended Sediments (TSS) during flood and ebb cycles at each hydrostation and in the nearshore zone of Knik Arm.

During the fall of 1994, two sensors were added to measure current velocity and water level. A Marsh–McBirney electromagnetic current probe was mounted about 1 m above the bed at the Bread Truck, Parachute and Spring gully sites (Fig. 16). Ultrasonic sensors by Campbell were installed at Otter and Spring gullies and the weather station adjacent to Knik Arm to monitor flooding duration and height above the mudflats.

Water characterization data were also collected using Seabird CTD (mdl 19) Profilers (Table 8) over shorter time periods at a variety of sites in gullies and the Knik Arm (Fig. 16). Also, a Seabird model SBE 26 wave and tide gauge was positioned north of Area D to record water depth and

Table 8. Specifications of sensors used in water quality parameter measurements.

Instrument type	*Sensor*	*Accuracy*	*Resolution*
Hydrolab	Temperature	± 0.15°C	0.01°C
(H2O Multiprobe)	pH	± 0.2 units	0.01 units
	Specific conductance		
	Fresh water	± 0.0015 to 0.1 mS/cm*	0.001 mS/cm
	Salt water	± 0.15 to 1.0 mS/cm*	0.01 mS/cm
	Salinity	± 0.2 ppt	0.1 ppt
	Dissolved oxygen	± 0.2 ppm	0.01 ppm
	Redox	± 20 mV	1 mV
	Depth	± 0.45 m water	0.1 m water
CRREL thermistor	Temperature	± 0.02°C	0.01°C
Druck (PDCR 950)	Pressure (water depth)	± 0.008 m water	0.001 m water
OBS-3	Turbidity	± 100 mV	1 mV
	5 V = 2000 FTU		
Marsh-McBirney	Water current (velocity)	± 6.10 cm/s	2.13 cm/s
(model 512)			
Cambell Ultrasonic	Distance (water depth)	± 1 cm	0.05 cm
(model UDG01)			
Seagauge wave/tide	Pressure (water depth)	± 0.003 m water	0.0015 m water
(model SBE 26-03)	Temperature	± 0.02°C	0.01°C
Seacat CTD	Pressure (water depth)	± 0.75 m water	0.045 m water
(model SBE 19-03)	Temperature	±0.01°C	0.001°C
	Conductivity	± 0.001 S/m	0.0001 S/m
	OBS [5 V = 2000 FTU]	± 100 mV	3 mV

* Depends on which of three auto-adjusting ranges is employed.

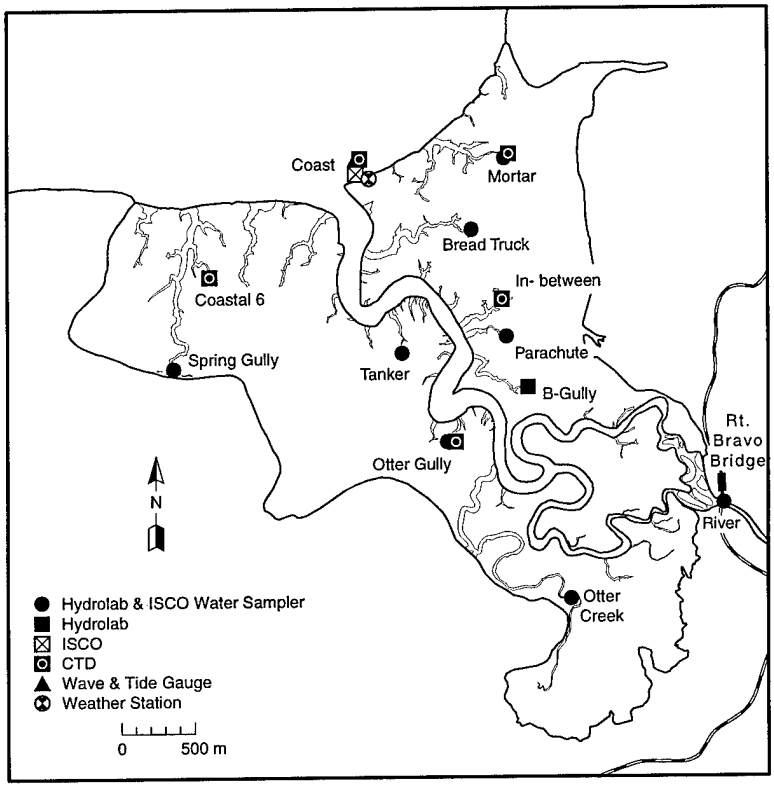

Figure 16. Locations of instrumentation recording water quality parameters and water depths.

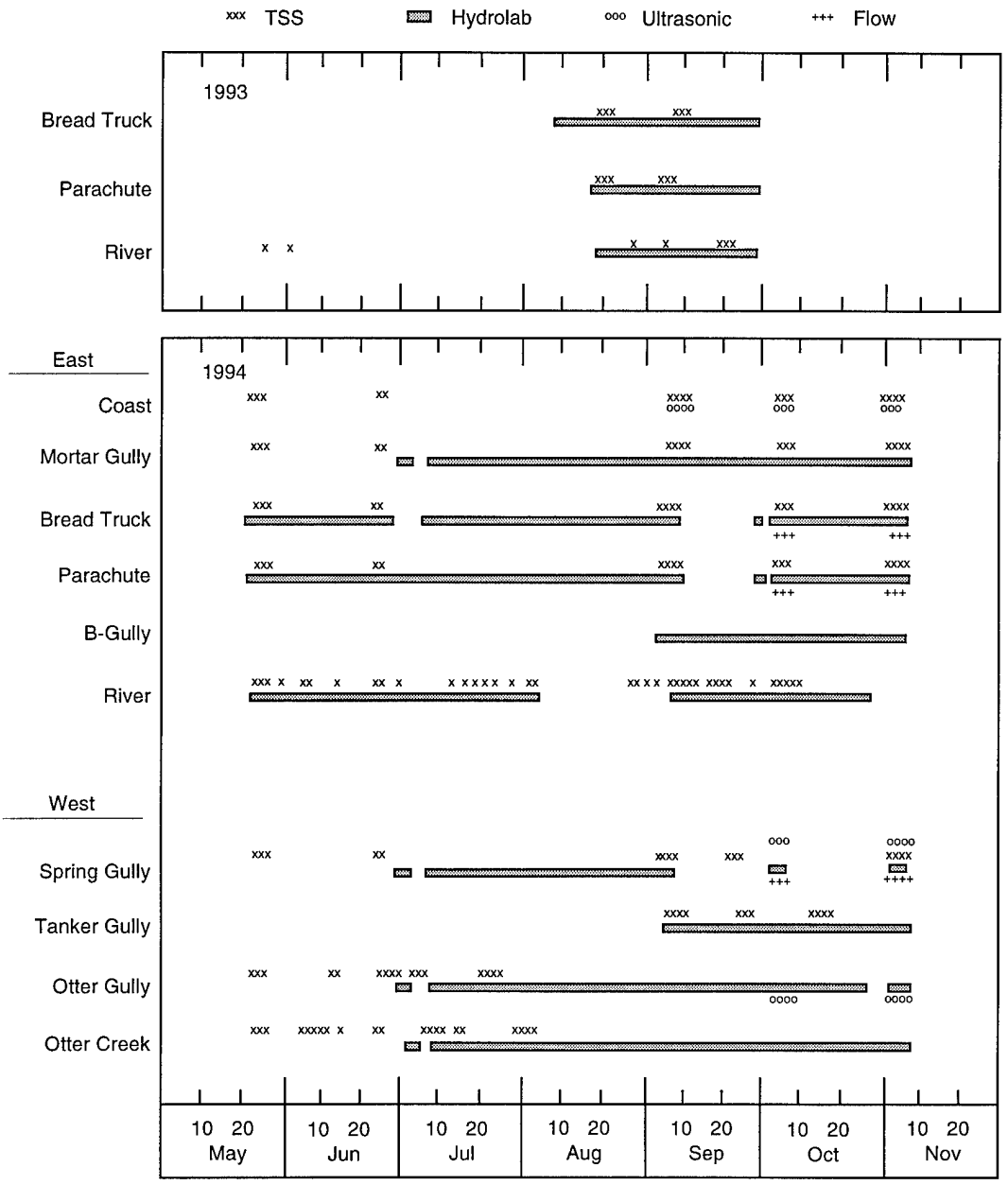

Figure 17. Active hydrostations during the 1994 season.

temperature of Knik Arm waters and to continuously record data from August through September 1993 and from May through November 1994.

At hydrostation sites, the sensors were mounted on a metal crossbar attached to a stake driven into the gully bed and positioned in plunge pools, where they would remain wet at all times, at an elevation of 15 to 45 cm above the bed. Flow probes were mounted about 1 m above the bed on separate stakes downstream of the plunge pool at Spring and Parachute gullies, and on a separate crossbar in a higher position at the Bread Truck Gully hydrostation (Fig. 16). Data were collected at 5-second intervals and averaged for a 4-minute output frequency. Wires from the sensors were bundled and strung to a Campbell CR10 datalogger, which was positioned on a floating platform next to the gully (Fig. 18).

Each platform was constructed of a 4-ft (1.2-m) square plywood deck with a wood frame made from 2- × 8-in. (~5- × 20-cm) studs. Large metal eyehooks were screwed into the frame on each corner. One and one-half meter sections of 0.75-in. (2-cm) -diameter steel pipe were mounted ver-

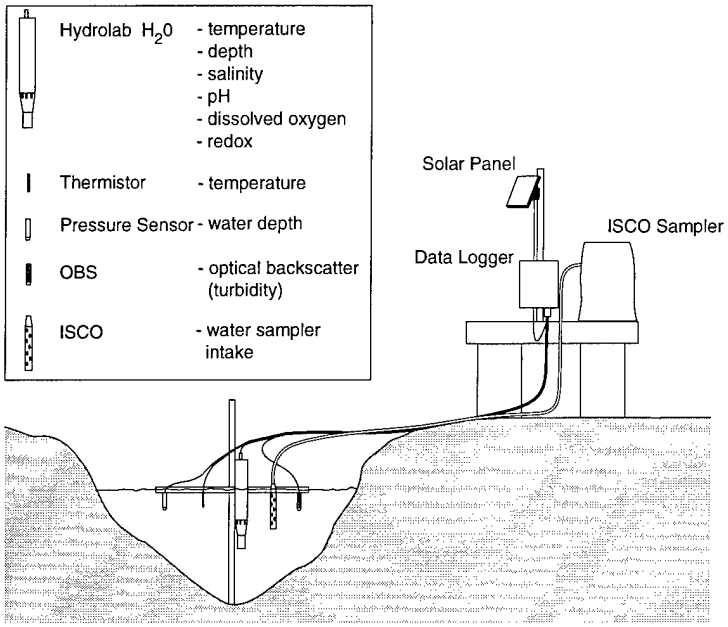

Figure 18. Schematic of hydrostation showing layout.

tically in 20-gal. (75-L) cans filled with concrete, and the eyehooks mounted on the platform's wood frame lowered over them. Foam filled the inner space of the deck framework and provided flotation so that the platform could move vertically up and down the steel pipes during tidal flood and ebb (Fig. 19). The platforms allowed us to establish monitoring stations without setting stakes or foundations in the ordnance-bearing mudflat sediments; however, the platform's main task is to keep the datalogger and related devices dry during the highest flood levels. Dataloggers were installed in NEMA plastic enclosure boxes mounted on 2-in. (~5-cm) vertical steel pipes. Solar panels of 18-W output were fastened to the pipes above the dataloggers to recharge the 12-V external battery. Ultrasonic sensors were also mounted on an arm attached to the support pipe and aimed downward towards the mudflat surface, which was covered by a metallic plate pinned to the ground.

An ISCO Model 3700 water sampler was also mounted on the platform at each site, except B-Gully (Fig. 18). A tygon tube extended from each sampler to an intake screen positioned on the same crossbar bearing the electronic sensors. The sampler was programmed to obtain 500-mL water samples at specific intervals through the flood and ebb cycles. These samples were processed for TSS concentration using vacuum techniques and 45-μm glass microfiber filters following procedure 2540D in *Standard Methods for the Examina-*

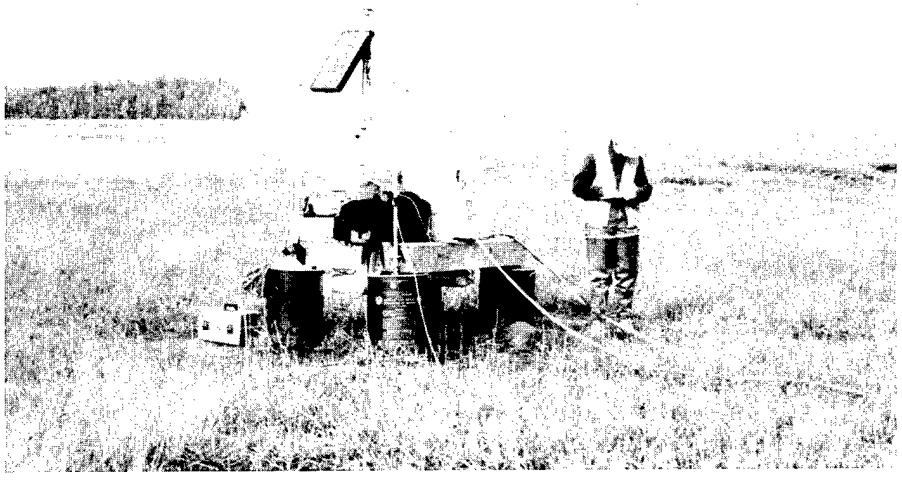

Figure 19. Platform and instrumentation measuring discharge characteristics at the Bread Truck Gully location.

Figure 20. Plankton net used for collection of WP in transport through gullies.

tion of Water and Wastewater (APHA, AWWA, WEF 1992). Our project modifications to this procedure are described in Appendix A.

WP transport sampling

A plankton net, 3 m long, with an opening of 1 m and a mesh size of 80 μm, was used to sample suspended and bed load sediments transported in the gullies during ebb. We then analyzed these samples by standard laboratory methods for the presence of WP particles.

The plankton net was tied to stakes driven into the gully bottom. It extended down-channel in the direction of ebb flow (Fig. 20). A cup at the apex of the net collected sediments that were trapped from water flowing down the gully. Nets were deployed in the Parachute Gully in May 1994, in the Bread Truck, Parachute and B gullies in September 1994, and again in the B-Gully in October 1994. These nets were set during multiple flooding tides to document whether or not WP was being transported out of the ponds and mudflats (see *White Phosphorus Erosion and Transport* section). In addition, grab samples were collected from recent deposits in various gullies across ERF on 4 June, 6–8 October and 6 November 1994. Samples of pond and mudflat sediments frozen-on to ice cover fragments were also collected in Areas C and D in November 1994.

Bathymetric profiling

Bathymetry of the Knik Arm near the Eagle River mouth was recorded for the first time this year to allow us to develop a baseline for assessing erosion and deposition and to help us identify potential areas for WP deposition. Bathymetry was measured using a Lowrance fathometer with a 50-kHz transducer–receiver. On 27 and 28 July, 20.1 km of fathometer transects were run in a 2-km-wide portion of Knik Arm just offshore of the Eagle River Flats (Fig. 21).

We made our profiles using a 14-ft (~4.3-m) inflatable skiff. The transducer was mounted on the transom with angle irons, screwed onto a wooden block made from a 2- × 4-in. (5- × 10-cm) stud that was tightened to the hull with C-clamps. The mounting bracket was wedged so that the bracket hung vertically off the stern, and the transducer–receiver was mounted on the bracket such that its surface was approximately parallel to the water surface.

We located and recorded our transects using a land-based Total Station. Seven benchmarks were established along the coast for setting up the surveying equipment to track the skiff. Personnel in the skiff pointed a prism and rod towards shore. Communication between shore and skiff was maintained to relay navigation commands using hand-held VHF radios.

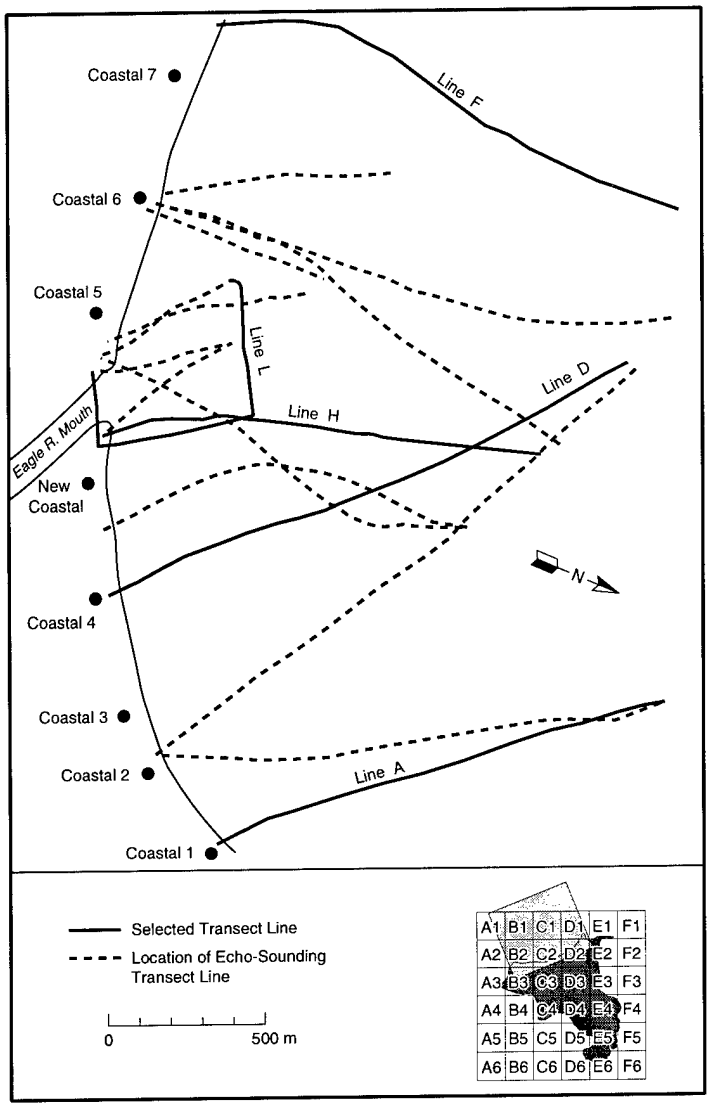

Figure 21. Location of selected bathymetric profiling transect lines.

Survey data have given us highly accurate bathymetric data. Water depth can be read to within 10 cm, while survey data provide us with the ability to compensate for variations in tidal height (±3 m) during bathymetric profiling. The timing of bathymetric profiling was centered around the predicted high tide in Anchorage, providing us with an appropriate 4-hour window of operation each day. This time was chosen to take advantage of maximum flooding so that transect lines would not be hindered by bars in Knik Arm and, more importantly, when tidal and fluvial currents are minimum around slack high tide. Elevation data collected during profiling allow us to subtract tidal effects from the raw bathymetric data and adjust the bathymetric records to mean Anchorage sea level. Bathymetry is therefore estimated to have accuracy that is better than a meter. All data are standardized to mean Anchorage sea level, as are all other surveyed data in ERF.

Length of data record

Table 9 summarizes the periods when various types of field data were acquired. The starting dates for acquisition reflect both the development of new methods for these investigations and expansion to analyze a larger proportion of the physical system across ERF. Gaps in the records of water quality sensors, other than during the winter period, resulted from either instrumentation failure or disruption by natural processes.

TIDAL HYDROLOGY AND INUNDATION

Erosional, transport and depositional processes are complexly related to Knik Arm tidal dynamics and Eagle River hydrology. Although sufficiently high tides can flood all of ERF, lower high tides may be supplemented by the river's discharge or wind-induced surges (or both) and flood more area to a greater depth than the predicted tide height indicates. An understanding of the tidal and river dynamics is critical to the evaluation of the physical system and WP attenuation. Several factors influence the timing, magnitude and duration of flooding, each of which must be evaluated since flooding drives many of the surface processes and modulates the moisture-dependent decomposition of WP particles (Walsh et al. 1995).

A typical flooding tidal cycle begins with a rise in the water level in the Eagle River and gullies. As the tide reaches its peak, the water floods over the banks of the gullies, letting it flow over a large area, causing a decrease in the rate of water level rise (Fig. 22). Once the peak is reached, there is a period of slack high tide when the water is dammed upon the Flats. During ebb, the water begins to drain nearest the coast and progresses inland. The channeling of ebb flow into tidal gullies, combined with the dammed fresh water, results in a longer runout time than flooding prior to complete inundation.

The damming of the river water during the flood tide causes the river to slow, pool, and even-

Table 9. Extent of data record for various measurement parameters.

a. Discrete samples.

	1992					1993								1994				
	M	*JN*	*JY*	*A*	*S*	*M*	*JN*	*JY*	*A*	*S*	*M*	*JN*	*JY*	*A*	*S*	*O*	*N*
White phosphorus																	
Sample type																	
Sediment grab	x		x x							xxx		xx			xx	xx	
Sediment trap			x							xx	x				xxx		
Plankton net											xx				xxxx	xxx	
Water									xxx	xx							
Bedload trap										xxx							
Ice																	x
TSS																	
Knik Arm										xx		xx					
Eagle River					x	x			x	x							
ISCO									xx	xxx		xx	xxx x xx	xxx	xx	xxxx x xx	xxx	xx
Ice																		xx
Grain size			x												xxxx			

b. Continuous data.

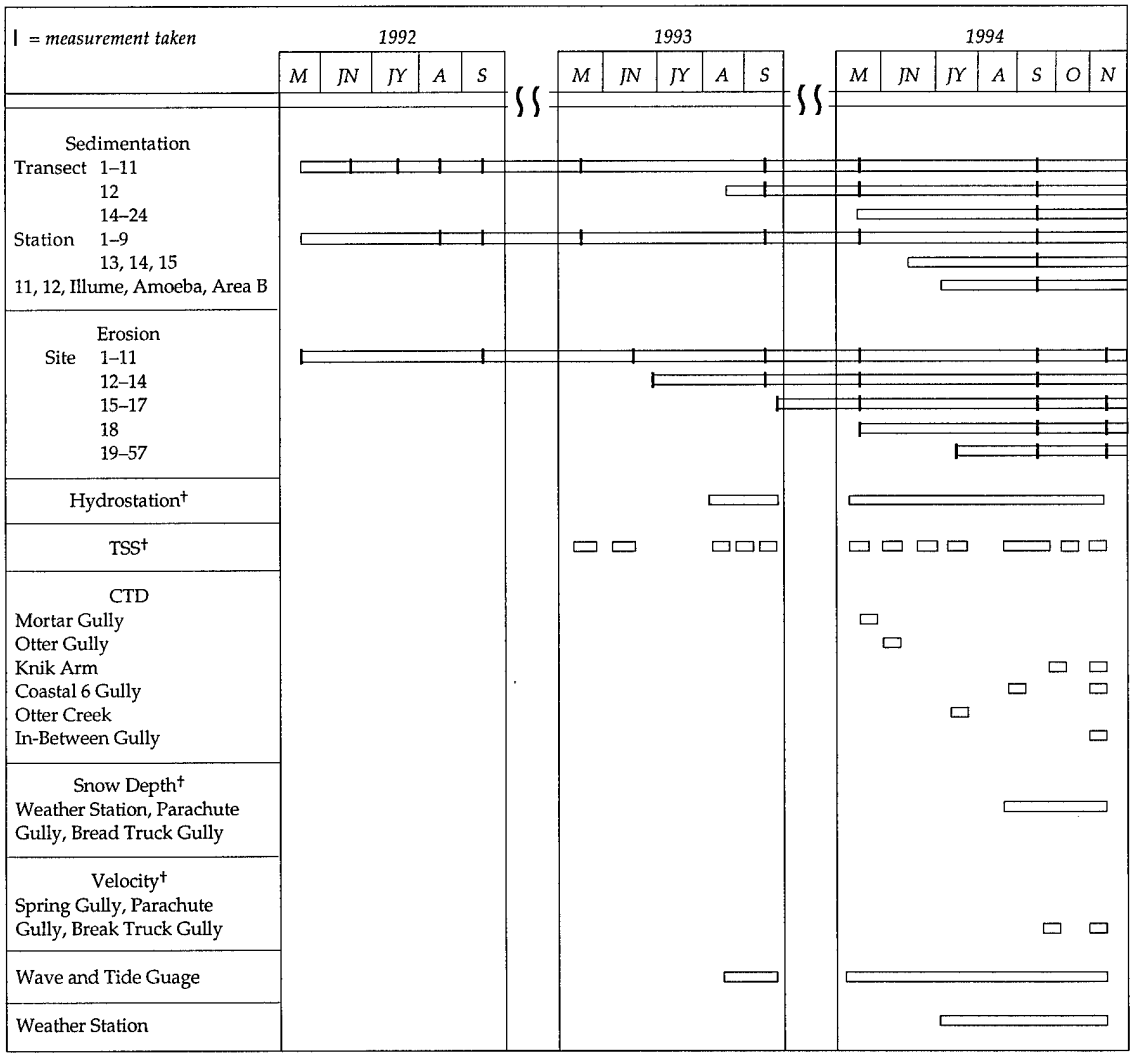

† see Figure 18

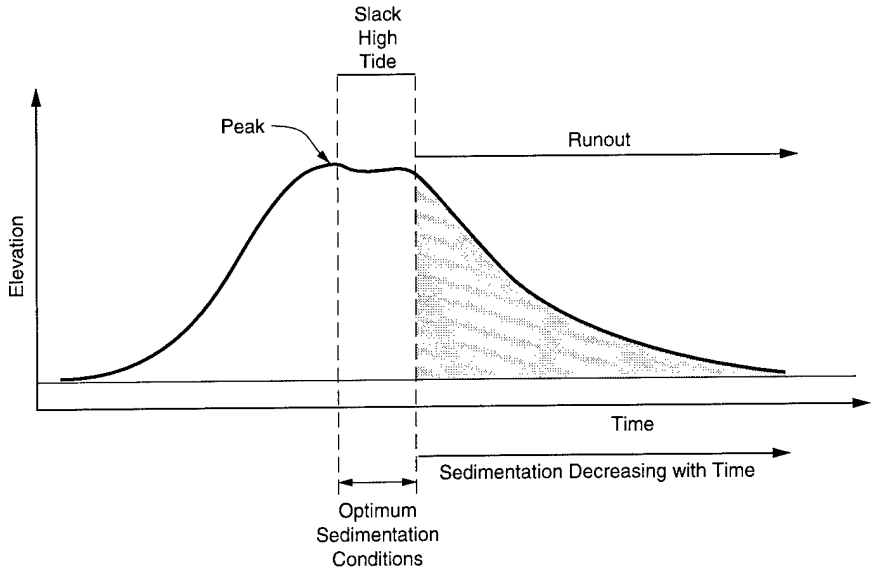

Figure 22. Typical high-tide curve showing period of sedimentation.

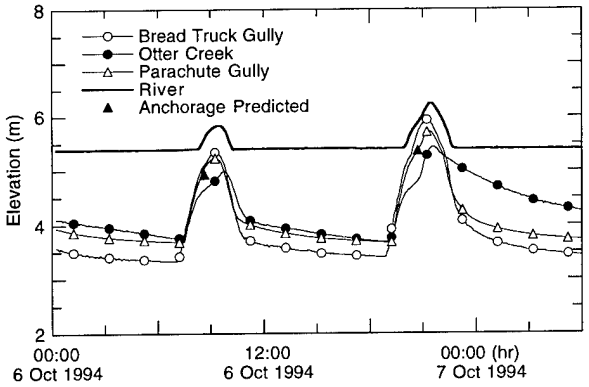

Figure 23. Water elevations as measured by pressure transducer for two flooding tide events.

tidal height for Anchorage by more than 0.9 m in some events (Fig. 23).

During periods of lower high tides, water depths matched well with the predicted Anchorage high tide values. Strong winds in Knik Arm and Cook Inlet can, however, cause either a higher or lower high tide elevation, depending on wind direction. As an example, let's observe two tidal events during the nights of 6–7 October that were predicted to be of the same height (Fig. 24). On 6 October, strong southerly (180°) winds blowing up Cook Inlet into Knik Arm amplified tide height on the Flats; however, in the latter case, northerly winds off the Flats produced a peak

tually reverse its flow direction in the upper Flats. This damming effect causes the water of the river to rise higher than the elevation of water in the gullies and reverses flow in the drainage system. We saw this happen in September and October 1994 during flooding events with a predicted high tide of at least 4.0 m. The damming effect may be accentuated during spring snowmelt or mid- to late-summer runoff peaks caused by a large volume of glacial melt in the Eagle River. Water depths measured at the hydrostations and the tidal gauge in Knik Arm show that during the September and October flood tides, the peak water elevation on the Flats exceeded the predicted

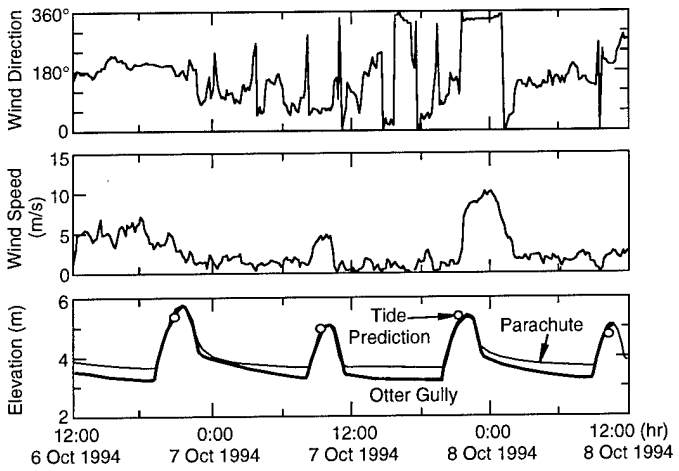

Figure 24. Wind characteristics and effects on tide heights at Parachute and Tanker gullies, 6–8 October 1994.

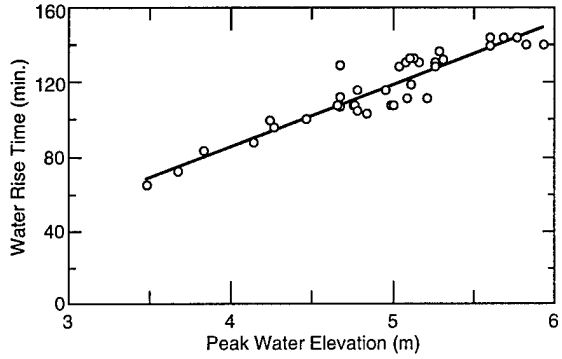

Figure 25. Relationship of water rise time to peak water elevation at Bread Truck Gully.

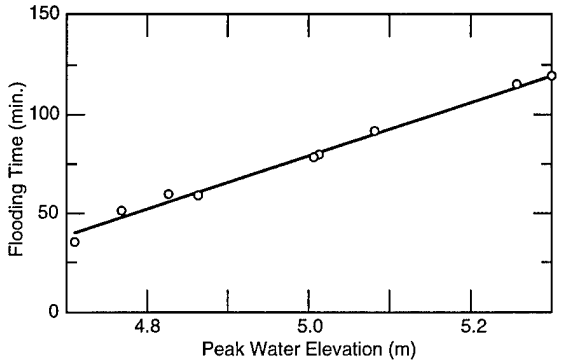

Figure 27. Peak water elevation vs. flooding time at Bread Truck Pond, September 1994.

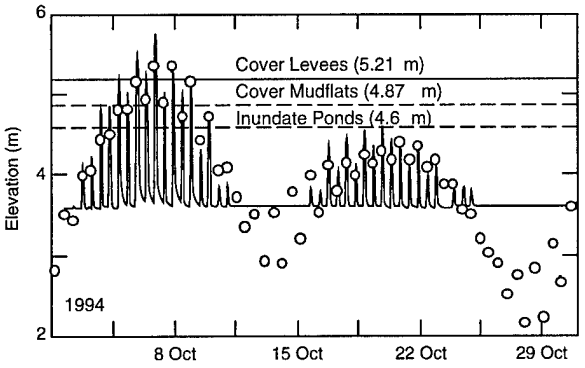

Figure 26. Water elevation record at Parachute Gully relative to elevations required to flood selected landforms. Open circles represent the time and elevation of predicted high tide at Anchorage.

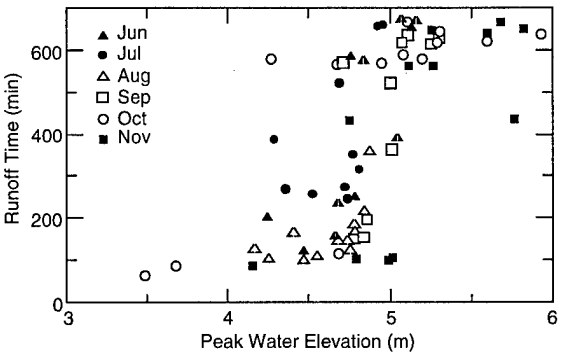

Figure 28. Peak water elevation vs. runoff time at Bread Truck Gully, June–November 1994.

height slightly below that predicted, reducing the inundation. Higher tides attributable to wind surge increase the height and volume of flood water and prolong the period of runoff during ebb.

The time between the start of water rise and peak high tide was calculated for each hydrostation site. We found a linear relationship between water rise time and peak elevation (Fig. 25). Then, average elevations for tidal flooding across the Flats were estimated from the surveyed transects (Fig. 7). These data reveal that ponds will begin to flood at a tidal height of 4.6 m, that mudflats are inundated at 4.9 m and that levees are covered at 5.2 m (Fig. 26). These elevations also yielded a linear relationship between the period of flooding (i.e., time when water elevation was greater than 4.6 m) and peak water elevation (Fig. 27). How often each landform is flooded in a given period can be estimated using these elevations. The length of time available for sedimentation during tidal inundation is directly related to the peak elevation and each landform's threshold for flooding.

During flooding, ponds have relatively high water levels, increasing the area available for sedimentation. Successive flooding tides move new material into the ponds and higher deposition rates can be maintained for extended periods. Pond drainage is restricted by the gullies' cross-sectional area, channel roughness and drainage density, which limit the volume of water that can escape from the pond. This produces a bottleneck where water in the pond remains dammed despite turbulent, fast flowing conditions in the gully heads. The response is a nonlinear relationship between pond elevation and runoff time (Fig. 28).

Pond sedimentation results mainly from settling-out of sediment suspended in the water column (Table 5); sediments are presumably deposited during and immediately following slack high tide (Fig. 22). Ponds commonly did not completely drain between consecutive tides during a high

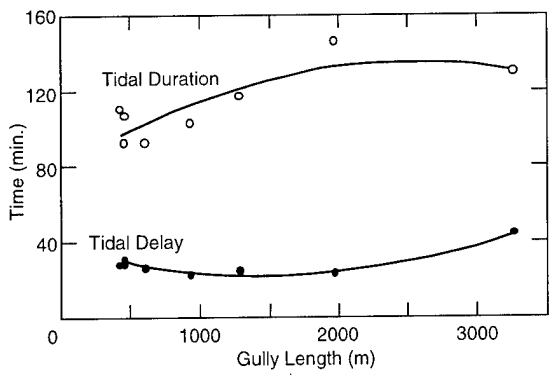

a. Gully length vs. tidal duration and delay. Regression line for tidal duration is expressed by $y = -8E\text{-}06x^2 + 0.0437x + 79.818$ ($R^2 = 0.6964$); *and for tidal delay,* $y = 7E\text{-}06x^2 - 0.0187x + 35.887$ ($R^2 = 0.9655$).

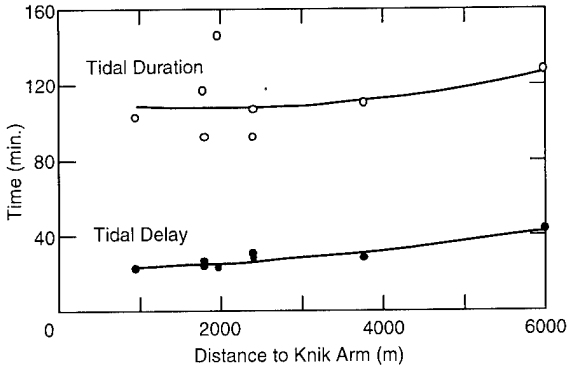

b. Distance to Knik Arm vs. tidal duration and delay. Regression line for tidal duration is expressed by $y = 1E\text{-}06x^2 - 0.004x + 112.72$ ($R^2 = 0.1283$); *and for tidal delay* $y = 5E\text{-}07x^2 + 0.0005x + 22.94$ ($R^2 = 0.8915$).

Figure 29. Relationships among the duration of tidal flooding and tidal delay with gully length and distance from gully headwall to Knik Arm.

flooding cycle, allowing even longer sedimentation times. This may be significant because ponded water has low turbulence and reduced particulate transport capacity. Increased runoff time may therefore allow for increased sedimentation. In addition, the mixing of flood waters with the pond and marsh waters increases the amount of sediment suspended in the ponds and marshes, and is the primary source of newly deposited materials.

The timing of flooding is a function of the elevation of the levees and mudflats surrounding the gullies, the distance of the gully headwall from the coast, and gully length. Water moving down the river can also alter the timing of flooding inland from the coast, depending upon its volume relative to the volume of tidal waters. Analyses indicate that tidal flooding is best described by a polynomial regression ($R^2 = 0.97$) for the relationship between gully length and tidal delay (Fig. 29a). A good correlation ($R^2 = 0.89$) also describes the relationship between tidal delay and gully headwall distance from the coast (Fig. 29b). A similar comparison using tidal duration indicates little relationship with either gully length or distance to Knik Arm.

The characteristic tidal response observed at our hydrostation sites is governed by gully characteristics (i.e., sinuosity, gradient, cross-sectional area, perimeter and channel roughness) that influence the tidal inundation rate in the gullies. Thinking intuitively, we feel that the distance to Knik Arm also must be an important factor, since the Arm is the primary source of water flowing into the gullies; however, secondary controls on water dynamics in the gullies modulate the individual site responses.

Water level measurements at the river and gully sites (Fig. 16) verified our observations that the flood cycle normally starts with a progressive rise in the river channel and adjacent gullies before the mudflats gradually flooded. Flooding begins first in the coastal mudflats on Knik Arm while water is moving progressively inland up the Eagle River channel. The delay in flooding at the hydrostation sites from that predicted for Anchorage is illustrated by data from June through November (Fig. 30).

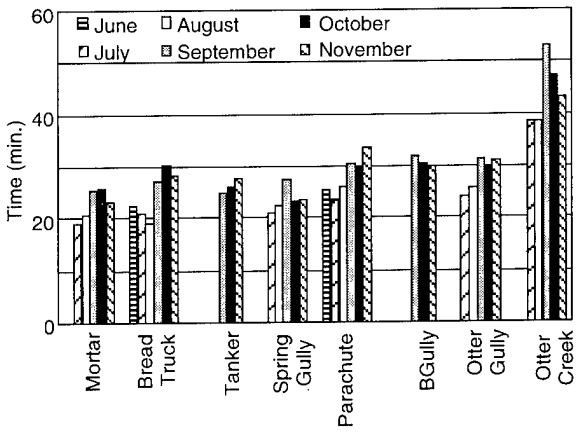

Figure 30. Delay in peak high tide from Anchorage to ERF sites, June through November.

Table 10. Pressure sensor elevations and peak high tide delay relative to predicted time at Anchorage gauge.

Site*	Sensor elevation (m)	Average delay time (min) Jun	Jul	Aug	Sep	Oct	Nov
Mortar Gully	2.79		19.1	20.9	25.4	25.8	23.0
Bread Truck Gully	2.76	22.3	21.0	18.9	27.1	29.9	28.2
Tanker Gully	3.08				24.9	26.2	27.8
Spring Gully	1.60		21.1	22.5	27.5	23.4	23.5
Parachute Gully	3.29	25.3	23.6	26.1	30.4	29.7	33.5
B-Gully	3.11				31.8	30.5	30.0
Otter Gully	2.87		4.0	25.9	31.3	30.1	31.0
Otter Creek	2.20		38.4	38.5	53.5	47.6	43.4

* Arranged by increasing distance from Knik Arm Coast.

Spring Gully and Mortar Gully are generally first to reach peak high tide because they are close to the coast and independent of river influence (Table 10). Otter Creek has the greatest lag time owing to incomplete drainage of the creek between flooding tides and distance from the coast. During periods of flooding tides from August to November, the tide was still rising at Otter Creek while the rest of the stations recorded ebb. This order of peak high tides between sites varies slightly from month to month, indicating that additional factors affect the rate of tidal inundation.

WATER QUALITY PARAMETERS AND TIDAL FLATS HYDROLOGY

Knowing water quality parameters during tidal flood and ebb is critical to understanding the interplay of tidal flood waters and river discharge and its influence on sedimentation in the Flats. The hydrostation data plotted in Figure 31 bespeak the parameters controlling sedimentation across the Flats. These data can be used to determine critical hydrological elements, such as duration of inundation (depth), river vs. tidal water domination (salinity and temperature), and sediment transport (OBS). For example, Figure 31a presents water quality data for about 1 month (18 August to 14 September) where an earlier sequence of high tides was only high enough to fill the gullies, and a later sequence flooded onto the mudflats. The record shows a daily sinusoidal water temperature pattern when tides are low (29 August–1 September). Perturbations to this regular temperature pattern and fluctuations in the salinity and OBS signify tidal flooding and mixing of different water masses, as will be discussed later in more detail.

Data from a single flood and ebb cycle show the basic relationships of water quality parameters and inundation (Fig. 32). Initially, as the water level in the gully rises during flood, parameters remain at values characteristic of the incom-

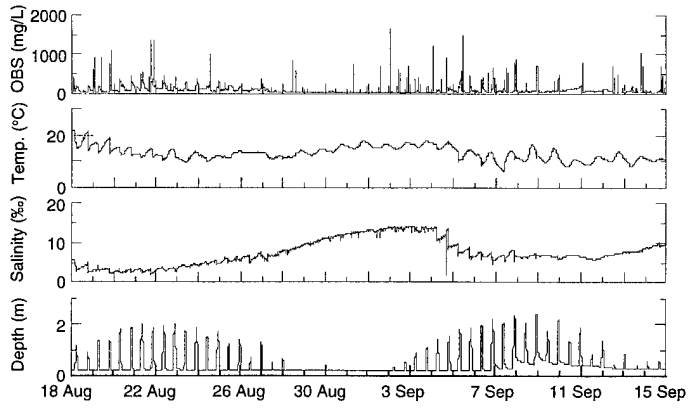

a. 18 August–14 September 1994.

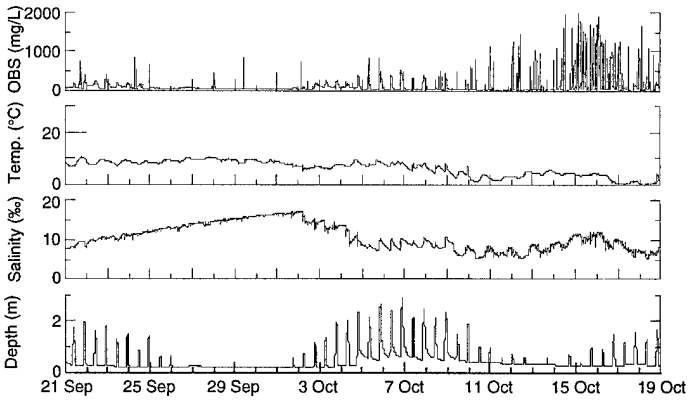

b. 21 September–18 October 1994.

Figure 31. Hydrostation record at Mortar Gully.

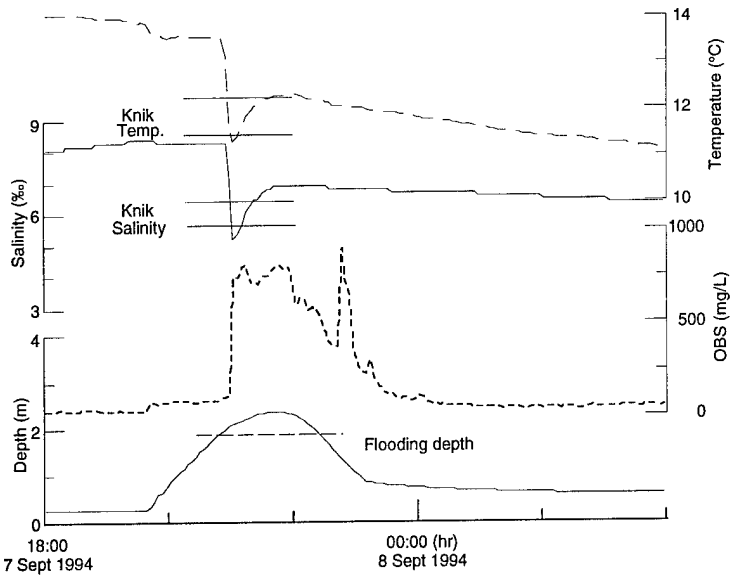

a. Mortar Gully

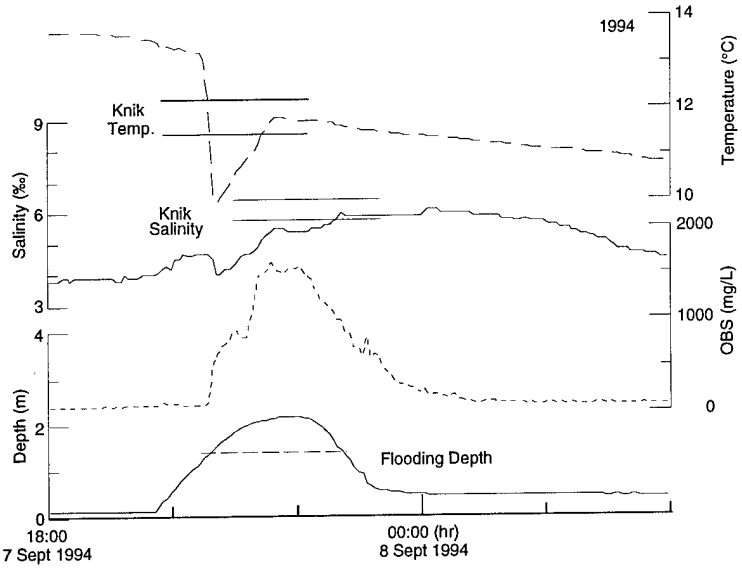

b. B-Gully

Figure 32. Variation in water quality parameters at two gully locations during 7–8 September flooding cycle.

ing water. When the water crests over the gully headwall (flooding depth mark), temperature and salinity change rapidly to values characteristic of the arriving flood water—either tidal, riverine or a mixture. During ebb, the parameters gradually change to levels that are, first, a mixture of flood waters, to one with more local water characteristics. Knik Arm waters are generally the dominant incoming water mass in the Mortar (Fig. 32a), Spring, Bread Truck and Tanker gullies. A more complex mixture of both riverine and Knik Arm waters occurs in the Parachute, B (Fig. 32b) and Otter gullies. Otter Creek often receives backed-up water from the Eagle River, but during the highest tidal events, Knik Arm waters penetrate even to this most southern part of the Flats, as will be discussed later.

Source waters

The characteristic signature of Knik Arm water varies through the season as air temperature and discharge from glacial meltwater in the Eagle River and in the rivers draining Knik Arm change (Table 11). Knik Arm water temperature reflects the seasonal rise and fall in air temperature. During May and October flooding events, temperatures were in a similar range (8–9°C), higher in September (11–12°C), and lower in November (about 1°C). Salinity was highest in May (15–16 ppt) prior to the start of the glacial meltwater season, lowest in September when glacial discharge had a large influence (5–6 ppt), and increased gradually during October (8–10 ppt) and November (11–13 ppt) as the discharges from rivers decreased.

The Eagle River is the primary incoming freshwater surface source for the Flats, with both glacial and seasonal changes (Table 12, see Fig. 36). While salinity, i.e., specific conductance, remains at near-zero (0.1 ppt) throughout the season, changing specific conductance levels document the relative influences of glacial sources. Higher conductance levels occur during early and late season when the ground water and local runoff components are greater than the glacial input, and solute concentrations in the glacial outflow are not diluted by meltwater (Sharp et al. 1995). Daily undulations in the specific conductance and temperature curves in midsummer mark the diurnal meltwater discharge variations from the Eagle Glacier.

Coastal sites

The two coastal sites where flood and ebb are controlled by Knik Arm must be treated separately, since the Mortar Gully drains ponds in Area D, and Spring Gully is fed by an upland spring and the northwestern-most section of Area A.

Table 11. Characteristic temperature and salinity of Knik Arm and Eagle River source waters during flood and ebb portions of selected flooding events.

	Knik Arm				Eagle River			
	Temperature (°C)		Salinity (ppt)		Temperature (°C)		Salinity (ppt)	
Date	Flood	Ebb	Flood	Ebb	Flood	Ebb	Flood	Ebb
May								
25	8.2–7.5	7.5–7.8	—	—	6.2–6.5	6.5–8.0	0.1	0.1
26	8.7–8.0	8.0–8.3	15.5–16.3		7.1–7.2	7.2–8.5	0.1	0.1
September								
7–8	11.4–12.4	12.4–12.2	5.8–6.2		5.5–7	5.7–6.2	—	—
8–9	11.5–12.5	12.5–12.2	5.9–6.5		7.3–7.0	7.0–6.8	0.1	0.1
October								
5–6	8.2–8.9	8.9–8.8			6.3–6.1	6.1–6.2	0.1	0.1
6–7	8.3–8.8	8.8–8.7	8.2–10.0	10.0–9.9	6.2–5.8	5.8–5.5	0.1	0.1
7–8	8.0–8.6	8.6–8.4			5.0–4.5	4.5–4.0	0.1	0.1
November								
3–4	0.8–1.6	1.6–1.5	11.2–12.7	12.7–12.6	—	—	—	—
4–5	0.7–1.7	1.7–1.3	11.4–13.0	13.0–12.8	—	—	—	—
5–6	0.4–1.3	1.3–1.0	11.6–13.0	13.0–12.9	—	—	—	—

Table 12. Gross sedimentation rates. Measurements for seasons through winter 1993–1994 are from transect lines 1–12 only, Summer 1994 measurements from lines 1–24.

	Range (mm)				
Morphological unit	Sum 92	Win 92–93	Sum 93	Win 93–94	Sum 94
Levee	1–6	1–12	0–6	0–11	0–15
Vegetated mudflat	1–6	1–16	1–14	1–21	1–30
Unvegetated mudflat	1–13	7–12	1–8	6–10	1–17
Pond – plate	1–4	8–28	6–26	2–17	1–21
Pond – cup	2–9	8–26	6–19	1–13	2–20
Marsh	ND	ND	ND	ND	1–20
Gully	1–77	20–33*	0–19	0–16	1–19

* Based on small sample size.

The Mortar Gully record (Fig. 31) displays the expected pattern of decreasing temperatures from mid-August to mid-October as air temperatures drop. This decrease in temperature, coupled with increases in salinity, causes the water to become denser, thereby increasing its capacity to transport sediment. Salinity changes at Mortar Gully are cyclic, opposite to the tidal flooding sequence, becoming more saline between flooding periods. This saline condition is likely caused by the discontinued exchange of water between Knik Arm and the ponds, allowing the salinity to increase in the ponds and the plunge pools at the gully heads through evaporation and stagnation. During flooding, the salinity drops to the relatively low levels of Knik Arm water.

Spring Gully, with significant freshwater input, maintains salinity levels near zero ppt when tides are low, but has increasing salinity semi-diurnally, marking periods of tidal inundations (Fig. 33). During fall flooding (6–8 September, 5–8 October), the salinity increase is longer as the higher flooding levels cause Knik Arm water to remain impounded in the northernmost section of Area A when freshwater spring discharge is apparently lower.

Central sites

Hydrostation sites in the central area of the Flats monitor gullies that hydrologically link ponds to the Eagle River. Observed patterns are cyclic and generally consistent from mid-summer to fall. Temperature decreases steadily through the period, while salinity levels during floods increase in response to the decreasing glacial meltwater input. Increased salinity between flooding events in Parachute and Tanker gullies means that their waters become stagnant and evaporate.

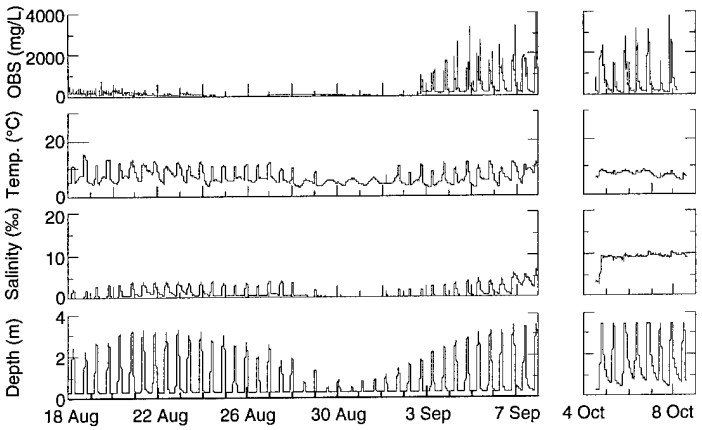

Figure 33. Hydrostation record at Spring Gully.

Salinity remains more uniform at the remaining sites—Bread Truck, B and Otter gullies—and this uniformity reflects the continuous flow of water out of the respective pond sources, each of which has ground water influx from springs. In general, the peak turbidity levels, which are consistent with those of Knik Arm, increased during flooding events through the season (e.g., Fig. 34).

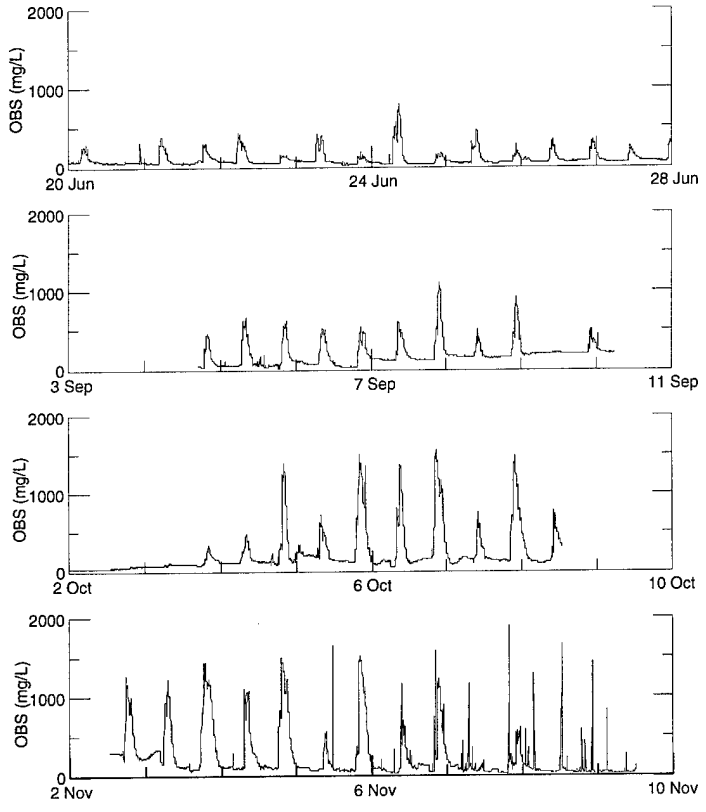

Figure 34. OBS levels at Parachute Gully during flooding periods in June, September, October and November 1994.

Otter Creek

Hydrostation data from the Otter Creek site appear to confirm our 1993 hypothesis that the dominant source water for this area is both Eagle River and the upland springs that feed Otter Creek, which enters ERF from the west. Salinity remained very low throughout the summer, indicative of the freshwater discharge from the uplands southwest of Area B (Fig. 35). During tides without floods, water temperatures drop semi-diurnally to levels similar to those recorded in Eagle River (Table 11). This behavior shows that when high tide levels are low, Knik Arm waters lack momentum and time to penetrate deep into the ERF river drainage system (i.e., Area B); however, backpressure from inflowing tidal water appears to dam the Eagle River and divert it into Otter Creek and the southwestern reaches of the Flats (Fig 35a). During the extremely high tides of late fall, Knik Arm waters did have enough energy and elevation to penetrate deep into this area, as indicated by the salinity increases in Otter Creek at that time (Fig. 24). The salinity increase at Otter Creek during the November floods is longer and more pronounced (Fig. 35c). The snow cover on the Flats at that time retarded the runoff during ebb because of its capacity to store flood water. Its slow release probably was the primary cause of the longer period of high salinity. Drainage through the porous snow is much slower than normal ebb runoff without snow.

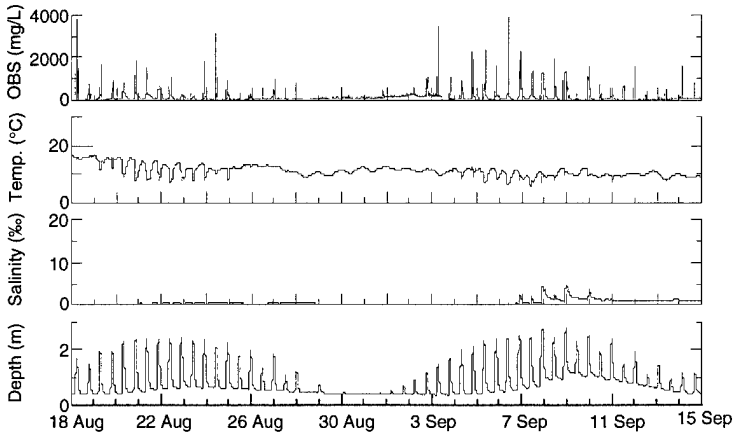

a. 18 August–14 September 1994.

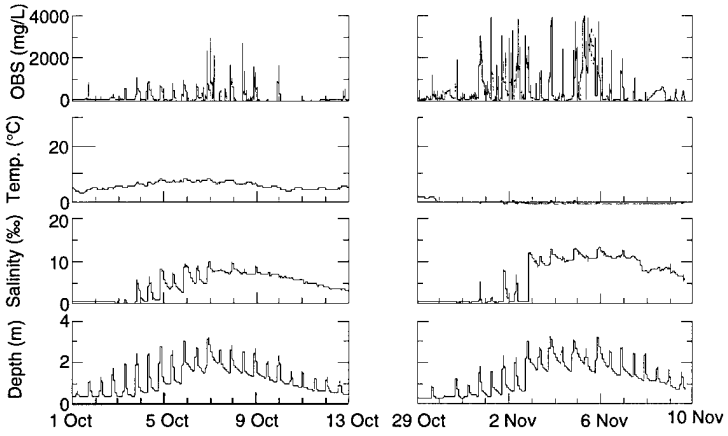

b. 1–13 October 1994. *c. 29 October–9 November 1994.*

Figure 35. Hydrostation record at Otter Creek.

SEDIMENT TRANSPORT AND SEDIMENT SOURCES

Sediments are deposited in ponds and mudflats mainly through suspension settling from pond and flood waters (Table 5). Sediment is derived from two external sources: the Eagle River and Knik Arm. Internally, the erosion of riverbanks, gullies, pond bottoms and mudflats by wind and water currents, ice, bottom feeding waterfowl, and other mechanisms provides remobilized materials.

Concentrations of suspended sediment vary seasonally, through monthly tidal inundation periods as well as through single tidal cycles (from flood to ebb) (Fig. 36). These concentrations appear to vary with distance from the river and coastal sediment sources (Fig. 36 and 37). Total suspended sediment (TSS) measurements also vary among sites through a single tidal cycle, depending upon local runoff variations, pond storage and how effectively the gully moves water out of the local area (Fig. 37).

A typical pattern in TSS response through a flooding cycle is a sharp increase owing to highly turbid flood water and resuspended gully bed sediment (Fig. 38). TSS values remain high through slack high tide and the start of ebb, but abruptly decrease during ebb runoff. The length of ebb runoff depends on how well the gully or network of gullies transfers water stored in the ponds and mudflats. The greater the volume of water stored in an area, the longer it will take for the gullies to effectively drain the ponds. The decrease in suspended concentration may reflect the loss of material by deposition on mudflats and in ponds.

TSS concentrations vary seasonally in the Eagle River, being high through July and August, with

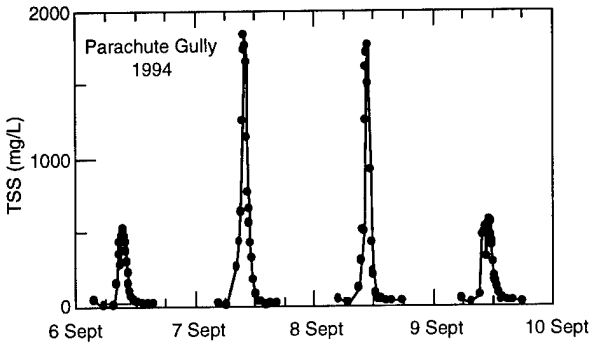

Figure 36. TSS measurements at Parachute Gully through four tidal cycles in September 1994.

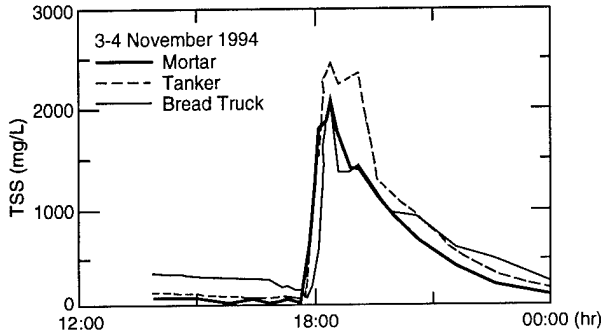

Figure 37. TSS measurements at coastal sites during single tidal cycle, 3–4 November.

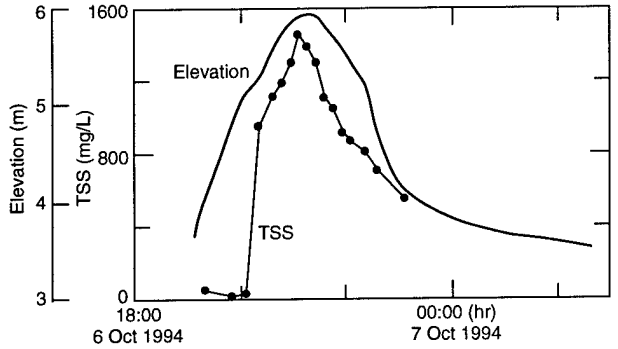

Figure 38. Typical TSS variation through a flooding cycle.

glacially induced sediment peaks in mid-June and early August (Fig. 39). However, the relative levels of TSS concentrations in the river are quite low compared with simultaneous values measured at mudflat gully sites and in Knik Arm.

These data tell us that Knik Arm, and not the Eagle River, is the main external sediment source for ERF. Coastal TSS measurements exceed those at the river throughout the monitoring period

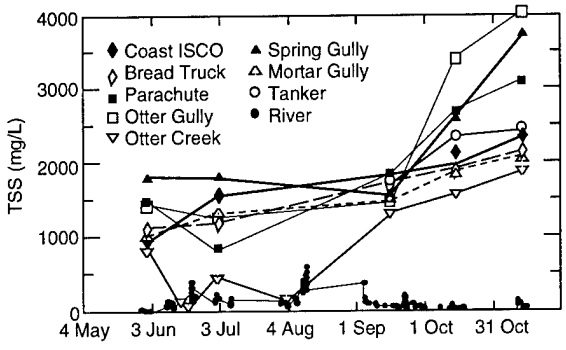

Figure 39. Maximum monthly TSS measurements.

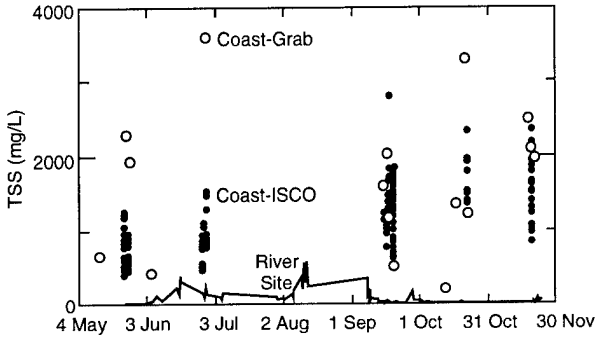

Figure 40. Coastal vs. river TSS measurements.

and show a general increase in sediment concentration through the season (Fig. 40). We observed gradual early season increases, as well as sharper, late-season increases in the peak TSS values of both the Knik Arm and gully sites. Late-season increases in TSS also correlate with increases in OBS turbidity measurements at the hydrostations, as will be described subsequently.

Trends in TSS related to location in the Flats were not observed until the October and November cycles, when TSS values of sites near the coast were generally lower than at other sites, but were comparable to those observed in Knik Arm waters (Fig. 39). The extremely high TSS values at inland sites during the fall flooding cycles probably reflect a stronger influence of sediment transport from internal sources such as riverbank and gully erosion, perhaps ascribable to freeze–thaw effects on bank and mudflat materials.

Unfortunately, the USGS stopped monitoring of the Eagle River by 1981, so that there is no continuous record of water or sediment discharge. However, the channel profile at Bravo Bridge was measured twice during the summer of 1994 (17

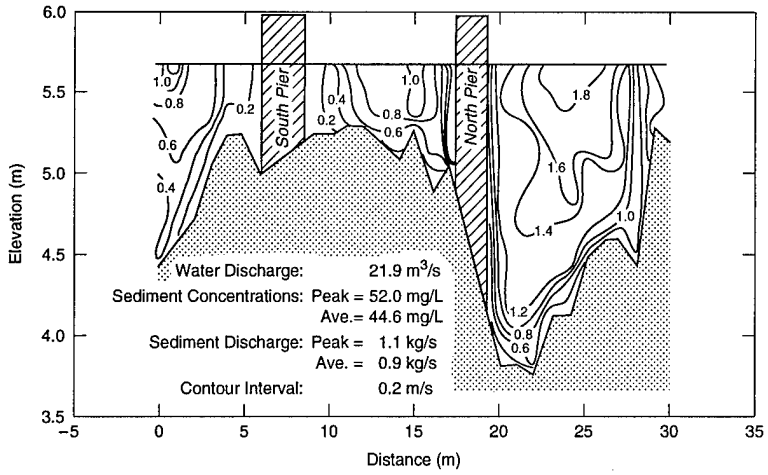

Figure 41. Velocity profile for Eagle River on 5 September 1994 with estimates of discharge (sediment and water).

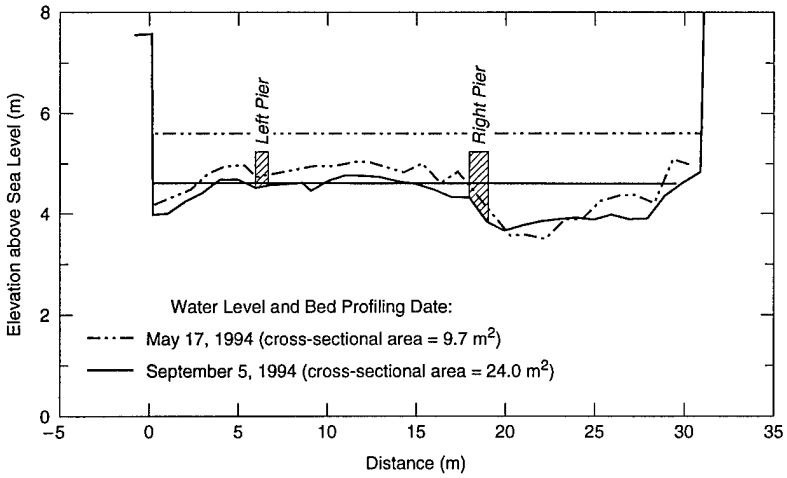

Figure 42. Comparison of Eagle River profiles from 17 May and 5 September 1994.

May and 5 September), the latter as part of an exercise to measure the velocity profile of the Eagle River (Fig. 41). Velocity was measured about every meter across the bridge at approximately 30-cm (1-ft) depth increments. The water stage in early September is relatively high because of seasonal runoff from Eagle Glacier, and velocity ranged from below 0.2 m/s to about 1.9 m/s with a discharge of 21.9 m^3/s. TSS values measured at the river ISCO averaged 44.6 mg/L with a peak of 52.0 mg/L. Using these values, we estimated average and peak sediment flux to be 0.9 and 1.1 kg/s respectively.

In May the channel profile was measured at Bravo Bridge, yielding a cross-sectional area of 9.7 m^2 (Fig. 42). TSS measurements during May averaged 11.1 mg/L with a peak of 30 mg/L. River discharge and sediment flux during the channel survey can be estimated if the discharge is assumed proportional to the cross-sectional area of the river. In May it was 40.6% smaller than in September. Using this assumption, we calculated a river discharge of 8.9 m^3/s, while the estimated average and peak sediment fluxes were 0.34 and 0.45 kg/s. This estimated discharge is similar to the 1966–1975 average of 6.8 m^3/s for the month of May from the USGS (USGS 1981).

SEDIMENTATION

Suspension settling occurs during slack high tide and the early stages of the ebb cycle. In ponded areas, it also happens between tides when water turbulence is low and fine particles settle out of the water column. Therefore, the longer

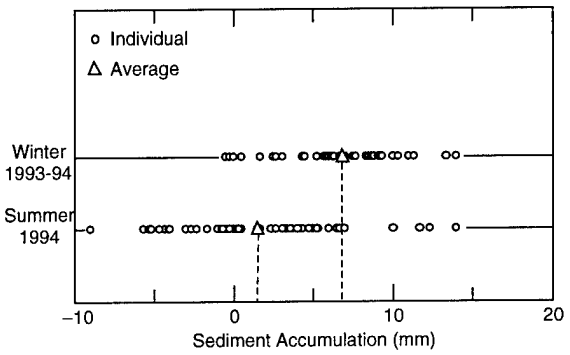

Figure 43. Net seasonal sedimentation rates at sites sprayed with paint in August 1993 (winter 93–94 represents September 1993 through May 1994, summer 94 represents May 1994 to September 1994). Circles represent individual sedimentation measurements; the triangle and dashed line show the averages.

quiet water conditions can be maintained, the greater is the time for deposition. The mixing and exchange of flood water with pond and marsh water increases the amount of suspended sediment in the ponds and marshes, and provides the primary source for deposition with each flooding tide. Additional processes in gullies include bedload deposition, sediment flows and slumping; these materials, however, may be remobilized and transported either into the pond areas or into the Eagle River, depending upon tidal stage.

Controls on sedimentation rates at any particular location include elevation, vegetation that traps sediment, and the frequency, height and duration of inundations by sediment-laden waters. The distance from the source water also plays a role in some areas, as sediment can be deposited or eroded during flood and ebb, altering its concentration. Local variability in deposition may also result from ice rafting of sediment plucked from other locations within the Flats.

Sedimentation rates vary with morphology and, in a general sense, elevation (Table 12). The overall trend in rates is an increase from levees to mudflats, ponds, marshes and gully bottoms, with the more heavily vegetated areas having higher rates of accumulation. Typical annual sedimentation rates range from about 10–30 mm among the various landform types.

Net accumulation rates are generally higher during the "winter" 8-month period from September to May than during the "summer" 4-month period from May to September. This difference may reflect the respective lengths of the seasons, an increase in available sediment as indicated by TSS values during the early winter months (Fig. 39), the trapping of sediment by the snow and ice cover, or the number of flooding events. Net accumulation of sediment above paint layers through August 1994 in Area C and D mudflats and levees are shown in Figure 43. Most winter values fall in the range 2–15 mm, while the summer values range between −5 and 6 mm. The negative summer values may result from compaction or erosion, or from the variability in sedimentation in the area from which measurements are taken.

The relationship of sedimentation rate to elevation is a response to the number of times the sites are inundated. Table 13 depicts the number of events that would reach critical elevations to flood different landforms, based on predicted tide heights at the Anchorage tide gauge. The number of inundations is highest for ponds and decreases with the increasing elevations of mudflats to levees, thereby correlating with the general decrease in sedimentation rates (Table 12). An example of decreasing sedimentation rate with increasing elevation is revealed in the summer 1994 data for Transect 19 on Racine Island (Fig. 44). Sediment accumulation along the northern part of the transect that crosses a low-lying, abandoned oxbow is much higher than in the elevated, vegetated mudflat to the south.

The number of flooding events that we show in Table 13 is a conservative estimate, since predicted tidal elevations do not account for higher tidal elevations from tidal amplitude increases caused by the geometry of Knik Arm (e.g., McCann 1980a,b; Syvitski et al. 1987, p. 163), river discharge, ice cover or wind. If the augmentation

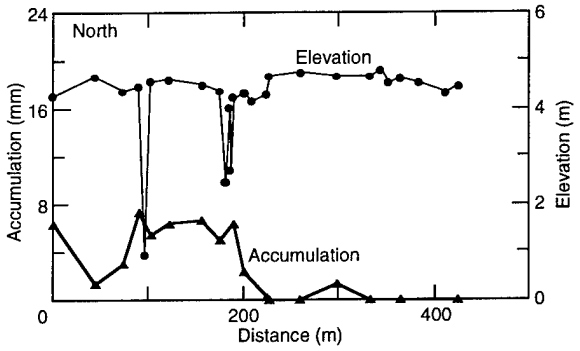

Figure 44. Sediment accumulation and elevation along transect 19 on Racine Island. Northern lower-lying section is located within an abandoned oxbow.

Table 13. Comparison of predicted and measured number of flooding events reaching critical heights during summer and fall 1994. Measured data based on depth transducer at Bread Truck Gully.

	Number of flooding events			
	Anchorage predicted		*Measured*	
Critical height	*Summer 1994**	*Fall 1994**	*Summer 1994*	*Fall 1994*
Inundate ponds (4.6 m)	16	21	52	23
Cover mudflats (4.87 m)	8	11	18	18
Cover levees (5.21 m)	0	5	4	7

*Summer 1994 (22 May to 15 Sept).
*Fall 1994 (16 Sept. to 9 Nov).

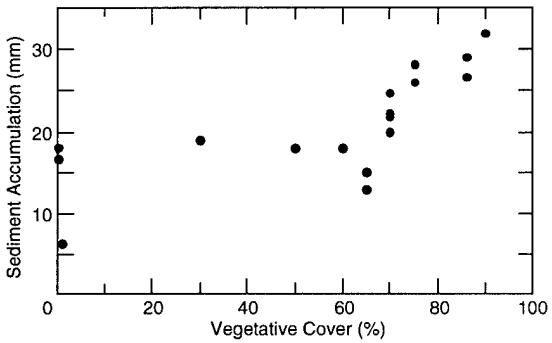

Figure 45. Relation between total sediment accumulation recorded in September 1994 and vegetative cover at sites sprayed with paint in 1992.

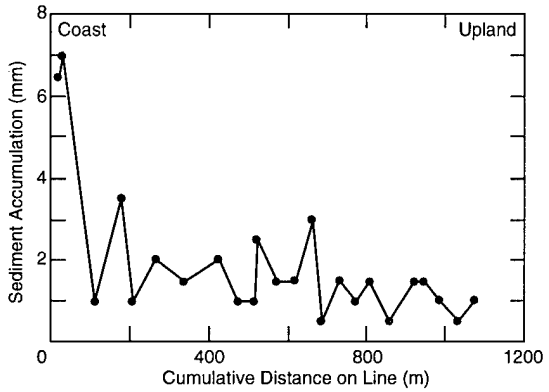

Figure 46. Accumulated sedimentation with distance inland from coast along line 16 in northwest Area A.

of the tidal effects by such factors is considered, the number of inundations increases (Table 13). There were significantly more tidal floods at the Bread Truck hydrostation during the 1994 season than were predicted by the tide chart elevations. The increase was on the order of twice that predicted for the summer period. The increase during the fall was much less evident and correlates with a seasonal reduction in river discharge.

The amount of vegetative cover in the mudflats influences the sediment accumulation rates. Sediment accumulation vs. vegetation cover at sites first established in 1992 are correlated in Figure 45. Gross sedimentation rates at these longest-established sites had 2-year total accumulations of 6–18 mm at sites with less than 60–65% vegetative cover, and 26–32 mm at sites with a vegetative cover greater than 70%.

Sedimentation rates also vary with distance from source waters. A decrease in sedimentation rate with distance inland is best documented along transect 16 (Fig. 46), which extends southward from Knik Arm in coastal Area A (Fig. 7). Decreased velocities of Knik Arm waters during

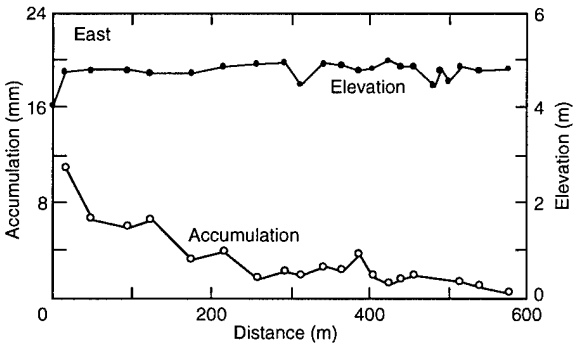

Figure 47. Sediment accumulation and elevation along transect line 18 in Area A. East end of line is located at river levee.

flooding reduces their ability to transport sediment, causing rapid sedimentation near the coast, with less material available further inland. The same effect is often seen along the scarp of many gullies where flow conditions change rapidly as flood waters overtop gully banks. Sedimentation rates in general decrease with distance from the Eagle River inland toward the marshes abutting the uplands (Fig. 47).

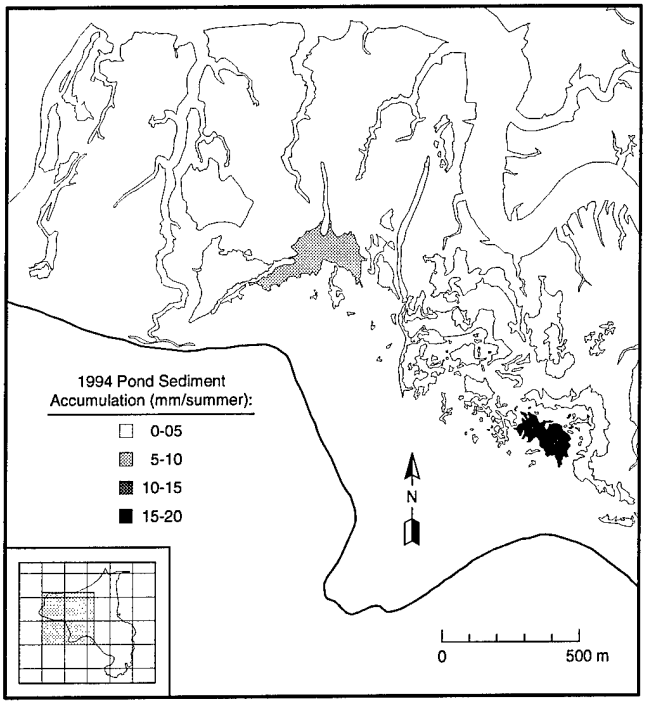

a. Northwest tile.

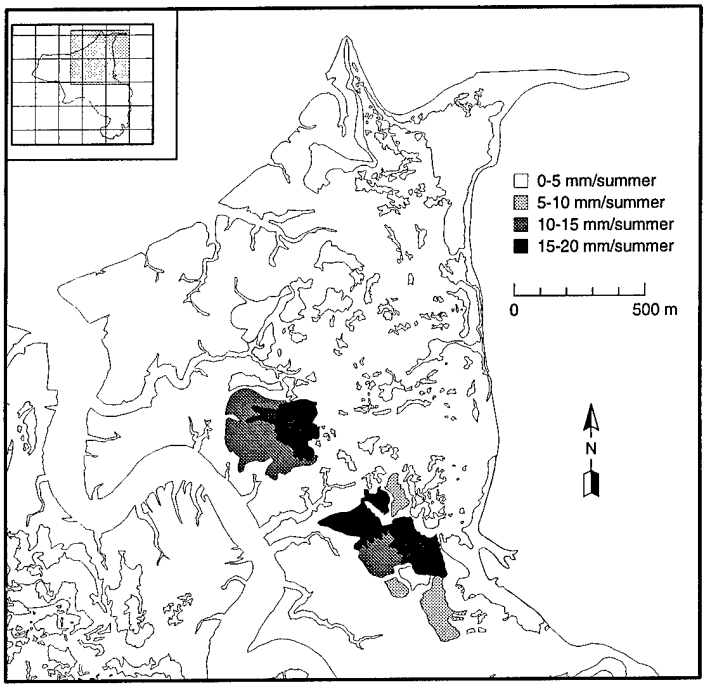

b. Northeast tile.

Figure 48. Summary of sediment accumulation in pond locations during summer 1994.

Sedimentation rates in the ponds are also quite high (Table 12). The amount of sediment that originated by resuspension of bottom sediments in ponds ranged from 8–16 mm for the summer of 1992, or approximately equivalent to the thickness of new sediments deposited in the ponds during the same period. During the winter 1992–93 period, sedimentation from resuspension ranged from 2–15 mm, or amounts similar to those of the summer 1993. Winter 1993–94 resuspension rates could not be calculated because the plate collection devices were not cleared in the fall of 1993. Using the sedimentation stations established in 1994, we found that summer resuspension sedimentation ranged from 0–7 mm (slightly less than in previous years).

Pond sedimentation rates vary in space and time across the Flats because of the interactions of processes and physical constraints described earlier. Summer sedimentation rates for monitored ponds across ERF are summarized in Figure 48. During the summer of 1994, the highest sedimentation rates (15–20 mm) were recorded in the ponds of Bread Truck, Area C and Area A (Fig. 48a, b). Sedimentation rates at intermittent ponds ranged from 1 to 15 mm per summer; however, the rate at station 1 (Fig. 10) was anomalously higher, having 24 mm per summer.

EROSION DYNAMICS

Gully erosion is one of the most visible mechanisms that is currently modifying and reshaping the Flats. Similarly, Eagle River migration also causes considerable change (Tables 1–4). Because of the rapid dynamics associated with river and gully erosion, the rates of erosion and recession need to be quantified and integrated into our modeling of the physical system. This quantification is critical because numerous gullies are experiencing headward erosion towards several of the most contaminated ponds on ERF.

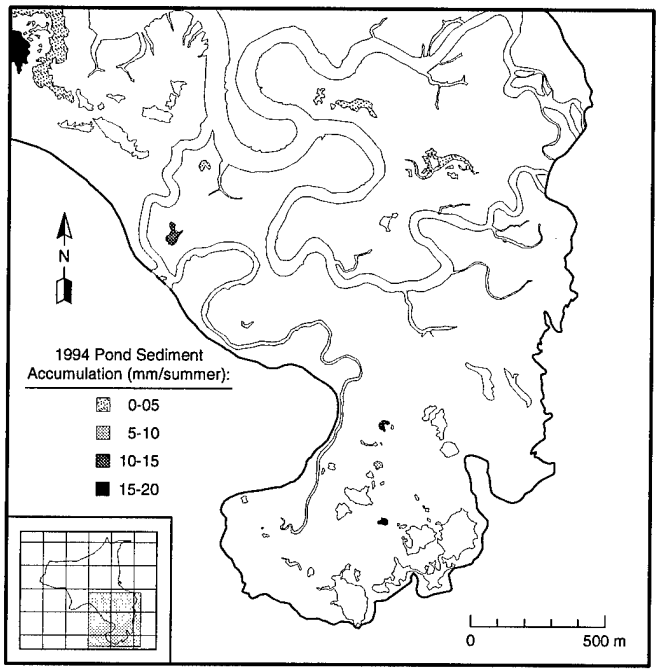

c. Southern tile.

Figure 48 (cont'd).

Driving mechanism and system response

Gully and river erosion in ERF may best be described as a complex response to external and internal factors (Table 7), particularly the 1964 Alaskan earthquake. Brown et al. (1977) concluded that the Anchorage area subsided 60–70 cm during the earthquake, followed by a post-seismic recovery of about 1.5 cm/yr. However, gravity and tide gauge data indicate that the rate of uplift has been decreasing. Accordingly, up to 45 cm (or about 65%) of the recovery may have occurred through September 1994. The physical system therefore has been and now is complexly responding to an initially rapid reduction in base level, which is now being followed by a gradual rise as isostatic recovery takes place.

The ponds' and mudflats' initial response to subsidence probably was a significant increase in deposition in them, as the potential energy decreased with the lowering of the surface elevation closer to that of mean Anchorage sea level. The lower elevation increased flooding frequency, and the volume of water entering the Flats increased the amount of sediment entering ponds and the time available for suspension settling in the ponds, marshes and mudflats. Deposition will augment the rate of surface rise and thus may reduce the length of time for recovery in base level than that expected from tectonic adjustment alone.

The subsequent uplift and increase in flood water volume also induced gully erosion across ERF; this is evident by an increase in gully entrenchment, the formation of knickpoints* and progressive headwall migration into the mudflats and ponds. The most prominent knickpoints are the steep headwalls at plunge pools in gully heads. As uplift continues, the gradient of the gully bed steepens relative to mean tide. Gully incision results from scour of the bed as the volume and rate of discharge increase. Gully knickpoints migrate up-gradient, reducing the slope of the longitudinal profile by scour and progressively lowering the down-channel gradient (Fig. 49). Gully incision and headwall erosion will continue as long as the overall base level is lower than the one that existed prior to the 1964 earthquake; once tectonic stability is attained, an equilibrium gully slope profile will develop and gully extension should cease.

Erosion and recession rates

Headwall erosion is progressively elongating gullies into the mudflats, towards the ponds. Eagle River is also laterally migrating, transporting the eroded sediment down-river towards Knik Arm.

The amount of recession of scarp crests is highly variable within a gully, as well as among the individual sites (Table 14, App. B). At each site, some parts of the scarp crests did not retreat at all, and in fact, extension was measured where tension cracks developed at an early stage of collapse. This variability in recession rates is evident in plots of the scarp crest location with time (Fig. 50 and 51). Recession rates for the September 1993 flooding cycle were a maximum of 1.4 m, while 3.8 m was observed at Bread Truck Gully during the fall of 1994 (Table 14, Fig. 50d). Recent monitoring of erosion along the Eagle River recorded recession rates of 2.3 m during the summer and 2.0 m during the fall of 1994 (Fig. 51), with maximum recession rates of 3.7 m. Headward erosion in 1994 resulted in

* Knickpoints are locations of abrupt slope change in the longitudinal channel or gully profile and represent system disequilibrium.

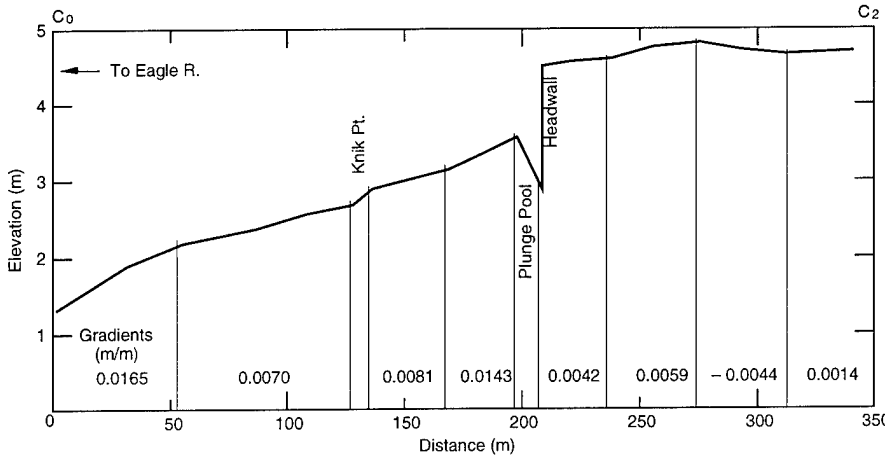

a. C_0 to C_2.

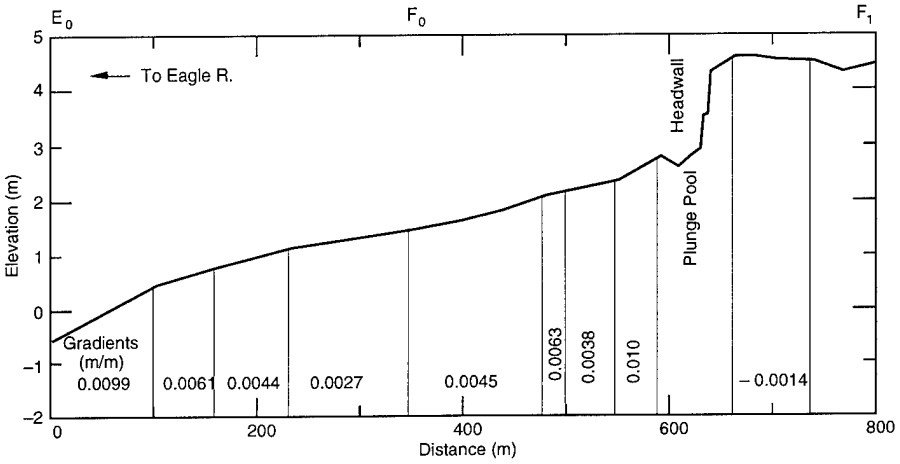

b. E_0 to F_0 to F_1.

Figure 49. Longitudinal profiles along two gully thalwegs (see Fig. 13). Gradients along sections of the gullies are indicated.

Table 14. Summary of gully and river erosion monitoring.

		Recession range (m)						
Area	*Position**	*Sum 92†*	*Win 92*	*Sum 93*	*Win 93*	*Sum 94*	*Fall 94*	*Net erosion*
Area A								
(coast)	H	—	—	—	—	0–0.47	0–1.17	0–1.09
	L	—	—	—	—	0–1.01	0–1.85	0–2.76
(interior)	H	—	—	—	—	0–1.59	—	0–1.59
	L	—	—	—	—	0–1.01	0–1.17	0–1.17
Area B	H	—	—	—	—	0	0	0
	L	—	—	—	—	0	0	0
Area C	H	0.09–3.06	0.17–0.37	0.04–3.79	0.13–1.35	0–1.16	0 –1.17	0.04–9.30
	L	0–4.90	0–6.30	0.17–9.80	0–2.08	0–2.57	0–1.03	0.27–8.17
Area D	H	0.01–6.95	0.05–0.35	0–4.31	0–0.61	0–2.10	0–3.77	0.04–4.61
	L	0–2.37	0–2.00	0–3.12	0–2.29	0–2.23	0–3.77	0–8.15 **
Racine Isl.	H	—	—	—	—	0	0	0
	L	—	—	—	—	0	0	0
River	L	—	—	—	—	0–2.32	0–2.03	0–3.69

* H —Head wall; L—Lateral wall.

† Summer (Sum) represents period May to September; Winter (Win) represents period September to May.

** Measured change since Fall 1993.

variable recession rates. No erosion was measured on Racine Island or Area B in 1994. Field observations in Area B showed that slopes are heavily vegetated and more gently sloping than in other sections of ERF. Lateral erosion in 1994 also had values ranging from 0 to 3.7 m (Table 14). The greatest change measured thus far was the extension of a shallow (0.5 m) gully by nearly 45 m into the mudflats near Lawson's Pond during the 1992–93 winter (Fig. 50e); little change has been observed since that time.

Recession by lateral erosion characterizes the B-Gully site, located about 75 m below the headwall (Fig. 50a). Erosion forms cuspate embayments that gradually enlarge, with a maximum measured recession of 8.2 m (Fig. 52). This site is significant because WP has been found in gully transport, but additional study is needed to see if WP is being flushed out of C-Pond or introduced by erosion and collapse of these bank sediments.

Parachute Gully (Fig. 50b) is a good example of the processes of headward erosion and recession. Up to 9.3 m of headward recession (~3.79 m/year; Table 14) but only 1.6 m of lateral recession have been monitored at this site since 1992. Recession has centered around a cratered drainageway that has become incised and enlarged.

Two additional drainages, Coastal 6 and Bread Truck, exhibit variable head and lateral recession rates characteristic of ERF (Fig. 50c and 50d). Bread Truck Gully receded headward 0–3.5 m (up to 1.9 m/year) and laterally 0–8.2 m since monitoring began in 1993 (Table 14). Coastal 6 Gully receded 0–2.8 m headward and 0–1.2 m laterally in a single summer season of 1994. Upwards of 1.9 m of headward and 1.2 m of lateral recession occurred here in early fall.

Rapid lateral erosion of about 3.7 m was recorded at River Section-North between July and November of 1994 (Fig. 53). Erosion takes place along large rotational slumps that are undercut by the river (Fig. 54). To start, large extension cracks develop parallel to the scarp, gradually leading to catastrophic failure. The location of the crack becomes the new scarp of the riverbank. Several locations where the river is meandering and slope processes are consuming mudflat sediments are given in Figure 55. Material at these sites is entering directly into the Eagle River and subsequently into Knik Arm.

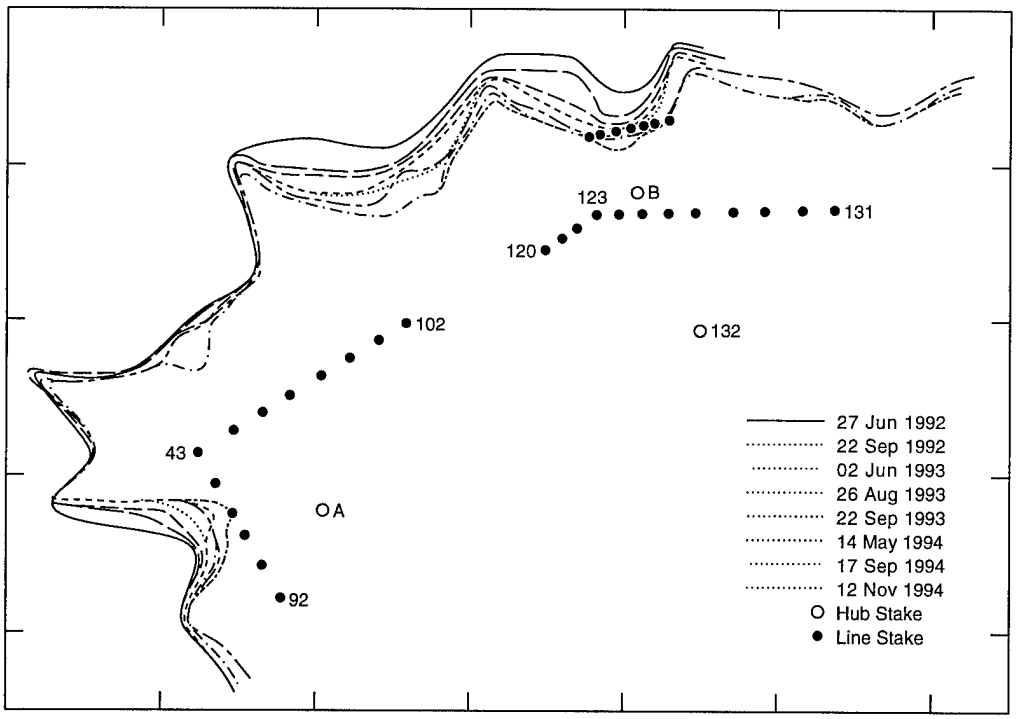

a. B-Gully.

Figure 50. Gully scarp locations for measuring erosion rates.

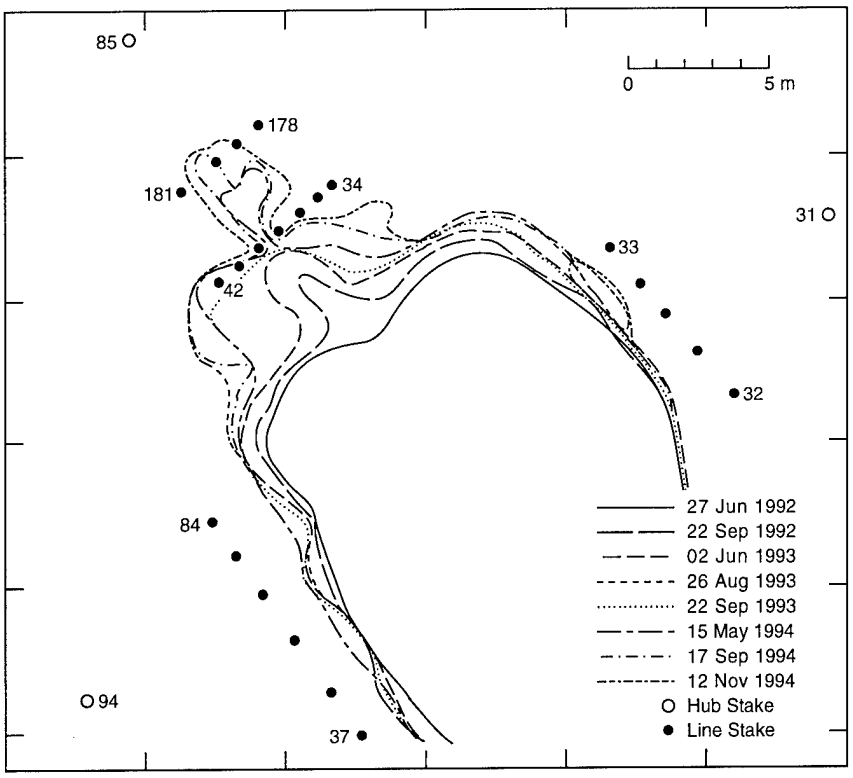

b. Parachute Gully.

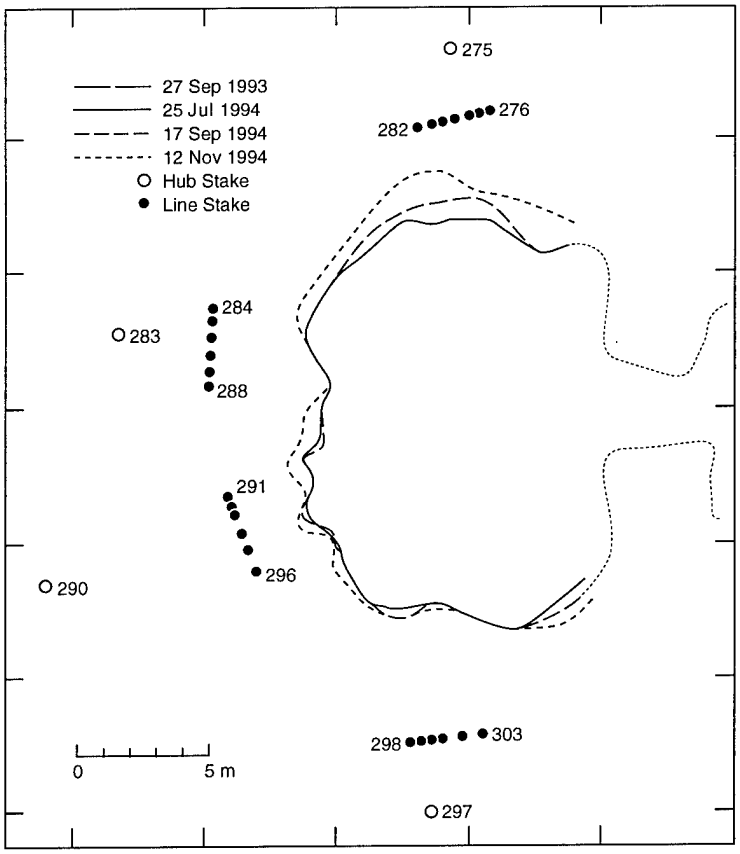

c. Coastal 6 Gully.

Figure 50 (cont'd). Gully scarp locations for measuring erosion rates.

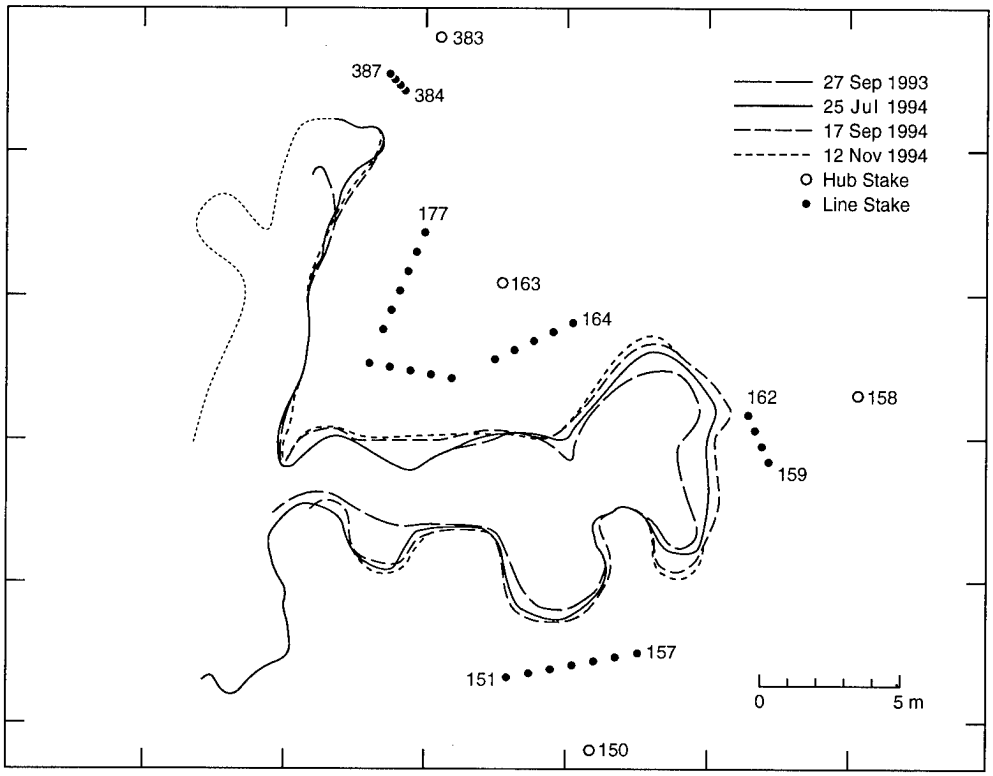

d. Bread Truck Gully.

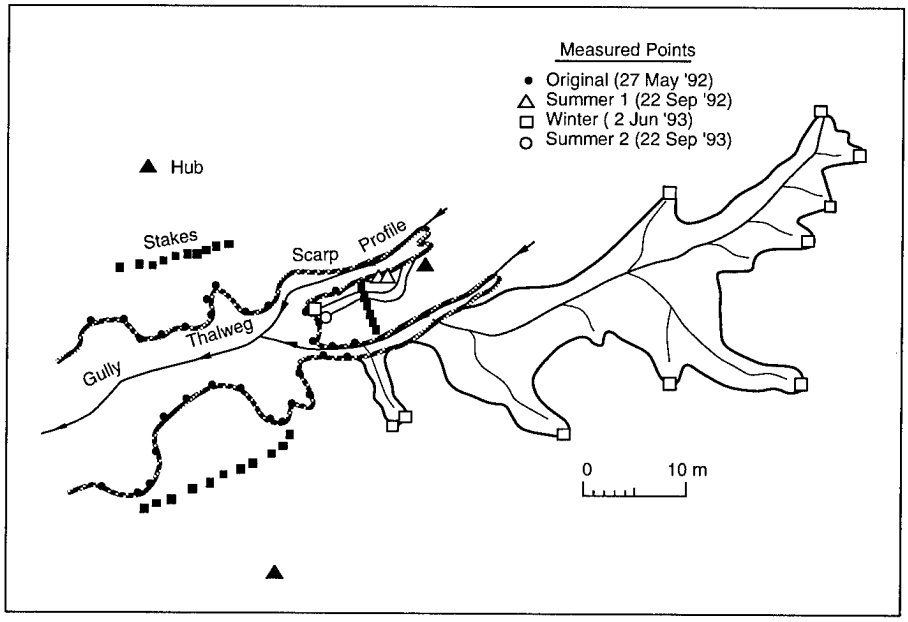

e. In-Between Gully.

Figure 50 (cont'd).

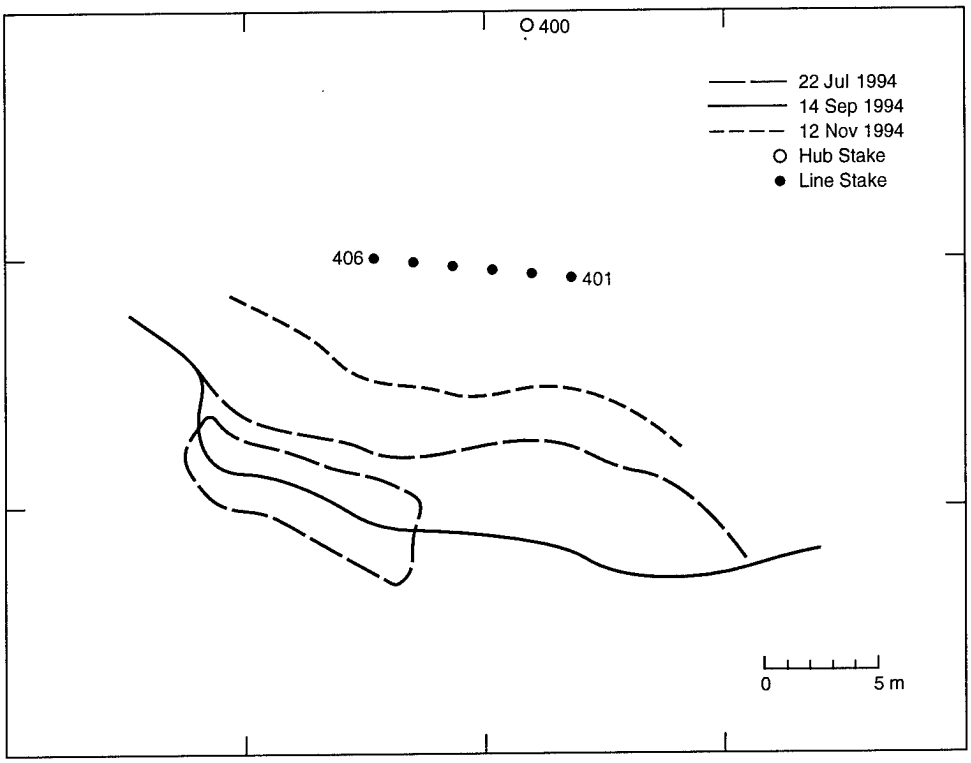

Figure 51. River bank erosion at the River Section-North.

Figure 52. Eastward view of eroded cuspate embayment at monitored section of B-Gully where white phosphorus was recorded in transport.

Recession rates vary because erosion takes place as rapid, short-duration events (Tables 1 and 2). Recession is mostly caused by current scour of the lower, unvegetated portion of gully walls during ebb tide when water velocities are high. Because the uppermost 20–30 cm of material is consolidated and rootbound, this soil and root mat fail only after an erosional niche of approximately 0.5 m or deeper is cut below it. Along steep scarps, blocks of consolidated, root bound sediments fall and roll into the gully bottoms, remaining intact until currents eventually break them down either by rolling them along the bed or by scour (Fig. 53). The lateral walls of gullies, which tend to develop low-angle slopes as headwalls, progressively recede inland, failing mainly by rotational slumping, but also by debris flow; both processes introduce sediment into the gully channel. On gentler slopes, blocks of rootbound material can remain intact as they are transported by these mudflows. This sequence of events happens at different times and rates, and therefore recession varies within as well as among the study sites (Table 14).

If our measurements of the average recession rates are representative of longer-term trends, then erosion may be expected to extend gullies into ponds over the next 15–50 years (Table 15).

a. Plunge pool of Mortar Gully.

b. Gully scarp of Coastal 6 Gully.

Figure 53. Examples of slope failure.

Table 15. Preliminary estimates of delay before natural pond drainage.

Gully	*Distance to pond (m)*	*Max. recession (m)*	*Max. recession rate (m/yr)*	*Min. time before natural drainage (yr)*
Bread Truck	65–100	3.4	1.9	35–50
In-Between	40	9.8	2.3	17–20
Parachute	~80	9.3	3.1	25–30

Figure 54. Rotational slump block failure at River Section-North.

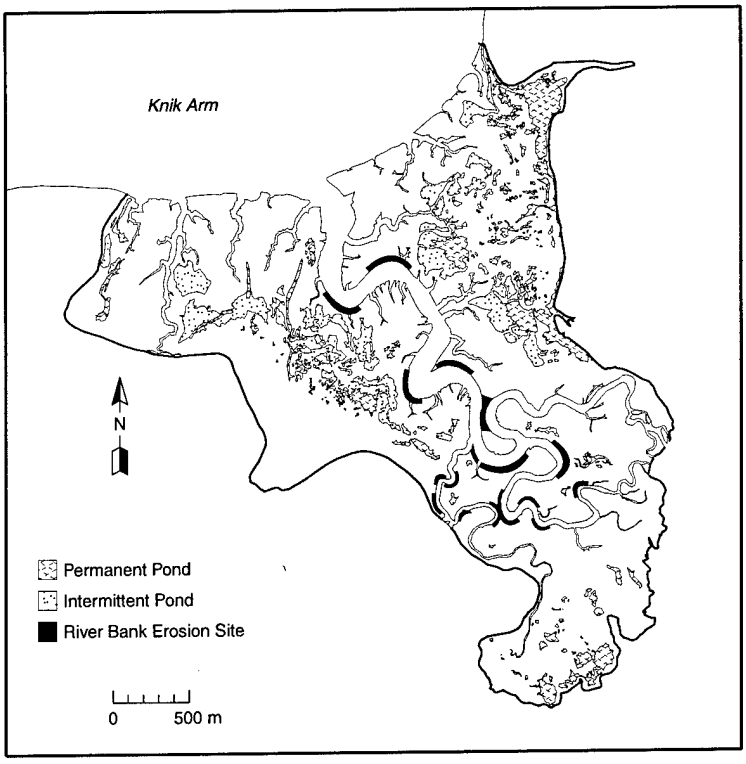

Figure 55. Sites of observed or suspected riverbank erosion.

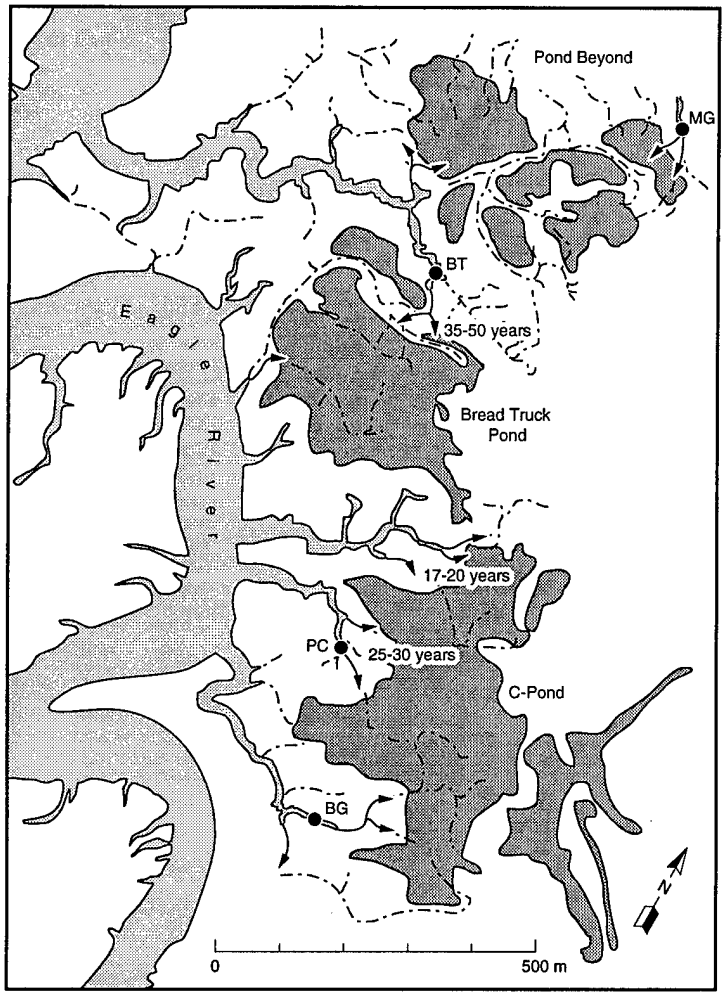

Figure 56. Drainages within C/D Area near permanent ponds with arrows showing locations of anticipated progressive erosion. Where rates have been measured, estimated time to natural draining of ponds is indicated (MG–Mortar Gully, BT–Bread Truck Gully, PC–Parachute Gully and BG–B Gully).

The two ponds most likely to be naturally drained by headward gully extension are Bread Truck in an estimated 35–50 years and C-Pond in an estimated 17–25 years (Fig. 56). Further analyses of both modern and historical recession rates are required to determine if the 1992–1994 data are representative of longer-term rates.

Implications for remediation methods

An understanding of gully recession enables us to better assess the effectiveness of the proposed remedial measures for WP contamination. In a positive way, headward recession will eventually drain C-Pond, Bread Truck Pond and Pond Beyond, thereby producing drying conditions that will favor a natural degradation of WP (see Walsh et al. 1995). Gully erosion, however, could threaten the integrity of capping measures (i.e., geotextiles and AquaBlock) if these are used in the wrong places. Erosion will undercut the capping material and damage or destroy its effectiveness.

Gullies are also routes for pond outflow and therefore are potential pathways for migration of WP off-site. As the gullies continue headward expansion into contaminated ponds and mudflats, WP-bearing sediment will be introduced into the water draining the ponds. As gullies encroach on pond margins, erosion will probably increase runoff, stimulating increased scour, and once reaching unvegetated pond bottoms, increase the rate of gully expansion within them.

Dredging has also been proposed as a potential method to remove WP from pond sediments. This method will, however, affect the physical properties of the dredged areas and will affect hydrological conditions, including drainage. Gullies intercepting a dredged area may deepen and extend rapidly through those areas because of the loss of vegetation and compaction of sediments. Extension could be rapid, and move large amounts of material while destroying the ponds.

GULLY HYDRAULICS AND DISCHARGE

Gully profiles

Longitudinal profiles of nine gullies, surveyed along their central channel or thalweg, have several characteristics in common. Each gully in the area east of Eagle River has moderate to relatively steep slopes downstream of an eroding headwall (e.g., Fig. 49). The headwall region has a nearly vertical face ranging from 1.2 m to over 2.0 m in height. At the base of the headwall is a depression or plunge pool scoured by water flowing over it (Fig. 57). These plunge pools range in depth from about 0.5 to over 2.0 m.

Channel gradients are steepest near the Eagle River (1.0 to 2.0 m/km). The steep bed slope here probably results from the large range in tidally controlled variations in water level and discharge in the river proper. Upgradient of this steep section, the gradient shallows (0.3 to 0.7 m/km), producing a concave upward profile that then progressively steepens with distance to the base of the headwall (Fig. 49). At one or more locations in the gully, short segments of the channel exhibit the sharp increases in gradient (knickpoints) that signify that the bed profile is not in equilibrium with the existing hydrological conditions. Further, they indicate active scour of the bed as the gully thalweg deepens and the channel gradient lessens.

Channels above each headwall are lined by vegetation and the bed slope ranges from 0.1 to 0.6 m/km, generally being less than gradients in the gully proper. With distance, slopes gradually reverse in direction and dip towards the ponds across the unvegetated mudflats. The divide represents a critical threshold beyond which gully extension will capture the pond and accelerate its drainage. As erosion continues, the lower threshold for pond drainage may extend the duration of and possibly the volume of water flow through the gully, further accelerating erosion and headwall recession.

Table 16. Discharge calculations for October and November 1994.

	Spring Gully	*Bread Truck*	*Parachute*
Cross-sectional area (m^2)	26.5	5.5	9.8
Peak flow (cm/s)			
Flood	51.82	84.17	64.97
Ebb	177.06	146.41	75.71
Mean flow (cm/s)			
Flood	15.07	21.92	10.48
Ebb	66.06	69.42	50.31
Peak discharge (m^3/s)			
Flood	13.73	4.63	6.65
Ebb	46.92	8.05	7.42
Mean discharge (m^3/s)			
Flood	3.99	1.21	1.03
Ebb	17.51	3.82	4.93

Figure 57. Water flowing over gully headwall at Parachute Gully plunge pool.

Gully discharge

The volume of water that flows through a gully is mainly a function of the height of tidal inundation, including its supplement by the river and any additive effects of wind, ice and any other factor that may reduce gully cross-sectional area. The velocity range and magnitude of the flood and ebb currents determine the flux of sediment and water from the ponds and mudflats, as well as gully erosion.

The velocity of tidal flood and ebb currents at the Bread Truck, Spring and Parachute gullies differs greatly in magnitude among these sites, but the peak ebb velocity in each instance is greater than the peak flood velocity (Table 16). Velocity asymmetry is greatest between the ebb and flood in Spring Gully and the smallest in Parachute Gully (Fig. 58). The magnitude also changes with the height of flooding (Fig. 59), the lower peak and range in velocities occurring during the lower elevation flooding tides. Velocities are greatest in Spring Gully, with moderate values recorded in Bread Truck Gully and the lowest values in Parachute Gully (Table 16).

The flood and ebb asymmetry determines the net transport of sediment. During flood, gully water levels generally rise passively before spreading onto the mudflats (Fig. 60). Then, the amount of sediment in suspension is probably limited to the amount in the water source, mainly Knik Arm. In contrast, higher velocities during ebb mean increased turbulence and potential for entraining sediment and thereby resulting in a net flux out of ERF. More energy is also available to cause bank and bed scour across the mudflats and within the gullies.

Discharge has been calculated for the Bread Truck, Parachute and Spring gullies, where current meters were located 1 m above the bed. The cross-sectional areas in each gully (Fig. 61) were used with the peak and mean velocities to estimate the discharge (Q) (Table 16, App. D) by

$$Q = VA$$

where V is velocity and A is the cross-sectional area.

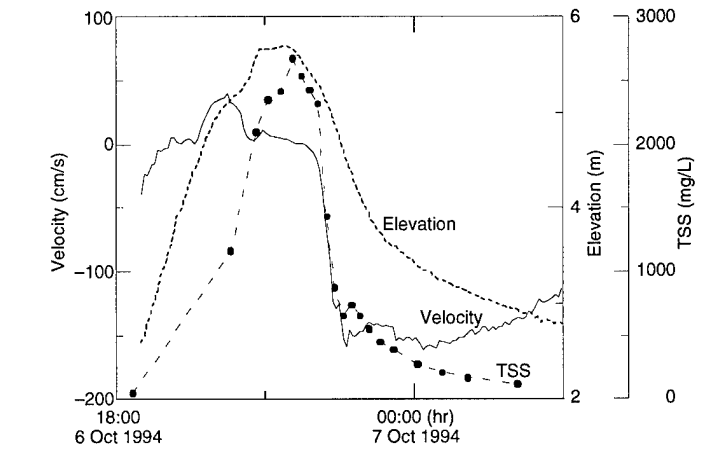

a. Spring Gully.

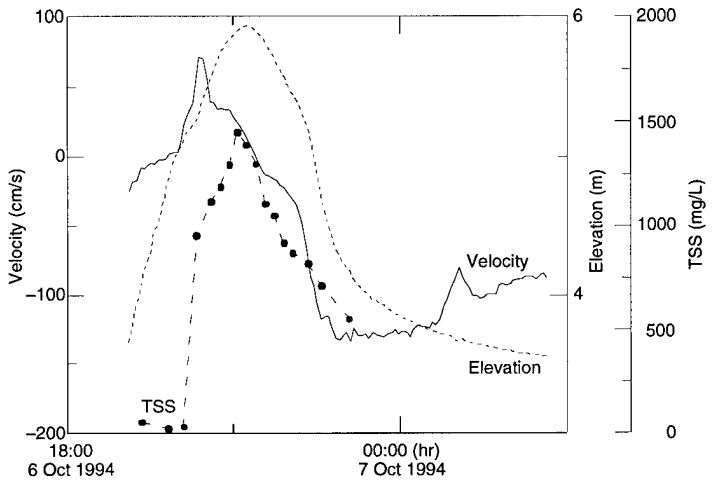

b. Bread Truck Gully.

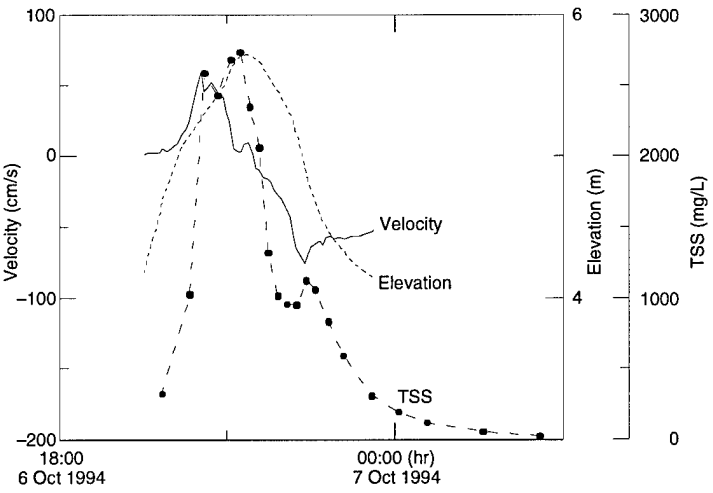

c. Parachute Gully.

Figure 58. Velocity during flood and ebb in a single tidal cycle.

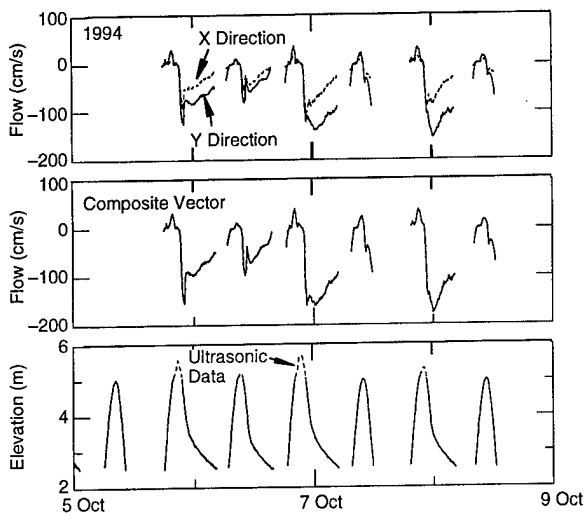

a. Spring Gully.

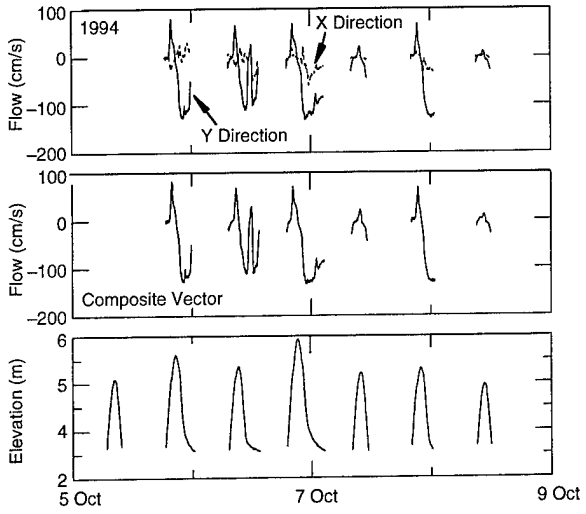

b. Bread Truck Gully.

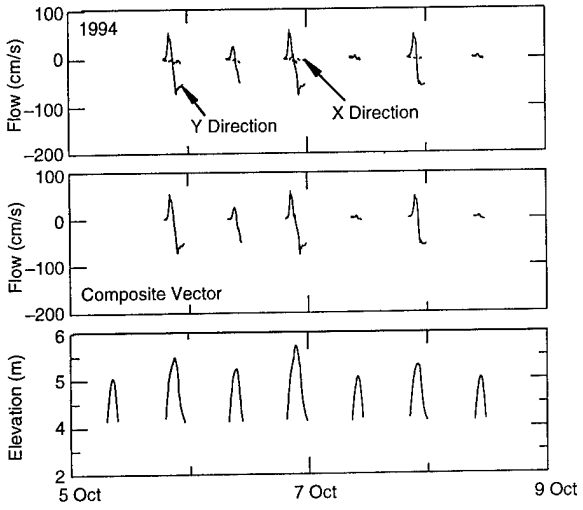

c. Parachute Gully.

Figure 59. Current velocity measurements for tidal inundation and ebb during the period 5–9 October. Flow velocity is in the x *and* y *directions; the composite velocity vector and flood–ebb elevations are shown.*

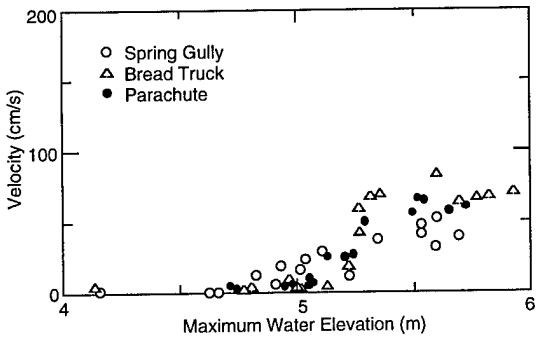

a. During flood.

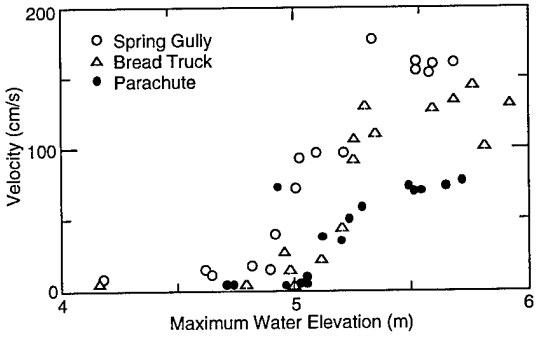

b. During ebb.

Figure 60. Comparison of peak velocities at the Spring, Bread Truck and Parachute gullies. Note the variability from site to site, which may be related to the area drained by each gully.

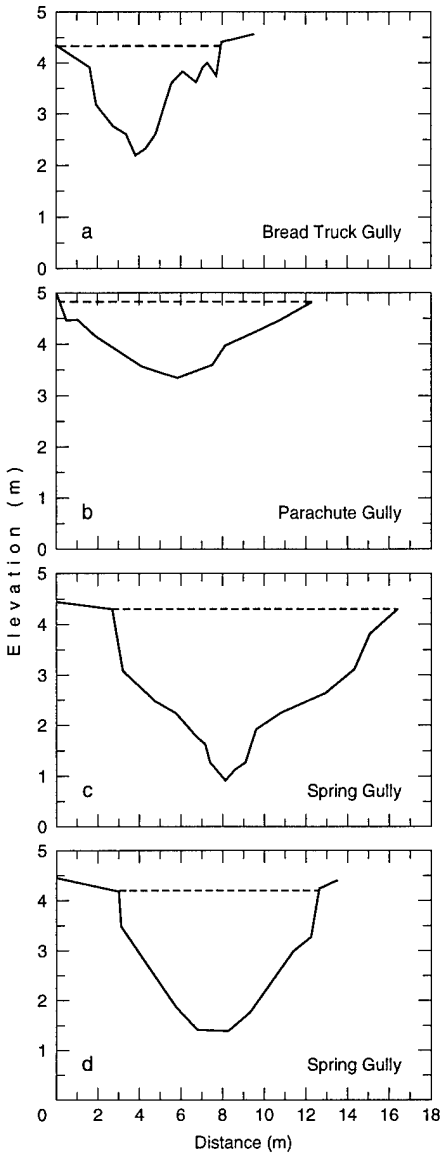

Figure 61. Gully cross sections at the location of flow probes in Bread Truck and Parachute. Two cross sections from Spring Gully represent the gully profile at the hydrolab (c) and the flow probe (d).

Data for October and November 1994 were divided into their flood and ebb components using the tidal inundation data in Appendix C. Calculations were based on average flood velocities ranging from 13.4 to 32 cm/s and ebb velocities ranging from 45 to 124.6 cm/s. Peak velocity ranged from 37.4 to 71.1 cm/s during flood and 72.0 to 176.2 cm/s during ebb.

Using the measured average and peak velocities, we estimated flood and ebb discharge for other months without measurements (App. D). Average velocities of 25.0 and 76.1 cm/s were used for Bread Truck Gully calculations, 27.1 and 47.0 cm/s for Parachute Gully, and 15.5 and 101.9 cm/s for Spring Gully.

Average discharge values in Bread Truck Gully were about three times greater during ebb than flood (~4.1 vs. 4.3 m^3/s), with a peak ebb discharge of 8.0 m^3/s. The difference in flood and ebb discharge at Parachute was slightly less overall (~1.2 vs. 2.6 m^3/s), peaking at 4.0 m^3/s. At Spring Gully, the difference is over 4 to 1 (~1.2 vs. 5.8 m^3/s); peak ebb is 9.7 m^3/s.

Peak and average TSS concentrations collected over the same time intervals were then combined with discharge calculations to make rough estimates of flood and ebb sediment fluxes (App. D). Ebb sediment flux exceeded flood sediment flux in each case, ranging from 2 to 3 times more during ebb. Peak sediment flux during ebb ranged from 33.7 kg/s at Spring Gully, to 11.2 kg/s at Parachute Gully, to 10.9 kg/s at Bread Truck Gully.

The calculated ebb and flood sediment flux data suggest that there should be a net transfer of sediment from ERF into Knik Arm, if these calculations are representative of the summer and this relationship holds during the winter when we don't have any data. Our sedimentation data indicate a higher overall rate during times of ice and snow cover. Without data on runoff, including sediment discharge, it is difficult to examine this problem further.

WHITE PHOSPHORUS EROSION AND TRANSPORT

White phosphorus may be eroded and transported with sediment by wind, river and tidal currents in summer. During winter, ice forming on the ponds and mudflats as frazil and anchor ice within both freshwater and saltwater bodies has the potential to entrain and transport sediments with WP (Fig. 62). It is critical to determine if transport of WP by these processes is quantitatively important in moving it to other locations in ERF proper or elsewhere in the Eagle River and Knik Arm. Ice and water may deposit WP-bearing sediments where waterfowl, fish, invertebrates or other potential receptors may ingest them.

WP-contaminated sediments transported as suspended or bedload in gullies were sampled using a plankton net (Fig. 19). Recent gully bottom deposits were also sampled as surrogates for

material in transport. Sediment in each sedimentation trap at the pond sites was sampled to see if WP particles were being resuspended and redeposited in ponds.

In addition, during November 1994, recently transported and deposited ice floes having sediments frozen to their bottom surfaces were sampled to determine if in fact ice was transporting WP-contaminated pond sediments (Fig. 63). Sediment and WP may be moved when the ice and frozen sediments are lifted off of the mudflat during flooding tides and drift with the wind and tidal currents (Fig. 64a). During tidal ebb, the ice can strand on the mudflat surface, and it often piles up at the heads of gullies (Fig. 64b).

The plankton net, gully bottom, pond and ice floe samples each carried WP-contaminated sediments (Fig. 62b and 63). WP concentration ranged from 0.0013 to 0.0493 mg/kg in three out of four plankton net samples taken during ebb discharge through B-Gully, following the four highest flood cycles in September. Four out of eight samples obtained from sediments frozen to ice floes yielded WP concentrations that ranged from 0.001 to 0.013 mg/kg. Two resuspended sediment samples from ponds in Area A and C ranged from <0.0014 to 0.003 mg/kg. These latter samples show that WP can be resuspended, but this may be limited since no samples from other sites have yet tested positive for WP.

Both the suspended load and bedload transport samplings and those from ice floes are significant. The ice floe samples that we obtained while walking along a transect from the EOD pad to the Bread Truck Gully site are the first from ERF. Samples were collected if the ice floes en-

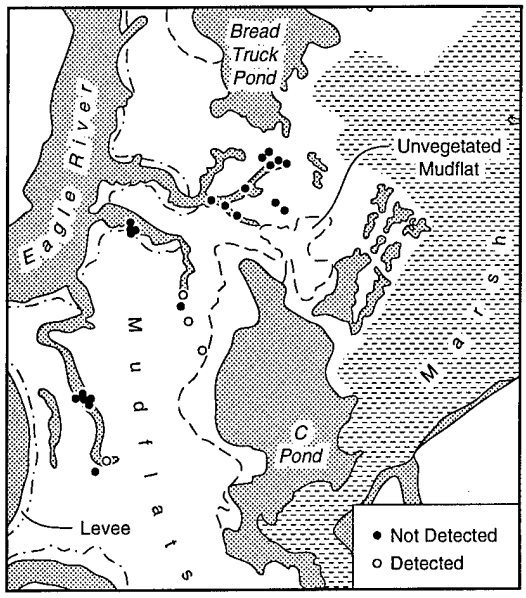

a. Positive results of previous sampling of gully bottom sediments.

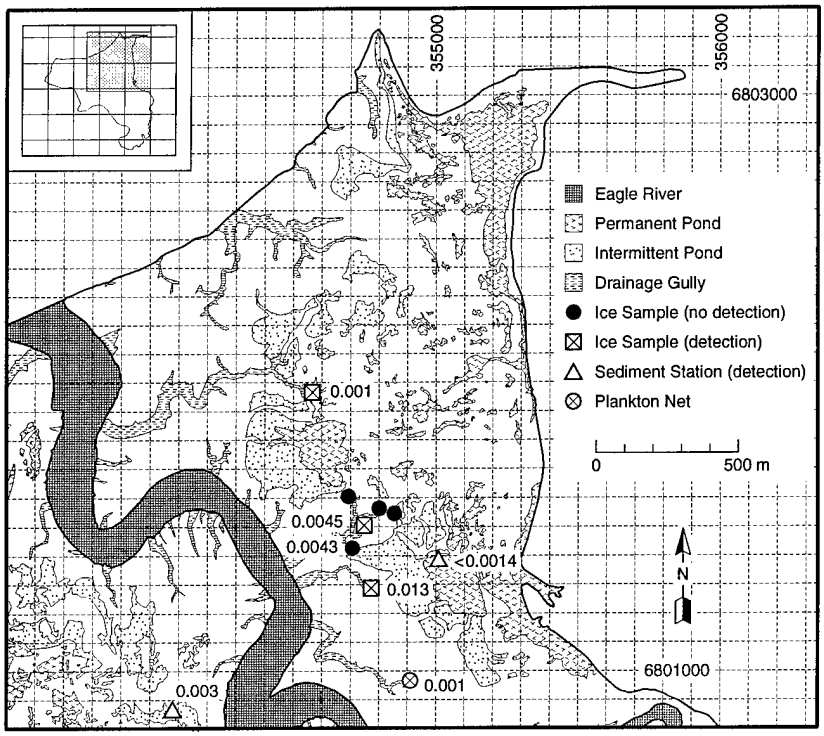

b. Positive results of 1994 sampling of sediment and water samples by gully currents and ice floes.

Figure 62. Location maps for WP.

a. Vegetated pond bottom sediments frozen onto ice near the In-between Gully.

b. Sediment layer frozen onto an ice block at Otter Gully.

Figure 63. Examples of freeze-on to pond ice at ERF.

countered had sediment frozen to them. The number of positive detections (~50%) out of the total number of samples indicates that this may be extremely important. This mechanism could entrain areas of pond bottom material of several square meters or more, with thicknesses of tens of centimeters. Ice floes move inland as well as out into Knik Arm and thereby can redistribute WP-contaminated materials. Further analyses are required to determine if these results are representative.

The plankton net samples are important because they point to water actively transporting WP-contaminated sediment from C-Pond or the

a. Aerial view showing distribution of ice blocks stranded during ebb tide.

b. Ice block pile along high point near gully margin.

Figure 64. Stranded ice blocks on the southern edge of In-between Gully.

surrounding mudflat, or both. Although other samples in 1994 from Bread Truck and Parachute gullies proved negative, they were taken during high tides of less than 5.03 m. Each flood when the B-Gully samples proved positive exceeded 5.15 m, so the former samples may not be representative.

The positive analyses for WP-contaminated sediments on ice floes and in gully runoff give some indication that migration of WP within the site and off-site is taking place. They clearly show the need for further investigation of WP transport and redeposition, including active deposition areas of Knik Arm.

BATHYMETRIC MONITORING AND WHITE PHOSPHORUS DEPOSITION

Bathymetric monitoring of Knik Arm near the mouth of Eagle River provides us with important information on the submarine and estuarine environment adjacent to ERF. Locations within this area may be sites where sediment and WP is deposited. Once identified, these areas should be sampled for analysis of WP.

The Knik Arm near the mouth of the Eagle River is 9–10 km wide (Fig. 65), having large tidal cycles (±9 m) that cause the Arm to alternate between being tidally and fluvially dominated. At low tide, this portion of Knik Arm essentially becomes a large anastomosing stream with a main channel located directly off the coast of ERF. Highly turbulent flow with large standing waves are common during low tide and as tidal flooding starts.

Bathymetric profiles

Examples of the bathymetric transect lines (Fig. 20) from which Figure 66 is developed are shown in Figure 67. The main channel just off ERF can be identified on each of the five bathymetric profiles. This channel changes from a broad (~500 m), smooth profile about 14 m deep along the northeastern corner of ERF to a more deeply incised (>16 m) and narrow channel (<200 m) near the mouth of the Eagle River. The asymmetrical profile has steeper slopes nearshore than those further out into the Arm (Line D, Fig. 67). Line F (Fig. 67), located near the northwestern corner of ERF, shows that the channel is wider (near 1 km) and appears to merge with a secondary channel at the intersection of Lines D and H. This secondary channel is located about 1–2 km offshore of ERF. It is characterized by sharp scarps, an uneven or scabbed bed profile with 3–5 m of relief, and shallower depth than the main channel. The main channel appears to handle most of the discharge during ebb, and low tide in particular, when two large intertidal bars in the center of Knik Arm are exposed (Fig. 65 and 67). The scabbed profile of the secondary channel suggests that localized and intense scour occurs in it.

The intertidal bar nearest ERF is located 0.2–1.2 km offshore and is greater than 1.5 km wide.

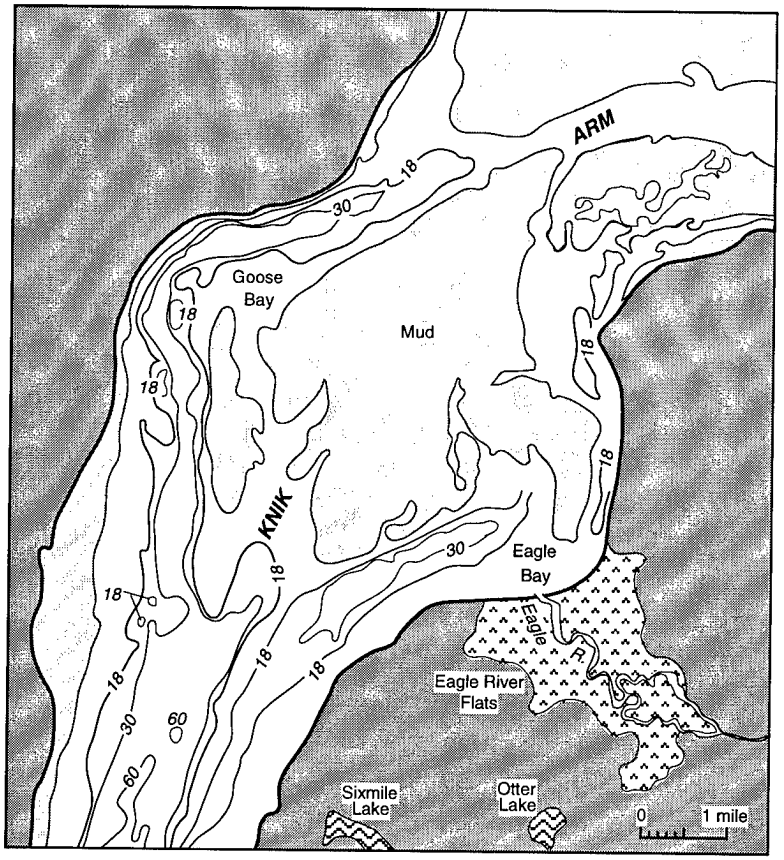

Figure 65. Knik Arm in the vicinity of ERF.

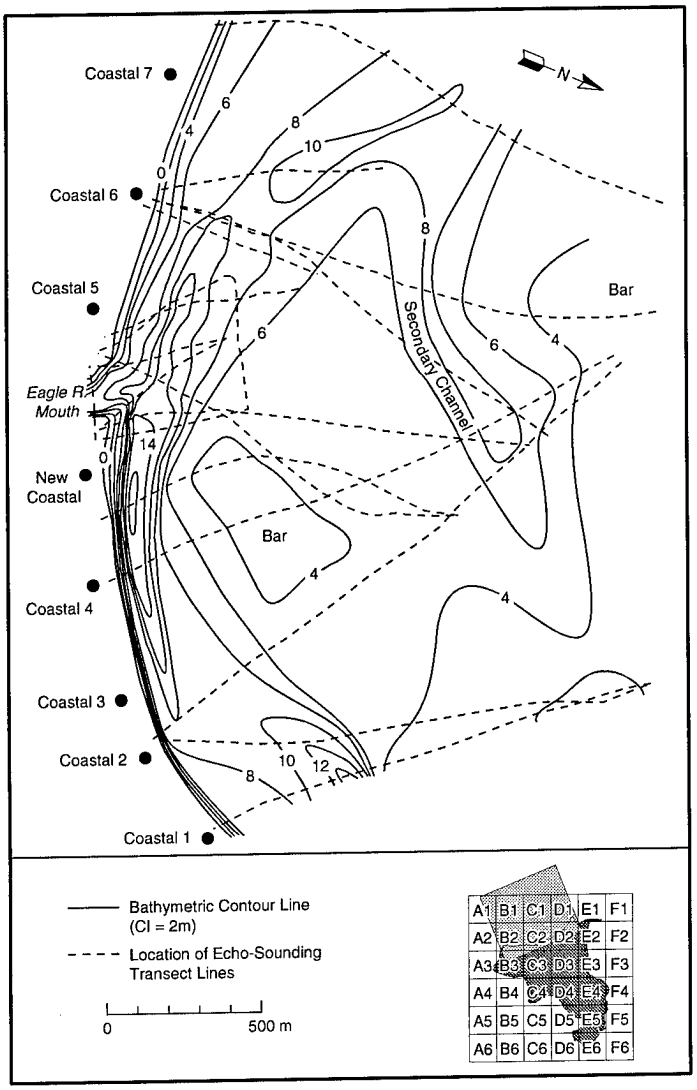

Figure 66. Bathymetric map of the Knik Arm near the mouth of the River and adjacent to the coast of ERF. Datum is mean Anchorage sea level.

The second bar extends north beyond the area that we have monitored. Both intertidal bars represent large zones of temporary sediment storage within Knik Arm.

A third, smaller intertidal bar forms a sharp peninsula that protrudes northwest into the Knik Arm from the northeast bank of the Eagle River mouth. Transect Line L (Fig. 67) turns at this bar across the Eagle River mouth, showing it to have a relatively flat bed and a depth of only 2–3 m below Anchorage mean sea level.

Potential areas of WP deposition

The bathymetric data show that several areas in Knik Arm are potential sites of sediment and WP deposition. These areas include the two intertidal bars mentioned previously (Fig. 66). In addition, there may be deposition along the coastline of ERF in zones where eddies develop during tidal inundation and in the early stages of ebb. Sediment appears to be accumulating along the upper beach slope as well. These sediments probably come from suspension settling near slack high tide and during the initial ebb.

Because our data indicate that WP-contaminated sediment is being transported by ice and water into gullies that drain into the Eagle River, we recommend that further analyses of offshore areas in Knik Arm be undertaken. These studies should include sampling of suspected areas of deposition for analysis of WP.

GROUND WATER INFORMATION

Data on ground water conditions in ERF are severely limited, but suggest that conditions may vary widely. We currently have four sources of data available (Fig. 68): piezometer measurements from three areas in 1994 and Druck pressure transducer measurements from a single shallow well in 1993. We established 4 piezometers in Bread Truck, 9 on a transect from C-Pond to the Eagle River and 15 piezometers in four groups in the C-Pond area for this study (Fig. 68). The other piezometer groups consisted of three to five piezometers per set, located at different depths below the ground surface, depending on site conditions. Each cluster provides data on vertical gradients. Between the initial installation and first measurement, three clusters went dry as the surface elevation of C-Pond lowered. These groups were then reestablished within the intermittently flooded area of the pond; they were measured twice after flooding in early September (Fig. 68). A single cluster in the permanently ponded area of C-Pond (Fig. 68) was measured three times during the summer.

Piezometers in C-Pond recorded elevated water levels in September whenever the sites were flooded (Fig. 69). Piezometers that were set deepest within the muddy substrate of the ponds generally recorded the highest level of elevation above

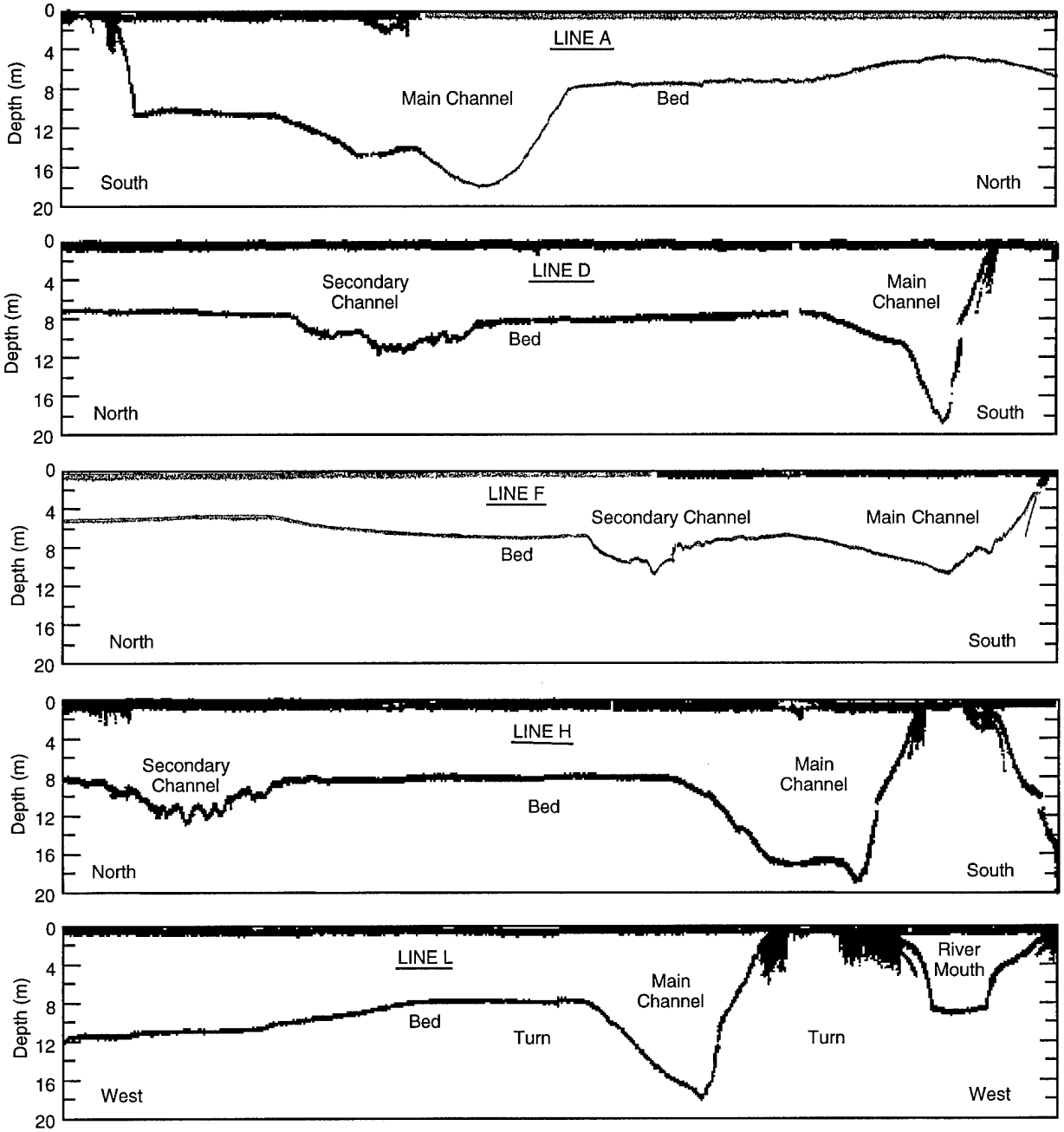

Figure 67. Bathymetric profiles. Refer to Figure 20 for profile locations.

the surrounding pond surface and indicate that C-pond was an area of ground water discharge.

The variability in water table elevation through time was only recorded from the monitoring well in B-Gully (Fig. 68 and 70). These data show that the water table fluctuates as a function of tidal flooding frequency in B-Gully, even when tides do not fully inundate the mudflats. There is, therefore, a subsurface hydraulic connection between tidal water and ground water at this site. However, there are no data available to determine the extent of this effect, and since the site was monitored only in 1993, these data cannot be correlated with our 1994 piezometer data.

The scanty data on ground water conditions suggest that tidal inundation interacts with the ground water system, but the precise nature of that interaction is unknown. There is a clear need for analysis of ground water conditions before its effects on WP remediation can be interpreted. Ground water fluctuations may be critical to measures requiring drainage and drying of sediment.

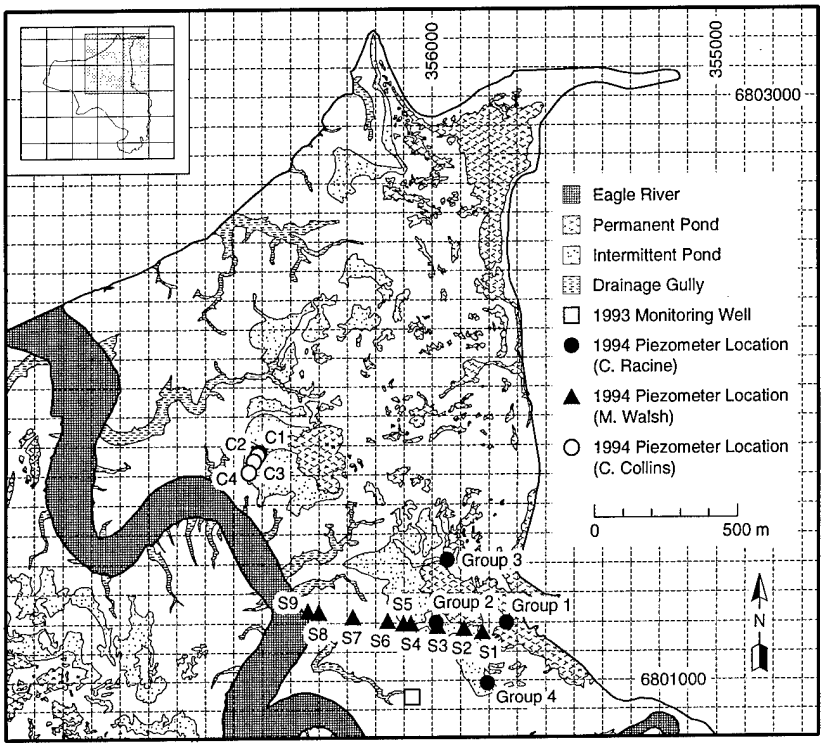

Figure 68. Locations of piezometers and monitoring well on ERF.

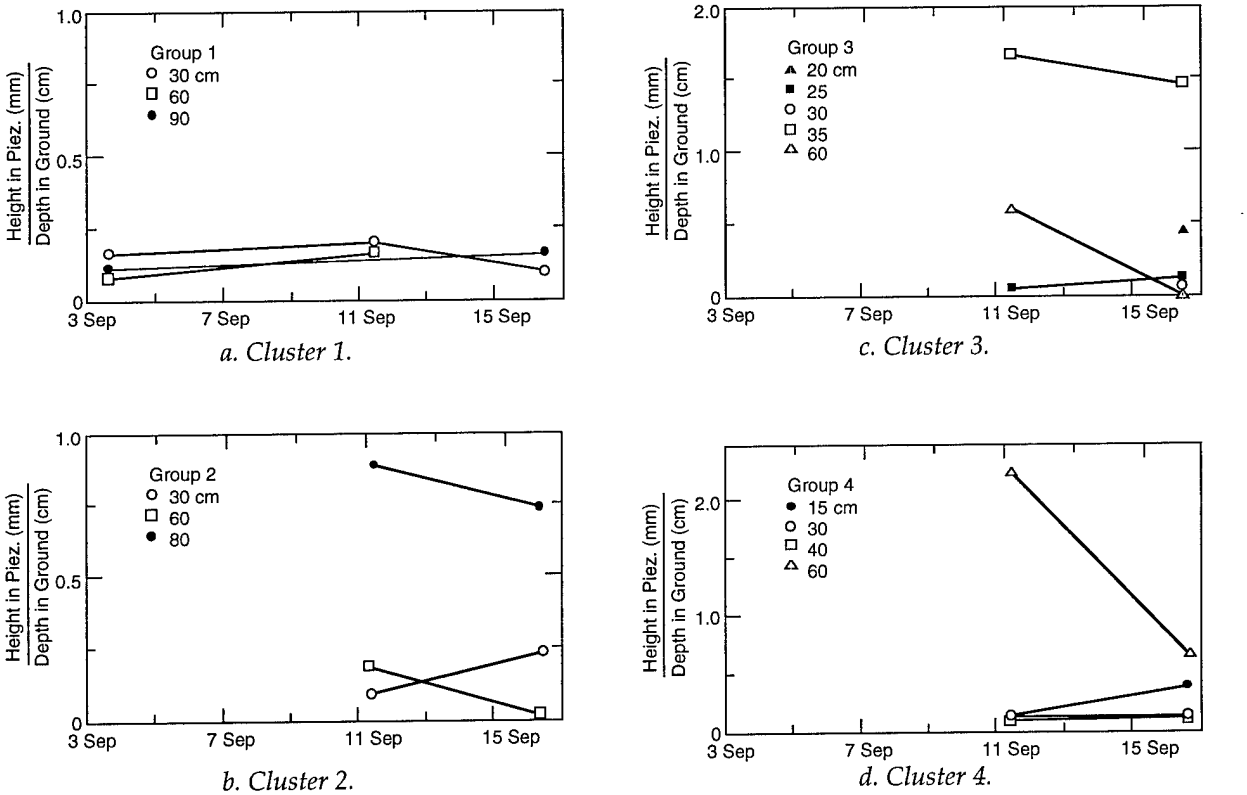

a. Cluster 1.

c. Cluster 3.

b. Cluster 2.

d. Cluster 4.

Figure 69. Plots of piezometer cluster data.

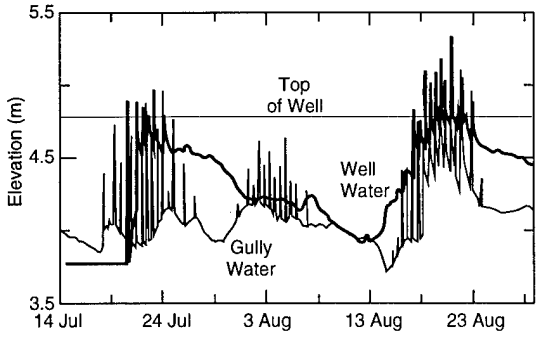

Figure 70. Ground water monitoring well levels and Hydrolab data at B-Gully. Elevations of top and bottom of monitoring well estimated at 4.78 and 3.78 m respectively (from C. Racine).

CONCLUSIONS: SYSTEM DYNAMICS AND REMEDIATION

Eagle River Flats is an estuarine salt marsh whose physical environment is undergoing progressive and significant changes. These changes result from the interaction and response of multiple physical processes to external forces such as tectonics, isostatic adjustment, macrotides, glacial river discharges and a cold climate. The location of ERF in an active earthquake zone adds to its complexity and to the potential for future rapid, but probably unpredictable, physical changes. If the area subsides again because of an earthquake, major changes in the hydrology and terrain can be expected. While pond areas may increase because of subsidence, the drainage system and river channel may also respond with increases in rates and locations of erosion if the base level is altered. In addition, ground explosions and cratering during the use of ERF as a military firing range since the early 1940s have caused physical changes to the terrain, hydrology and surface drainage. Craters act to divert and capture surface flow, causing changes in drainage and sediment storage patterns that can locally increase erosion and enhance gully expansion.

The inherent complexity of this dynamic environment makes it extremely difficult to predict what effects potential remedies for WP contamination will have on the physical system and, conversely, what short- and long-term effects the physical system will have on the effectiveness of proposed remediation. Understanding both the system's response to remediation and whether the remediation process will be enhanced or hindered by the physical environment is critical to their success in this dynamic environment. Further, site-specific process analyses of tidal flat hydrology, as well as continued measurements of erosion and sedimentation, will allow us to determine if this system will naturally attenuate the WP contamination.

LITERATURE CITED

Andrew, J. and G. Cooper (1993) Sedimentation in a river dominated estuary. *Sedimentology,* **40:** 979–1017.

Allen, J.R.L. (1982) *Sedimentary structures: Their character and physical basis.* Volume 1, 2. *Developments in Sedimentology,* vol. 30A, B. New York: Elsevier.

Allen, J.R.L. (1990a) Constraints on measurements of sea-level movements from salt marsh accretion rates. *Journal of the Geological Society London,* **147:** 5–7.

Allen, J.R.L. (1990b) Salt marsh growth and stratification: A numerical model with special reference to Severn estuary, S.W. Britain. *Marine Geology,* **95:** 77–96.

Allen, J.R.L. (1992) Large-scale textural patterns and sedimentary processes on tidal salt marshes in Severn Estuary, Southwest Britain. *Sedimentary Geology,* **81:** 299–318.

Allen, J.R.L. and J.E. Rae (1988) Vertical salt marsh accretion since the Roman period in the Severn estuary, southwest Britain. *Marine Geology,* **83:** 225–235.

APHA, AWWA, WEF (American Public Health Association, American Water Works Association, Water Environment Federation) (1992) Method 2540D total suspended solids dried at 103–105°C. *Standard Methods for the Examination of Water and Wastewater,* p. 2–56.

Bartsch-Winkler, S. and A.T. Ovenshine (1984) Macrotidal subarctic environment of Turnagain and Knik Arms, Upper Cook Inlet, Alaska: Sedimentology of the intertidal zone. *Journal of Sedimentary Petrology,* **54:** 1221–1238.

Bloom, A.L. (1984) Peat accumulation and compaction in a Connecticut coastal marsh. *Journal of Sedimentary Petrology,* **34:** 599–603.

Boon, J.D. (1975) Tidal discharge asymmetry in a salt marsh drainage system. *Limnology and Oceanography,* **20:** 71–80.

Brown, L.D., R.E. Reilinger, S.R. Holdahl and E.I. Balazs (1977) Post-seismic coastal uplift near

Anchorage, Alaska. *Journal of Geophysical Research,* **82** (23): 369–378.

Carling, P.A. (1981) Sediment transport by tidal currents and waves: Observations from a sandy intertidal zone (Burry Inlet, South Wales). In: *Holocene Marine Sedimentation in the North Sea Basin* (S.D. Nio, R.T.E. Schüttenhelm and Tj.C.E. van Weering, Eds.). I.A.S. Special Publication 5, p. 65–80

Carling, P.A. (1982) Temporal and spatial variation in intertidal sedimentation rates. *Sedimentology,* **29:** 17–23.

Cohen, S., S. Huldahl, D. Caprette, S. Hilla, R. Safford and D. Schultz (1995) Uplift of the Kenai Peninsula, Alaska, since the 1964 Prince William Sound earthquake. *Journal of Geophysical Research,* **100** (B2): 2031–2038.

Collins, L.M., J.L. Collins and L.B. Leopold (1987) Geomorphic processes of an estuarine marsh: Preliminary results and hypotheses. *International Geomorphology,* 1986, p. 1049–1072.

Dionne, J.C. (1988) Characteristic features of modern tidal flats in cold regions. In: *Tide-influenced Sedimentary Environments and Facies* (P.L. deBoer, A. van Gelder and S.D. Nio, Eds.). Boston: D. Reidel Publishing Company, p. 301–332.

Evans, C.D., E. Buch, R. Buffler, G. Fish, R. Forbes and W. Parker (1972) The Cook Inlet environment: A background study of available knowledge. University of Alaska Sea Grant Program.

French, J.R. (1991) Eustatic and neotectonic controls on saltmarsh sedimentation. In: *Coastal Sediments '91* (N.C. Kraus, K.J. Gingerich and D.L. Kriebel, Eds.). New York: American Society of Civil Engineer, p. 1223–1236.

French, J.R. (1993) Numerical simulation of vertical marsh growth and adjustment to accelerated sea-level rise, north Norfolk, U.K. *Earth Surface Processes and Landforms,* **18:** 68–81.

French, J.R. and T. Spencer (1993) Dynamics of sedimentation in a tide-dominated backbarrier salt marsh, Norfolk, U.K. *Marine Geology,* **110:** 315–331.

Frostick, M.E. and I.N. McCave (1979) Seasonal shifts of sediments in an estuary mediated by algal growth. *Estuary and Coastal Marine Science,* **9:** 569–576.

Gurnell, A.M. and J.C. Clark (Ed.) (1987) *Glaciofluvial Sediment Transfer.* New York: John Wiley and Sons.

Hanson, H.C. (1951) Characteristics of some grassland, marsh and other plant communities in western Alaska. *Ecological Monographs,* **21:** 327–378.

Harrison, E.Z. and A.L. Bloom (1977) Sedimentation rates on tidal salt marshes. *Journal of Sedimentary Petrology,* **47:** 1484–1490.

Hubbard, J.C.E. and R.E. Stebbings (1968) Spartina marshes in southern England III. Stratigraphy of the Keyworth Marsh, Poole Harbour. *Journal of Ecology,* **56:** 707–722.

Kearney, M.S. and L.G. Ward (1986) Vertical accretion rates in brackish marshes of a Chesapeake Bay tributary. *Geo-Marine Letters,* **6:** 41–49.

Keene, H.W. (1971) Postglacial submergence and salt marsh evolution in New Hampshire. *Maritime Sediments,* **7:** 64–68.

Kohsiek, L.H.M., J. Alphen, P. Bloks and P. Hoekstra (1981) A water and sediment balance of a salt marsh in the Eastern Scheldt Estuary. Published Research Report RWS nota nr. DDWT 81.042.

Krone, R.B. (1987) A method for simulating historic marsh elevations. In: *Coastal Sediments '87* (N.D. Krause, Ed.). New York: American Society of Civil Engineers, p. 316–323.

Lawson, D.E. (1993) Glaciohydrologic and glaciohydraulic effects on runoff and sediment yield in glacierized basins. USA Cold Regions Research and Engineering Laboratory, Monograph 93-2.

Lawson, D.E. and B.E. Brockett (1993) Preliminary assessment of sedimentation and erosion in Eagle River Flats, southcentral, Alaska. USA Cold Regions Research and Engineering Laboratory, CRREL Report 93-23.

Lawson, D.E., S. Bigl, J. Bodette and P. Weyrick (1995) Initial analyses of the hydrology and sedimentology of Eagle River Flats, Ft. Richardson, Alaska. USA Cold Regions Research and Engineering Laboratory, CRREL Report 95-5.

Leopold, L.B., M.G. Wolman and J.P. Miller (1964) *Fluvial Processes in Geomorphology.* San Francisco: W.H. Freeman, Co.

Letzch, W.S. and R.W. Frey (1980) Deposition and erosion in a Holocene salt marsh. *Journal of Sedimentary Petrology,* **50:** 529–542.

McCann, S.B. (ed.) (1980a) The coastline of Canada. Geological Survey of Canada, p. 80–10.

McCann, S.B. (ed.) (1980b) Sedimentary processes and animal–sediment relationships in tidal environments. Halifax: Geological Society of Canada Short Course No. 1.

McCann, S.B., J.E. Dale and P.B. Hale (1981) Subarctic tidal flats in areas of large tidal range, southern Baffin Island, eastern Canada. *Geogr. Phys. Quarterly,* **35:** 183–204.

McLaren, P., M.B. Collins, S. Gao and R.I.L. Powys (1993) Sediment dynamics of the Seven

Estuary and Inner Bristol Channel. *Journal of the Geological Society of London*, **50:** 589–603.

Ovenshine, A.T., D.E. Lawson and S.R. Bartsch-Winkler (1976a) The Placer River Silt: An intertidal deposit caused by the 1964 Alaskan earthquake. *Journal of Research, U.S. Geological Survey*, **4:** 151–162.

Ovenshine, A.T., S.R. Bartsch-Winkler, N.R. O'Brien and D.E. Lawson (1976b) Sediment of the high tidal range environment of upper Turnagain Arm, Alaska. In: *Recent and Ancient Sedimentary Environments in Alaska* (T.P. Miller, Ed.). Memoir, Alaskan Geological Society, p. M-1 –M-26.

Racine, C.H., M.E. Walsh, C.M. Collins, D.J. Calkins, B.D. Roebuck and L. Reitsma (1992a) Waterfowl mortality in Eagle River Flats, Alaska. USA Cold Regions Research and Engineering Laboratory, CRREL Report 92-5.

Racine, C.H., M.E. Walsh, B.D. Roebuck, C.M. Collins, D. Calkins, L. Reitsma, P. Buchli and G. Goldfarb (1992b) White phosphorus poisoning of waterfowl in an Alaskan salt marsh. *Journal of Wildlife Diseases*, **28**(4): 669–673.

Racine, C.H., M.E. Walsh, C.M. Collins, D. Lawson, K. Henry, L. Reitsma, B. Steele, R. Harris and S.T. Bird (1993) White phosphorus contamination of salt marsh sediments at Eagle River Flats, Alaska. USA Cold Regions Research and Engineering Laboratory, CRREL Report 93-17.

Reed, D.J. (1990) The impact of sea-level rise on coastal salt marshes. *Progress in Physical Geography*, **14:** 465–481.

Richard, G.A. (1978) Seasonal and environmental variations in sediment accretion in a Long Island salt marsh. *Estuaries*, **1:** 29–35.

Rosenberg, D.H. (1986) Wetland types and bird use of Kenai Lowlands. Anchorage, Alaska: U.S. Fish and Wildlife Service, Special Studies.

Sharp, M., M. Tranter, G.H. Brown and M. Skidmore (1995) Rates of chemical deundation and CO_2 drawdown in a glacier-covered alpine catchment. *Geology*, 61–63.

Stoddart, D.R., D.J. Reed and J.R. French (1989) Understanding salt marshes. *Estuaries*, **12:** 228–236.

Small, J.B. and L.C. Wharton (1969) Vertical displacements determined by surveys after the Alaska earthquake of March 1964. In: *The Prince William Sound, Alaska Earthquake of 1964 and Aftershocks.* Volume III, *Research Studies and Interpretive Results, Geodesy and Photogrammetry* (L.E. Leipold and F.J. Wood, Eds.). Washington, D.C.: U.S. Coast and Geodetic Survey, p. 21–33.

Syvitski, J.P.M., D.C. Burrell and J.M. Skei (1987) *Fjords: Processes and Products.* New York: Springer-Verlag.

U.S. Geological Survey (1981) Water resources data—Alaska, water year 1980. Washington, D.C.: U.S. Geological Survey.

Vince, S.W. and A.A. Snow (1984) Plant zonation of an Alaskan salt marsh. II. An experimental study of the role of edaphic conditions. *Journal of Ecology*, **72:** 669–684.

Walsh, M.E., C. Collins and C.H. Racine (1995) Persistence of white phosphorus particles in sediment. USA Cold Regions Research and Engineering Laboratory, CRREL Report 95-23.

APPENDIX A: TSS ANALYSES

TSS samples were analyzed in a field laboratory following the standard procedures, with minor modifications to the methods that were relevant to this project. Our procedure differed in the following ways.

1. Glass fiber filters were not pre-washed, dried and weighed. Control tests performed in 1993 and 1994 determined that the weight changes were insignificant.

2. Oven temperature remained between 103 and 105°C since volatile solids were not measured. Temperature was checked and recorded daily as was the balance calibration.

3. Owing to the small particle sizes of sediment, filters readily clogged. We minimized filtration time by carefully pouring the majority of settled sample into a graduated cylinder, recording the volume, then vigorously shaking the remaining portion and quickly transferring it to a graduated cylinder. This volume was recorded and added to the initial value. The sample container, graduated cylinder and filter funnel were thoroughly rinsed with distilled water, with all washes added to the filtered sample.

4. The final cycle of drying, cooling and reweighing of filters was deemed unnecessary for the concentration ranges encountered.

APPENDIX B: SEASONAL SUMMARY OF EROSION RATES

			Recession range (m)						
	SITE	*POS*	*S92*	*W92*	*S93*	*W93*	*S94*	*F94*	*NET*
River-Meander	32	L	—	—	—	—	—	0–0.59	0–59
	33	L	—	—	—	—	—	0–1.62	0–1.62
	34	L	—	—	—	—	—	0	0
River-North	36	L	—	—	—	—	—	0	0
	37	L	—	—	—	—	1.02–2.32	1.05–2.03	2.59–3.69
	38	L	—	—	—	—	—	0	0
	39	L	—	—	—	—	—	0	0
Racine Island	31	L	—	—	—	—	—	0	0
	29	H	—	—	—	—	—	0	0
	30	L	—	—	—	—	—	0	0
River South	28	L	—	—	—	—	—	0	0
Area A Near Coast									
Coastal 6	52	L	—	—	—	—	0.01–0.91	0.23–1.85	0.93–2.76
	55	L	—	—	—	—	0–1.0	0–0.63	0–1.65
	53	H	—	—	—	—	0–0.02	0–0.74	0–0.74
	54	H	—	—	—	—	0–0.27	0–0.64	0.25–0.58
Coastal 7	56	L	—	—	—	—	0–0.47	0–0.71	0–1.65
	57	H	—	—	—	—	0.12–0.43	0.1–1.17	0.07–1.09
Area A Inland									
Coastal 5	45	L	—	—	—	—	0–0.62	—	0–0.62
	47	L	—	—	—	—	0–1.0	—	0–1.10
	48	L	—	—	—	—	0–0.35	—	0–0.35
	43	H	—	—	—	—	0–0	—	0
	44	H	—	—	—	—	0–0.53	—	0–0.53
	46	H	—	—	—	—	1.33–1.59	—	1.33–1.59
	49	H	—	—	—	—	0	—	0
Tanker	40	L	—	—	—	—	0	0–1.17	0–1.17
	42	L	—	—	—	—	0	0–0.27	0–0.27
	41	H	—	—	—	—	0	0	0
Area D—In Between	7	H	0.01–1.09	0.05–0.35	0–2.79	0–0.61	0–0.25	—	0.13–2.14
	9	H	0.01–6.95	0.05–0.1	1.7–4.31	—	0.04–0.19	—	0.04–4.61
	6	L	0.05–2.37	0–2	0.35–2.34	0–2.29	0–0.4	—	0.02–4.37
	8	L	0.002–0.142	0–0.95	0–0.41	0–0.37	0–0.03	—	0.08–0.56
	10	L	0–0.16	0–0.5	0–0.03	0–0	0–0	—	0.3–0.041
	11	L	0.02–0.52	0–0.4	0–1.02	0–0	0–0.05	—	0.02–0.96
Bread Truck	16	H	—	—	—	—	0.99–2.1	0.065–1.39	20.03–2.97
	18	H	—	—	—	—	0–1.2	0–0.77	0–1.44
	19	H	—	—	—	—	0.18–1	0–3.77	0–3.54*
	20	H	—	—	—	—	0–0.03	0.01–0.04	0.03–0.05
	12	L	—	—	0.84–3.12	0–1.29	0.03–0.69	—	8–5.1
	13	L	—	—	0–1.68	0–0.93	0–0.6	—	0–3.33
	14	L	—	—	0.01–1.16	00.03–1.42	0–1.02	—	0.66–2.37
	15	L	—	—	—	0–2.34	0.03–1.44	0–0.62	0.44–8.15
	17	L	—	—	—	0.43–1.99	0–2.23	0–0.52	0.02–2.6
Area D—Coastal 1	26	L	—	—	—	—	—	0–0.82	0–0.82
	26	H	—	—	—	—	0–0.78	0.07–1.65	0.19–1.65
	27	H	—	—	—	—	0–0	0–0.4	0–0.04
	25	H	—	—	—	—	0	0.41–0.9	0.41–0.9
Area C									
B–Gully	1	L	—	0.17–4.5	0.70–1.82	0.13–2.08	0–2.57	0–0.97	0.12–7.32
	2	L	0–4.9	0–1.95	0.24–0.92	0–1.37	0–1.16	0–1.03	0.27–8.17
Parachute	3	L	0.13–0.61	0–0.37	—	0.16–0.75	0.02–6.02	0–0.71	0.3–1.63
	5	L	0.1–1.314	0.12–0.75	0.17–0.21	0–0.7	0–0.4	0	0.49–1.5
	4	H	0.09–3.06	0.09–3.06	0.04–3.79	0.24–1.35	0–0.07	0–1.17	0.04–9.30

* Records initial phase of extension prior to collapse.
L = lateral erosion, H = headward erosion.

APPENDIX C: TIDAL INUNDATION DATA FOR BREAD TRUCK, PARACHUTE AND SPRING GULLIES

	Start rise		*Peak*		*End runout*	
Site	*Julian time*	*Elev. (m)*	*Julian time*	*Elev. (m)*	*Julian time*	*Elev. (m)*
Bread Truck	274.704	2.959	274.749	3.479	274.793	2.959
	275.201	2.962	275.251	3.671	275.31	2.962
	277.74	2.995	277.835	5.287	278.265	*3.28
	278.268	3.28	278.349	5.091	278.757	*3.205
	278.76	3.205	278.86	5.606	279.29	*3.326
	279.293	3.326	279.388	4.671	279.782	*3.397
	279.785	3.397	279.885	5.933	280.326	*3.395
	280.329	3.395	280.413	5.206	280.815	*3.046
	280.818	3.046	280.913	5.307	281.36	*3.112
	281.363	3.112	281.446	4.956	281.843	*2.999
	281.846	2.999	281.943	5.1	282.407	*3.05
	282.415	3.05	282.482	4.268	282.885	*2.955
	307.213	3.174	307.304	5.263	307.696	*3.158
	307.699	3.158	307.796	5.82	308.246	*3.092
	308.251	3.092	308.332	5.115	308.724	*3.099
	308.726	3.099	308.826	5.688	309.288	*3.143
	209.29	3.143	309.365	5	309.438	3.166
	309.757	3.191	309.857	5.769	310.16	3.107
	310.315	3.085	310.396	4.987	310.468	3.063
	310.796	3.037	310.89	5.263	311.34	3.096
	311.343	3.096	311.429	4.748	311.729	3.017
	311.84	3.017	311.915	4.786	311.988	3.012
Parachute	275.746	3.603	275.776	4.094	275.976	3.603
	276.246	3.603	276.288	4.261	276.513	3.603
	276.743	3.603	276.801	4.838	276.979	3.606
	277.26	3.61	277.318	4.897	277.524	3.606
	277.76	3.602	277.835	5.206	278.285	*3.642
	278.288	3.642	278.349	5.044	278.729	3.614
	278.779	3.612	278.868	5.49	279.31	*3.685
	279.313	3.685	279.385	5.23	279.799	*3.669
	279.801	3.669	279.89	5.719	280.346	*3.678
	280.349	3.678	280.413	5.049	280.835	*3.625
	280.838	3.625	280.915	5.288	281.379	*3.668
	281.382	3.668	281.446	5.023	281.865	*3.619
	281.868	3.619	281.943	5.158	282.435	*3.64
	282.438	3.64	282.479	4.325	282.774	3.614
	306.693	3.697	306.776	5.407	307.235	*3.619
	307.238	3.619	307.301	5.119	307.715	*3.643
	307.718	3.643	307.799	5.653	308.271	*3.693
	308.274	3.693	308.329	5.049	308.749	*3.625
	308.751	3.638	308.829	5.541	309.313	*3.742
	309.315	3.742	309.368	4.926	309.668	3.619
	309.785	3.628	309.868	5.514	310.34	*3.685
	310.343	3.685	310.401	4.958	310.818	*3.659
	310.821	3.659	310.89	5.196	311.382	*3.734
	311.385	3.734	311.435	4.705	311.865	*3.641
	311.868	3.641	311.918	4.738	312.135	3.623
Spring Gully	277.71	1.888	—	—	278.229	2.202
	278.243	2.206	278.349	5.019	278.735	*2.047
	278.738	2.047	—	—	279.265	*2.351
	279.268	2.354	—	—	279.763	*2.303
	279.765	2.303	—	—	280.307	*2.332
	280.31	2.332	280.41	5.027	280.79	*2.304
	280.793	2.034	—	—	281.335	*2.265
	281.338	2.265	281.438	4.986	—	—
	308.224	1.88	308.329	4.921	308.701	1.839
	308.704	1.839	—	—	309.054	2.205
	309.26	1.908	309.365	4.823	309.46	1.907
	309.735	1.879	—	—	310.265	1.908
	310.288	1.9	310.396	4.902	310.765	*1.798
	310.768	1.798	—	—	311.324	*1.872
	311.326	1.872	311.426	4.623	311.807	*1.785
	311.81	1.785	311.915	4.657	312.365	*1.806

* Water elevation never reached base level before next tidal inundation.

APPENDIX D: PRELIMINARY ESTIMATES OF GULLY WATER DISCHARGE AND SEDIMENT FLUX

Month	Tidal stage	Velocity (cm/s)		TSS (mg/L)		Discharge (m^3/s)		Sediment flux (kg/s)	
		Peak	Average	Peak	Average	Peak	Average	Peak	Average
Bread Truck Gully; Cross-sectional area = 5.5 m^2									
May	Flood	NA	25.0	739	170	NA	1.38	NA	0.23
	Ebb	NA	76.1	1148	669	NA	4.19	NA	2.80
June	Flood	NA	25.0	715	227	NA	1.38	NA	0.31
	Ebb	NA	76.1	1175	512	NA	4.19	NA	2.14
September	Flood	NA	25.0	1714	429	NA	1.38	NA	0.59
	Ebb	NA	76.1	1423	467	NA	4.19	NA	1.95
October	Flood	71.1	22.6	1930	847	3.9	1.24	7.55	1.05
	Ebb	133.0	81.0	1329	758	7.3	4.46	9.72	3.38
November	Flood	68.6	29.9	2152	1186	3.8	1.64	8.12	1.95
	Ebb	146.0	74.0	1363	885	8.0	4.07	10.94	3.60
Parachute Gully; Cross-sectional area = 9.8 m^2									
May	Flood	NA	27.1	983	222	NA	1.49	NA	0.33
	Ebb	NA	47.0	1507	485	NA	2.59	NA	1.25
June	Flood	NA	27.1	638	250	NA	1.49	NA	0.37
	Ebb	NA	47.0	854	221	NA	2.59	NA	0.57
September	Flood	NA	27.1	1740	646	NA	1.49	NA	0.96
	Ebb	NA	47.0	1840	373	NA	2.59	NA	0.96
October	Flood	37.4	13.4	2733	1752	2.1	0.74	5.62	1.29
	Ebb	76.0	45.0	2073	723	4.2	2.48	8.67	1.79
November	Flood	56.4	32.2	3102	2420	3.1	1.77	9.62	4.29
	Ebb	72.0	49.0	2838	1285	4.0	2.70	11.24	3.46
Spring Gully; Cross-sectional area = 26.5 m^2									
May	Flood	NA	15.5	1850	420	NA	0.85	NA	0.36
	Ebb	NA	101.9	1439	689	NA	5.60	NA	3.86
June	Flood	NA	15.5	5626	1765	NA	0.85	NA	1.50
	Ebb	NA	101.9	1888	834	NA	5.60	NA	4.67
September	Flood	NA	15.5	1458	763	NA	0.85	NA	0.65
	Ebb	NA	101.9	1586	608	NA	5.60	NA	3.41
October	Flood	59.7	24.5	2733	1752	3.3	1.35	8.97	2.36
	Ebb	176.2	124.6	2538	619	9.7	6.85	24.60	4.24
November	Flood	51.8	17.2	3049	1757	2.8	0.95	8.69	1.66
	Ebb	162.4	84.5	3776	1883	8.9	4.65	33.73	8.75

REPORT DOCUMENTATION PAGE

Form Approved
OMB No. 0704-0188

1. AGENCY USE ONLY (Leave blank)	2. REPORT DATE	3. REPORT TYPE AND DATES COVERED
	August 1996	

4. TITLE AND SUBTITLE
Physical System Dynamics and White Phosphorus Fate and Transport, 1994, Eagle River Flats, Fort Richardson, Alaska

5. FUNDING NUMBERS

6. AUTHORS
Daniel E. Lawson, Lewis E. Hunter, Susan R. Bigl, Beth M. Nadeau, Patricia B. Weyrick and John H. Bodette

7. PERFORMING ORGANIZATION NAME(S) AND ADDRESS(ES)
U.S. Army Cold Regions Research and Engineering Laboratory
72 Lyme Road
Hanover, New Hampshire 03755-1290

8. PERFORMING ORGANIZATION REPORT NUMBER
CRREL Report 96-9

9. SPONSORING/MONITORING AGENCY NAME(S) AND ADDRESS(ES)
U.S. Army Alaska, Fort Richardson, Alaska
and
U.S. Army Engineer District, Alaska
Anchorage, Alaska

10. SPONSORING/MONITORING AGENCY REPORT NUMBER

11. SUPPLEMENTARY NOTES
For conversion of SI units to non-SI units of measurement consult ASTM Standard E380-93, *Standard Practice for Use of the International System of Units*, published by the American Society for Testing and Materials, 1916 Race St., Philadelphia, Pa. 19103.

12a. DISTRIBUTION/AVAILABILITY STATEMENT
Approved for public release; distribution is unlimited.
Available from NTIS, Springfield, Virginia 22161

12b. DISTRIBUTION CODE

13. ABSTRACT (*Maximum 200 words*)

Eagle River Flats (ERF) is a subarctic estuarine salt marsh where human and natural forces are causing significant changes in the environment. Multiple internal and external forces govern the physical and chemical processes by actively altering surface conditions, sometimes in unpredictable ways. ERF is also used as an artillery range by the U.S. Army, where past use has resulted in white phosphorous (WP) contamination of the sediments within ponds and mudflats. Bottom-feeding waterfowl ingest this WP, which causes rapid death. This report documents analyses of the physical environment, describing the nature of the physical systems and factors controlling them. It includes data on sedimentation, erosion and hydrology. These investigations provide knowledge necessary to designing and evaluating remedial technologies. They also help determine the system's capacity to naturally attenuate the WP contamination.

14. SUBJECT TERMS
Erosion, Factors, Processes, Remediation, Sedimentation, Salt marsh, Tidal flat, WP

15. NUMBER OF PAGES
76

16. PRICE CODE

17. SECURITY CLASSIFICATION OF REPORT	18. SECURITY CLASSIFICATION OF THIS PAGE	19. SECURITY CLASSIFICATION OF ABSTRACT	20. LIMITATION OF ABSTRACT
UNCLASSIFIED	UNCLASSIFIED	UNCLASSIFIED	UL